UNIVERSITY OF CALIFORNIA SAN DIEGO

Intelligent Bioprinting for Structure and Mechanical Property Modulation

A Dissertation submitted in partial satisfaction of the requirements
for the degree Doctor of Philosophy

in

Electrical Engineering (Intelligent Systems, Robotics, and Control)

by

Jiaao Guan

Committee in charge:

Professor Shaochen Chen, Chair
Professor Zhaowei Liu, Co-Chair
Professor Zeinab Jahed
Professor Tse Nga Ng

2023

The Dissertation of Jiaao Guan is approved, and it is acceptable in quality and form for publication on microfilm and electronically.

University of California San Diego

2023

DEDICATION

To my encouraging and thoughtful mother, my hardworking and beloved father who cares about me dearly, and all my loving family.

TABLE OF CONTENTS

LIST OF FIGURES

LIST OF TABLES

ACKNOWLEDGEMENTS

First of all, I would like to thank Professor Shaochen Chen, for advising and supporting me through my research and study. Dr. Chen has been open to answering all aspects of my research and career questions and providing great help.

I would like to also acknowledge my talented and heartwarming labmates in Chen lab for providing so much help in my research and life and creating an awesome environment. I would like to thank Dr. Shangting You, Dr. Wei Zhu, Dr. David Berry, Dr. Henry Hwang, Dr. Zheng Zhong, Dr. Kathleen Miller, Dr. Min Tang, Dr. Daniel Wangpraseurt, Dr. Xuanyi Ma, Dr. Claire Yu, Wisarut Kiratitanaporn, Yi Xiang, Jacob Schimelman, Yazhi Sun, Ting-yu Lu, all former and past lab members, visiting scholars and all undergraduate volunteers who worked in the lab. I would like to especially give my thanks to Dr. Shangting You for his helpful guidance on my research.

I would like to thank my collaborators, Dr. Hao Su, Ronald Yu, and Dr. Netanel Kramer. I have learned a lot from the collaboration projects.

I am thankful for the time and advice from my thesis committee members Dr. Zhaowei Liu, Dr. Zeinab Jahed, and Dr. Tse Nga Ng.

Most importantly, I would like to give my deepest thanks to my parents, without whom I would have no chance of achieving my present life and education.

Chapter 1 introduction contains unpublished material coauthored with S. You, J. Alido, H. H. Hwang, S. Chen. The dissertation author was the primary author of this work.

Chapter 2, in full, is a reprint of the published article “Compensating the cell-induced light scattering effect in light-based bioprinting using deep learning”, J. Guan, S. You, Y.

Xiang, J. Schimelman, J. Alido, X. Ma, M. Tang, S. Chen. *Biofabrication*, 2022. The dissertation author was the primary researcher and the first author of this paper.

Chapter 4, in part, has been submitted for publication entitled “Multi-modal Vat Photopolymerization for Microscale Modulation of Scaffold Stiffness Assisted via Machine Learning”, W. Kiratitanaporn, J. Guan, D. Berry, A. Lao, S. Chen, as it may appear in Additive Manufacturing 2023. The dissertation author was the one of the primary researchers and co-first author of this paper.

VITA

2017 B.Eng. in Electrical Engineering, McGill University

2018 M.S. in Electrical Engineering (Intelligent Systems, Robotics, and Control), University of California San Diego

2023 Ph.D. in Electrical Engineering (Intelligent Systems, Robotics, and Control), University of California San Diego

PUBLICATIONS

1. C. Yu, J. Schimelman, P. Wang, K. L. Miller, X. Ma, S. You, J. Guan, B. Sun, W. Zhu, S. Chen, "Photopolymerizable biomaterials and light-based 3D printing strategies for biomedical applications", Chemical Reviews, 120.19 (2020): 10695-10743.

2. S. You, J. Guan, J. Alido, H. H. Hwang, R. Yu, L. Kwe, H. Su, S.C. Chen, "Mitigating Scattering Effects in Light-based 3D Printing Using Machine Learning", Journal of Manufacturing Science and Engineering, 142.8 (2020): 081002.

3. J. Guan, S. You, Y. Xiang, J. Schimelman, J. Alido, X. Ma, M. Tang, S.C. Chen, "Compensating the cell-induced light scattering effect in light-based bioprinting using deep learning", Biofabrication, 14.1 (2021): 015011.

4. Z. Zhong, J. Wang, J. Tian, X. Deng, A. Balayan, Y. Sun, Y. Xiang, J. Guan, C. Ma, J. Schimelman, X. Shi, E. Yao, S. X. Deng, S.C. Chen, "Rapid 3D Bioprinting of a Multicellular Model Recapitulating Pterygium Microenvironment", Biomaterials, 282 (2022): 121391.

5. Y. Xiang, K. Miller, J. Guan, W. Kiratitanaporn, M. Tang, S.C. Chen, "3D Bioprinting of complex tissue in vitro: state-of-the-art and future perspectives", Archives of Toxicology, 96.3 (2022): 691-710.

6. N. Kramer, J. Guan, S. Chen, D. Wangpraseurt*, Y. Loya, "Morpho-functional traits of the coral Stylophora pistillata enhance light capture for photosynthesis at mesophotic depths", Communications Biology, 5.1 (2022): 861.

7. S. You, Y. Xiang, H. H. Hwang, D. B. Berry, W. Kiratitanaporn, J. Guan, E. Yao, M. Tang, Z. Zhong, X. Ma, D. Wangpraseurt, Y. Sun, T. Lu, S. Chen*, "High cell density and high-resolution 3D bioprinting for fabricating vascularized tissues", Science Advances, 9.8 (2023): eade7923.

ABSTRACT OF THE DISSERTATION

Intelligent Bioprinting for Structure and Mechanical Property Modulation

by

Jiaao Guan

Doctor of Philosophy in Electrical Engineering (Intelligent Systems, Robotics, and Control)

University of California San Diego, 2023

Professor Shaochen Chen, Chair
Professor Zhaowei Liu, Co-Chair

Intelligent additive manufacturing is one of the pathways projected to be critical to the future of manufacturing. Among the many technologies that can facilitate advanced manufacturing, 3D printing provides high-quality customizable manufacturing with a wide variety of materials. Researchers have also investigated tissue engineering and cell-encapsulated biomaterials using 3D printing technologies, resulting in bioprinting which could help drug discovery, organoid fabrication, organ-on-a-chip devices, and many other

bioengineering fields. Increasing research and industrial interests have made 3D printing an easily accessible and productive tool, yet there are still challenges associated with different 3D printing technologies. Machine learning is another emerging technology that shows promising abilities to solve complex problems in a data-based experiential manner. The application of machine learning to enhance 3D printing performance is of great interest to both the research and industrial communities. Therefore, it is interesting to utilize machine learning technology to solve problems in 3D printing technology and enable more advanced functional fabrication.

In this dissertation, as an example of using machine learning to solve 3D printing challenges, we demonstrated the use of machine learning to first solve the significant light-scattering problem in light-based bioprinting with cell-encapsulated photopolymer material. The machine learning method was able to compensate for the cell-induced light scattering effect by modifying the local exposure doses for digital light processing-based 3D bioprinting.

After that, we developed a two-photon polymerization 3D nanoprinting method for its high fabrication fidelity in making sub-micron structures and the flexible control of the microfabrication. On top of that, a machine learning algorithm is developed to suggest the printing parameters for modulating the scaffold stiffness with the two-photon 3D printing process as well as the digital light processing-based 3D printing. The flexible control of both the microarchitecture and the mechanical properties of the 3D printed biocompatible scaffolds could enable a broad range of bioengineering applications.

Chapter 1 Introduction to 3D printing and machine learning

1.1 Introduction

Intelligent manufacturing describes the combination of intelligent systems and advanced fabrication technologies, and is considered to be one of the key components in the next generation of industrial manufacturing, which demands better metrics across domains such as production, throughput, quality, customizability, and environmental sustainability. [1–4] Intelligent systems are computer-controlled machines that has the capacity to communicate with human or machines, collect and analyze data, and automatically change their behaviors based on the analyzed data (self-learning). The use of intelligent systems may benefit resource management and utilization, as well as process optimization, thus achieving greater economic and environmental merit in manufacturing. There are many technologies that can contribute to intelligent manufacturing, including but not limited to: cyber-physical systems (CPS), Internet of Things (IoT), big data analysis, machine learning (ML), artificial intelligence (AI), 5th-generation wireless communication (5G), 3D printing (3DP), photolithography, click chemistry, genetic engineering, and so on. Recently, research focusing on the application of ML technology to 3D printing are emerging. [5–8] Various interesting strategies of integrating machine learning with different 3DP methods have been explored. In this work, we aim to provide a comprehensive review of intelligent manufacturing strategies that combine machine learning and 3D printing techniques (Fig. 1.1).

3D printing [9–16] is a principally additive manufacturing (AM) technology, usually involving tools that structure material from the ground up in a controlled manner, as opposed to subtractive manufacturing techniques that remove material from raw stock. Compared to commonly-used manufacturing techniques such as milling or molding, the initial cost and setup

time required for 3DP is minimal. Additionally, 3DP techniques can directly construct complex geometries, such as hollow structures, without need for secondary assembly. Various 3DP technologies can utilize a wide range of construction techniques and materials, making 3DP as a whole quite versatile for fabricating customized parts on a short time scale.

Machine learning [17–21] is a concept of training a computer algorithm's behavior based on examining relationships between input and output data without knowledge of the mediating process. Some tasks, such as hand-written number recognition, are difficult for process-based algorithms which require to develop an explicit mathematical solution beforehand; however, these kinds of problems can be solved via ML's self-learning capability, where humans need only to provide data to train the algorithm, without explicitly programming the algorithm to solve the problem. A popular subfield of ML, deep learning, makes use of artificial neural networks (NNs), which are sets of algorithms loosely based on human neural architecture, and excel at recognizing patterns[17]. Deep learning has recently shown great success in solving highly-sophisticated problems which were previously considered only solvable with human-level intelligence, and has enabled advances in fields such as market analysis[22], computer vision[23,24], and automatic driving[25].

Recent researches have showed great interest on using ML to assist 3DP [5–8]. To briefly summarize the significance of ML in the 3DP workflow, we first conclude that an intelligent system can usually be involved in the 3DP process on two aspects: 1) prediction, or system modeling and 2) optimization. For the first aspect, prediction, the most commonly used non-ML approach is the finite element analysis (FEA) which analyzes the system with finite element method (FEM)[26]. The FEM is a numerical method that approximates a system with small interconnected elements and simulates the system behavior in a bottom-up manner at a cost of long

run time and a precise modeling of the system. Using ML, we can greatly reduce the process time on executing the trained system model, and also eliminate the need for manually modeling the system. The only risk for ML is that the trained model quality greatly relies on the quality and quantity of the training data. For the second aspect, the optimization, actually ML and non-ML tends to follow the same way of using global iterative optimization methods. However, since the iterative method normally relies on the access to the system model, a fast ML model will result in a fast optimization speed. Besides, there are also a few recent attempts on using ML methods to model the inverse of the system model as a way to get optimized input. Since if we have the inverse model, any 3DP optimization problems can be simply solved by entering the optimization performance goal into the inverse model and the result would be the optimal system input factors. While this approach still lacks empirical practices, it has the potential of speeding up 3DP optimization problem solving and will allow more precise real time control adjustment.

Researchers have developed various ways to explore the combination of ML and 3DP in their studies. These studies can be loosely categorized into three types: 1) ML used in 3DP for high performance production; 2) ML used in 3DP for fast design turnaround; and 3) special uses of ML with 3DP. The details of the categories and the reviewed studies will be discussed in Section 1.4.

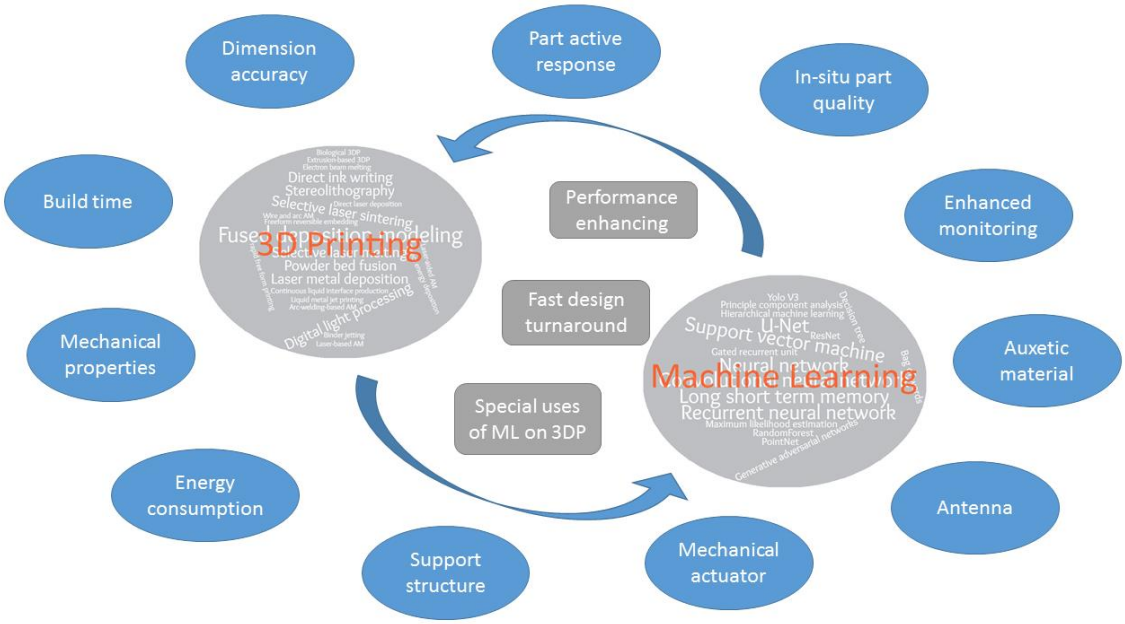

Fig. 1.1. Summary of 3D printing and machine learning applications.

1.2 3D Printing

1.2.1 3D printing technologies

3DP has emerged as a powerful additive free-form 3D fabrication technology in the past decades because of its low cost, simplicity, and versatility. To date, multiple variants of 3DP technologies have been developed. Generally, there are two classes of 3DP technologies. One is to selectively deposit the building material to the desired location, and the other is to selectively deliver energy to the desired location to induce phase change of the building material. For a comprehensive review of various 3DP techniques, please see these earlier publications. [12,10,9,15]

Material-deposition based 3DP methods such as fused deposition modeling (FDM), powder bed 3D printing, and ink-jet 3D printing[13,27,28] use one or more nozzles that can move under the control of a computer to selectively deposit material to the desired location. By scanning the nozzle through the 3D space of the designed object, a 3D construct can be built. However, as

the material is deposited serially, whether it be drop-by-drop, line-by-line, or layer-by-layer, distinct interfaces often form between depositions, which often affect the final mechanical performance or integrity of the 3D printed construct [9,11].

Energy-delivery based 3DP methods deliver energy, typically light energy, to the desired location and induce melting, sintering, photopolymerization, photocrosslinking, or photoreduction.[15,29–33] By spatially controlling the exposure dose, a desired 3D object can be formed. These technologies include selective laser sintering (SLS), stereolithography (SLA), digital light processing (DLP) 3D printing, etc. As light can be precisely manipulated by optical systems, energy delivery based 3DP methods typically achieve finer resolution and higher quality compared to their material-deposition based counterparts.

Regardless of the particular method of any given 3DP technology, every 3D printer requires a 3D model of the desired construct, and its associated processing parameters. Improper 3D modeling and/or processing parameters can lead to poor fabrication quality, or even failure to print. For example, when a 3D object is desired to be printed with overhanging structures or voids, support features need to be added to the base 3D model to prevent collapse during printing. Thus, expertise is required to operate a 3D printer, especially when fabricating high precision structures, or using customized materials. By introducing intelligent systems to assist in the design and optimization of 3DP, failed product rates can be reduced and fabrication quality can be improved.

1.2.2 Optimization problems in 3D printing

There are two common problems in 3D printing, the performance prediction and performance optimization. In practice, both of these problems can be modeled as mathematical optimization problems and can be solved by any appropriate optimization algorithms. For instance

the genetic algorithm (GA)[34], particle swarm optimization(PSO)[35], Taguchi's method[36], and Bayesian optimization[37] were used in some of the applications in the following sections.

The typical optimization problem has the following form[38]

$$\begin{array}{lll} minimize & f_0(x) & \\ subject\ to & f_i(x) \leq 0, & i = 1, \dots, m \\ & h_j(x) = 0, & j = 1, \dots, p \end{array} \tag{1.1}$$

Such a problem aims to find an x that minimizes the objective function f_0, while satisfying the inequality constraints $f_i(x) \leq 0, i = 1, \dots, m$ and the equality constraints $h_j(x) = 0, j = 1, \dots, p$. The constraints are normally subject to the specific problem setup in the actual problems.

For 3D printing performance optimization, the problem is either to maximize or minimize certain output performance by finding the optimal optimization variable x, or to reach a designated performance goal T. The x here can be any controllable factors that effect the 3D printing performance. For the case of maximizing or minimizing the performance, the objective f_0 simply represents the 3D printing process g_0 or the negative of it. For the case of reaching a designated performance T, the objective is then $f_0(x) = D(g_0(x), T)$ where $D(*,*)$ is a measure of difference between two variables.

For 3D printing performance prediction, the goal will be to find a function that mimics the 3D printing process. In this case, the optimization variable can be an arbitrary function, but in practice, we usually predetermine a parametric function $g(*; x)$ with optimization variable x being the function parameters. The objective function in this case would be $f_0(x) = D\big(g(a_k; x), g_0(a_k)\big), k = 1, \dots, n$, where a_k represents the point from the 3D printer input space. Since we usually have limited access with the 3D printer, we are expecting n to be a finite number. Such optimization problem can be formulated as shown below.

$$\begin{array}{lll} minimize & D\big(g(a_k;x), g_0(a_k)\big), & k = 1, \dots, n \\ subject\ to & f_i(x) \le 0, & i = 1, \dots, m \\ & h_j(x) = 0, & j = 1, \dots, p \end{array} \tag{1.2}$$

For all these problems, the constraints functions are normally induced from the system physical limitations. On the other hand, the preemptive knowledge of the distinctions about the data can also be injected into the optimization formula in the form of regularizers, which works as soft constraints. For example, the nature of a 3D object in voxel representation is generally sparse in the voxel and gradient domain, so a sparsity and total variation [39] term can be added to the objective. Moreover, a partial cycle-consistent regularizer can also be applied in some problems, which has been demonstrated by You et al.[40].

1.3 Machine Learning

Machine learning (ML) [17–21] is a powerful subset of the artificial intelligence domain, and is a technique enjoying quick growth and usage in many fields in recent years. Generally speaking, ML algorithms extract patterns from raw dataset and predict the unseen data distribution from the extracted patterns. ML algorithm normally constructs a parametric model that can represent the data distribution and fit the model to the given training dataset. Learning, or training, of the model involves iteratively optimizing model parameters according to an objective function defined by the model and the task. Unlike traditional data analyzing tools that preprogrammed some physical rules with human knowledge, ML assumes a generic model that has the potential to represent all different kinds of rules and allows the algorithm to learn the rules from the dataset without explicit human programming. The properties of ML allow many advantages compared to conventional data analysis algorithms: first, a given ML algorithm does not need human operators to explicitly define a task-specific model, and instead learns to achieve the task from the training

data with a simple generic model and objective function, which enables ML to complete tasks that are hard to explicitly define the underlying physics, like many computer vision tasks[23,24]. Second, ML can learn highly complex and non-linear models from data alone, a task that data analysts may find challenging to specifically program for, especially for data sets of high-dimensionality. Furthermore, while the training of a ML algorithm takes time, its ability to infer results is often very fast, thus enabling the ability to conduct analysis in real-time. ML algorithms can be loosely divided into three main types: supervised learning[41,42], unsupervised learning[43], and reinforcement learning(RL)[44,45]; with subtypes such as semi-supervised learning[46] and weakly-supervised learning[47] beginning to emerge in recent years.

Supervised learning[41,42] assumes that each input comes with a label, or desired output, and the ML algorithm simply learns the relation between the inputs and their corresponding labels. After training, the supervised learning algorithm will infer proper labels for unseen inputs. The supervised learning algorithms can be further categorized into classification and regression algorithms. Classification algorithms are for tasks with a discrete set of all possible outputs, and regression algorithms are used when the possible outputs include all values within a continuous value range. A popular supervised learning algorithm in recent times is the artificial neural network (NN) and its various extensions, such as the convolutional neural network (CNN) and the recurrent neural network (RNN). Supervised learning is widely used for tasks that can clearly define the desired output, and thus is suitable for most tasks in 3D printing.

Unsupervised learning[43] does not require any label or output from the training data, but instead learns the correlation and distribution of the unlabeled input data. The most common unsupervised learning algorithm is clustering analysis, which finds multiple data centers and groups data points according to those centers, therefore discovering the proper grouping and all

group-associated properties for any new data point. Since the un-labeled data usually does not represent a specific physical process, unsupervised learning is often only used for feature extraction or dimension reduction but not for the detection or optimization type of tasks in 3D printing.

Besides the supervised and unsupervised ML, there are also subtypes in between, such as semi-supervised learning[46] and weakly-supervised learning[47]. Semi-supervised learning makes use of the un-labeled data to support the training of supervised learning where labels are usually hard to obtain. However, semi-supervised learning requires more specific model design with the task and does not guarantee a performance improvement compare to supervised learning. Due to this performance inconsistency and the difficulty associated with implementing it, we have observed no applications of semi-supervised learning on 3D printing. A similar situation applies to weakly-supervised learning, which learns from data with incomplete labels.

Reinforcement learning[44,45] trains a software agent to select the best actions in an environment to maximize the cumulated reward signal coming from the environment. In a common setup, the agent can execute actions to interact with the environment and get rewards for each action and resulting state. Compare to supervised learning, reinforcement learning does not learn from labeled data pairs, but instead learns from exploring actions, states and the cumulation of rewards. The reinforcement learning is often used for sequences of decision-making problems, modeled as Markov decision processes, that involve rapid interaction with complex environments, such as autonomous driving, robotic controls, and games. As 3D printing relies on the initial input parameters instead of a sequence of inputs during the process, it is often trivial to apply reinforcement learning instead of other ML algorithms. However, reinforcement learning is still a good tool to use in cases such as in-situ control adjustments for 3D printing.

On top of these categories, there is a special ML technique, deep learning[17,48,49], that makes use of the artificial neural networks, recently achieved great success on many applications among all three ML categories. The deep learning is about cascading multiple layers of the simple building block, a perceptron composed of vector dot products and a non-linear activation function, and therefore forming a deep graph of parametric model. Such model is then called the artificial neural network, also known as the deep neural network. In this context, we will simplify the artificial neural networks as neural networks or NNs. Since the NNs could model arbitrary functions[50], we can apply NN to model the parametric function $g(*;x)$ in formula (2). The current standard method for training the NNs is the backpropagation method, which is basically gradient descent method with chain rule that allows accessible gradient calculation for each layer of NN thanks to the hierarchical structure of the NN. One issue of NN training, just like any gradient descent method, is that the result may fall into local minima. The local minimum issue is often compensated by applying stochastic gradient descent method to promote broader exploration on the input space, and by involving momentum at the weight updating step. Besides, global minimum is not always desirable for NN. Study shows that for deep learning, a global minimum for a large network means that the NN model is likely overfitting the training data[51]. Overfitting is another big issue of NN training. Unlike common optimization methods that aim to fit a model to the given data, ML tries to fit the model to some unknown data distribution with comparatively small training data sampled from that distribution, which requires the model to be able to generalize to unseen data. There are several ways to improve the generalizability of a NN. One common way is to preserve some verification data out of the training data, and early terminate the training when the error of verification data starts to increase during the training process. There are also ways like adding specific regularizers or averaging multiple NNs. If we want to look for

solutions aside from the algorithm, the essential solution is to increase the quantity and quality of the data samples. More discussions on improving the NN training for 3D printing problems can be found in Section 1.7.

1.4 Machine Learning Applications in 3D Printing

1.4.1 ML used in 3DP for high performance manufacturing

As a manufacturing technique, 3D printing has its own production flow. The key factors that are often controlled or monitored in 3DP are print part design, input parameters, in-situ process condition, and final printed product. We will explain previous research on performance prediction and optimization of key factors with the help of ML algorithms. Performance in this context refers to such factors as product quality, product properties, operation speed, and energy consumption.

The following subsections will discuss the performance prediction and optimization problems based on three different types of factors: 1) part design, 2) tunable parameters, 3) in-situ process condition.

1.4.1.1 Performance prediction and optimization by ML assisted part design

Design for Additive Manufacturing (DfAM)[52] is a study concerning the performance properties which could be affected by the design of the part that will be 3D printed. The part design we focus in this section mainly includes the geometric design of the 2D slices or 3D print structures and the design of the supporting structures. The following applications consider the time, energy cost, and the printed part quality as the resulting performance properties of the part design.

The topology optimization (TO)[53,54] is a common way of solving the DfAM problems. However, the TO often solve the DfAM problem by applying some iterative optimization method with finite element analysis (FEA), which does not involve ML in a typical sense. Therefore, we will not go into details of TO. The major difference between TO and ML in DfAM is that the ML approach usually uses a ML method to learn the system behavior instead of using the FEA or FEM. This use of ML allows significantly faster forward processing of the learned or simulated system behavior, and therefore also speeding up the optimization steps.

The most common performance issue is the printed part deformation or dimension deviation, meaning the printed part differs from the designed shape, which may be caused by various reasons depending on the 3DP technology used. Noriega et al.[55] used NN to predict the manufactured part dimensions from the computer-aided design (CAD), and Nelder-Mead method was used together with NN to optimize the dimension accuracy of printed parts for fused deposition modeling (FDM). Huang et al.[56] proposed a physical based mathematical model for the shape deviation effect of stereolithography (SLA). They used maximum likelihood estimation (MLE) to fit the physical model to data, and therefore can predict the shape deviation from any design shape. However, the physical model can only work for specific 3D shapes, and a more complex physical model is required for arbitrary shapes. Xiong's group[57,58] used a 3D U-net based CNN model to learn the transformation from 3D voxel design to the deformed printed 3D shape as well as the inverse for digital light processing (DLP)-based 3D printing. Therefore, the model can directly compute the proper 3D design to counter the deformation effect. You et al.[40] investigated the light scattering effect of ink material in DLP-based 3D printing. They applied U-Net based CNN to mitigate the scattering by optimizing the input layer-wise design. They designed

a master-slave two-NN algorithm to make use of the partially cycle-consistent property of the 3D printing system, and showed improvement compared to the single network design.

The Thermal deformation effect can also affect the fabrication fidelity in 3DP. Chowdhury and Anand[59] used two layer NN to learn the inverse relation between the CAD design surface coordinates and the corresponding coordinates after thermal deformation effects during the powder bed fusion (PBF) printing process. This allows them to directly compute the deformation-compensated design for any target part. Their team also extended the thermal deformation compensation into a two-step optimization methodology, where the other step finds the optimal build orientation for a maximum score combining eight design parameters with a global search algorithm[60].

The mechanical properties of the printed part are also commonly monitored performance indicators. Koeppe et al.[61] applied long short term memory (LSTM) recurrent neural network (RNN) to predict maximum stresses for the lattice cell structure based on different design parameters for FDM. Khadilkar et al.[62] developed a two-stream NN consists of CNN and PointNet to predict the stress distribution on each cured layer for SLA based on the slices of layer design trained with the data from finite element simulation. The predicted stress distribution can be further used to optimize the print orientation for minimum inter-layer stresses. Fan et al.[63] used a two-layer NN to predict a special structure's mechanical properties for direct ink writing (DIW) 3D printing according to four geometric parameters of the chosen structure.

Researchers are also concerned with energy consumption, usually in energy-delivery based 3DP methods. Yang et al.[64] investigated power consumption in DLP for different layer-wise geometry using three ML techniques and two feature extractors. According to their result, the NN with principal component analysis (PCA) has the best overall performance, and the stacked

autoencoder (AE) has the best testing performance. Qin et al.[65] developed a NN-based approach to predict energy consumption in selective laser sintering (SLS), using the design relevant data. They proposed a deep learning driven PSO that makes use of the prediction NN weights to enhance the PSO performance and used this special PSO to optimize design parameters for minimum energy cost. Another work from Qin's team[66] included not only the design data but also process, material, and in-situ monitoring data to do the energy consumption prediction for SLS. They applied IoT technology to sense and collect the multi-source data. All the different data are separated into two levelled datasets based on the frequency of these data being collected. The data like process parameter settings keep constant for each build, and is therefore classified into the build-level dataset. The data like work environment and material condition may change very often during each printing process, and these kinds of data, requires data collection once or several times per layer, are considered layer-level. The authors used clustering to unify the size of different layer-level data, and they designed a merged NN to combine the layer-level data with build level data as input to the NN. The authors proved that their hybrid method combining IoT, clustering and deep learning outperforms some other ML algorithms, namely linear regression, k-nearest neighbors, and decision tree.

Support structure design often aims to use as little support as possible to achieve a successful main structure print. Huang et al.[67] developed a CNN to predict whether a local surface element, which is represented by a special local topological representation, needs support structure or can be self-supported. This method is proved to best previous support detection methods and could help with better support generation for various 3DP technologies.

4D printing is a subfield of 3D printing focusing on creating an active or environmentally responsive 3D printed part. The design of such printable active parts is intuitively more complex

than the normal DfAM, and researches are recently exploring the use of ML and other optimization algorithms for such design problems. Hamel et al.[68] applied gradient-free evolutionary algorithms (EAs) with finite element method (FEM) to find the desired designs of active composite structures aiming to achieve certain degree of shape shifting upon heating the printed beam structure. Similarly, Wu et al.[69] used EAs with FEM on designing the magnetization of hard-magnetic soft active materials with DIW printing. They encoded the material design into a voxel form to represent magnetic density and direction distributions during the printing. Using this method, the authors can produce active soft magnetic part with desirable complicated shape morphing ability.

There is also research concerning multiple performance parameters at once. McComb et al.[70] trained an NN Autoencoder to learn the feature representation of voxelated 3D designs, and they re-used the encoder part of autoencoder to build a new NN and further trained it to predict printed part mass, required support material mass, and build time. Caiazzo and Caggiano[71] explored the use of NN on prediction and optimization of the laser power, scanning speed and powder feeding rate in laser metal deposition (LMD) based on geometric parameters.

1.4.1.2 Performance prediction and optimization by ML assisted parameters tuning

The tunable parameters in 3DP include process parameters, material related parameters, and environment parameters. Different 3D printing technologies usually have different process parameters and different available materials.

Dimensional accuracy is considered a critical performance parameter. The intuitive method of measuring the dimensional accuracy is to compare the whole or a part of the printed product

with the initially-designed dimensional data. Sood's team[72,73] explored the prediction and optimization of part dimensional accuracy for FDM, in terms of four dimensional parameters, with five process parameters using NN, fuzzy inference system and grey-Taguchi optimization method. Chen et al.[74] invented a new method of 3D printing spatial wireframes, which uses a NN-based approach to predict the quality of the printed curve based on input process parameters, as well as predicting the proper parameter set to achieve a selected curve. For the authors' case, fully connected NN performs better than CNN and LSTM. Conev et al.[75] investigated the use of random forest method for predicting the printing quality of porous polymer scaffolds printed with extrusion-based 3DP. Zohdi[76] had developed a sophisticated kinematic and dynamic model for the robotic arm controlled material extrusion additive manufacturing system, and used GA to optimize control parameters for the best match of extruded filament structure following the author's own series of works. This method showcased a typical way of predicting the performance of 3D printing by constructing a mathematical model that describes the physical 3DP system. Compared to the ML approach, this method has the benefit of constructing a precise model, but with the cost of a comprehensive human analysis of the system dynamics. Jiang et al.[77] applied NN and GA on biological 3D printing forming process to predict and optimize the printed bone scaffold quality. Lee et al.[78] trained a NN to predict the dimensional errors for SLA using layer thickness, hatch over-cure, and hatch spacing. He et al.[79] explored various ML algorithms to predict the success or failure of the printed surface quality for continuous liquid interface production using nine parameters and optimize printing speed for good surface quality. They found that Siamese NN works the best among the ML algorithms they tried.

The dimensional accuracy can also be represented or interpreted from some indirect measures. Sood et al. [80,81] used NN and quantum-behaved PSO to predict and maximize part

compress stress as well as minimizing part sliding wear, which could indicate the print quality, for FDM. Zhang et al.[82] used NN to predict the powder spread speed and layer roughness for PBF, considered as quality indicators, according to the spreader translational and rotational speed. Wang et al.[83] predicted and minimized shrinkage ratio using NN and GA for SLS. Chen and Zhao[84] explored the use of NN in binder jetting to predict shrinkage rate and surface roughness based on four process parameters. The authors also developed a workflow for choosing parameters based on NN and a mathematical model for print time estimation. Li et al.[85] used NN to predict the offset distance of weld beads for wire and arc AM, and developed a reasoning algorithm to minimize the offset. Aoyagi et al.[86] applied support vector machine(SVM) to predict good quality prints in terms of low pore density for electron beam melting, and found the parameter window with minimum defects using process maps of each pairs of process parameters. Menon et al.[87] used hierarchical ML to predict and optimize for print score for freeform reversible embedding, which is calculated from layer fusion, stringiness, and infill, using six process and material parameters. Mozaffar et al.[88] used various process parameters and a few specific geometric size and shapes to predict the thermal history of printing process for direct energy deposition(DED) 3DP using gated recurrent unit(GRU)-based RNN. Ren et al.[89] also developed a RNN and NN combined network to predict thermal history of different laser scanning patterns for laser aided additive manufacturing. The part density is also important in SLS. Shen et al.[90] applied NN to predict part density with four process parameters. Wang et al.[91] built a similar application to predict part density with three more process and environment parameters.

In terms of the products' mechanical properties, Malviya and Desai[92] used two-layer NN to learn the relation between build orientation and printed part strength and used Bayesian optimization to find the optimal build orientation for maximum part strength in FDM. Yadav et

al.[93] used NN and hybrid GA-NN tool to predict and maximize tensile strength using input parameters. Wang et al.[94] looked at tensile strength prediction for SLS using NN with seven process parameters.

In terms of energy consumption, Chen et al.[95] used regularized backpropagation NN to predict equipment energy consumption for FDM from process parameters.

Build time is also a useful performance parameter. Munguía et al.[96] focused on build time prediction for SLS using NN with four different process parameters.

1.4.1.3 In-situ/In-process performance analysis and control

Other than predicting the performance from the design or input parameters, monitoring and analyzing the performance during the actual printing process will often give more precise information than predicted ones. The critical part here is the analysis of the monitored information, as analyzation normally requires human expert knowledge, which means that the analyzation speed is limited, and the quality is inconsistent among different operators. In this scenario, ML is a useful tool, as the ML algorithm can learn expert knowledge from expertly labeled data, and any analyzation thereafter would require no human in the loop and would be consistent.

The quality analysis of in-situ 3DP system conditions often result in a classification of defect or quality levels. Wu et al.[97] applied naive Bayes classifier and J48 decision trees for infill defect detection for FDM based on extracted features from layer images during a printing process. Delli and Chang[98] built a similar defect detector with top view image extracted features, and they used SVM as the classification tool. Jin et al.[99] also investigated quality classification with layer images. However, they classified the quality into four levels, and instead of classifying the extracted image features, they used CNN to directly classify the images into three quality

conditions. They also developed an automated flow rate correction method based on quality prediction through a feedback loop. When the quality prediction is over- or under-extrusion, their feedback system will automatically correct the printing parameters to compensate for the error and refine the printing result of the next time step. The same team[100] built another CNN to predict the nozzle offset level according to on-line nozzle head image. The nozzle offset here is an indirect indicator for the in-situ system defect level. They applied transfer learning, which took a pretrained ResNet model and customized the two finishing layers and only did additional training on these two layers. Transfer learning allows better performance with less data.

Caggiano et al.[101] built an on-line defect classifier with a bi-stream CNN for selective laser melting(SLM), that analyzes both laser scanning images and powder recoating images, and proved that it is more accurate than using SVM with visual word or histogram of oriented gradients (HoG) feature extractor. Wasmer et al.[102,103] built a system to collect acoustic signatures from the part during the SLM printing process and developed a CNN to analyze the acoustic feature for printed part quality classification. The quality was classified into three levels. The authors also extended the work on using encoded acoustic features on PBF quality monitoring and classification[104], their following work also applied RL instead of CNN[105]. Zhang et al.[106] also conducted a quality level prediction with SVM and CNN according to process images for PBF.

Scime and Beuth[107–109] have done a series of work using ML techniques to apply in-situ quality classification for laser powder bed fusion (L-PBF). In [107], they used a composition of filter bank to extract the features from the powder bed images and used bag-of-words to learn the powder bed anomaly classification. In [108], they used the AlexNet CNN and transfer learning to directly learn the anomaly classification from the powder bed images. In [109], they used scale

invariant feature transform (SIFT) and histogram of oriented gradients (HOG) to extract feature from the melt pool images and used multi-class SVM for defect classification. The melt pool quality is directly linked to the quality of L-PBF printing. Similarly, Yang et al.[110] analyzed melt pool image directly using CNN, and concluded into four melt pool quality categories. Imani et al.[111] used CNN for flaw detection on layer-wise spatial characterization images. The spatial patterns were characterized from the subregion region of interest (ROI), which were extracted according to the CAD design and delineated into unique regions with the same size and in multiple scales. For Arc Welding based AM, Tang et al.[112] applied CNN and SVM to predict welding beads status, which directly affects the printing quality, using the surface images during printing. Gonzalez-Val et al.[113] developed a CNN based modular system called ConvLBM for real-time dilution estimation and feedback control in LMD, and defect detection in laser welding processes. Wang et al.[114] considered the system voltage level as the quality factor for liquid metal jet printing (LMJP). They trained a NN to predict the voltage change according to the extracted features from droplet frozen and dynamic images.

Some works showed the quality analysis by enhancing the monitored system condition instead of directly computing quality levels. This allows easier and better human interpretation of the in-situ system condition. Patel et al.[115] applied Yolo v3, which is a CNN based object detector, on layer images to detect bounding boxes of impurity or dross in L-PBF. Williams et al.[116] applied Spatially Resolved Acoustic Spectroscopy (SRAS) for in-process monitoring of the production-scale L-PBF system and used CNN to enhance the acoustic signature to an optical micrograph level quality image, therefore allowing easier in-process defect analyzation.

Aside from analyzing the intermediate printing quality, the in-situ condition can be used to predict the final completed part quality as well. For laser-based AM, Francis and Bian[117] used

both CNN to analyze the thermal images and NN to analyze process and material parameters, and together were able to predict pointwise distortion of the printed part. Zhang et al.[118] used CNN to detect the porosity occurrence and predict the local volume porosity for direct laser deposition according to melt pool images.

In-situ monitored system conditions can also be used to predict the mechanical properties of the final printed part. Zhang et al.[119] considered the thermal history as input and used LSTM to predict tensile strength of the final product for FDM. Later, they combined the process parameters and material properties together with the LSTM extracted thermal data, and together better predicted the tensile strength[120].

1.4.2 ML used in 3DP for fast design turnaround

For material and structural design, designers traditionally would propose designs based on mathematical simulations, which normally require long time scales. It is desirable to have ML to quickly predict the quality or property of the design to replace the simulators, and even to directly build a ML system to suggest designs instead of human designers. As 3D printing facilitates an effective way to quickly prototype and validate designed materials or structure properties, the combination of ML and 3D printing can greatly accelerate the design process.

Gu's group[121–123] investigated composite design as well as auxetic metamaterial design with ML and validated the designs with 3D printing. Their team encoded the composite designs as a data matrix of unit cell basic structures and explores the relation between the different arrangements of unit cells and the resulting mechanical properties. The ground truth mechanical properties in the training data are calculated by finite element modeling. After they trained a CNN to predict the mechanical property of any of their structures, they applied a self-learning-based

sampling method to explore the structure space and find the ones with high performance. Similarly in their auxetic material design, they chose their unit cell to be a simple reentrant honeycomb structure with tunable Poisson's ratio. Therefore, by combining the unit cells, the resulting structure will have different local auxetic property. Bonfanti et al.[124] demonstrated the use of RL for automatic design of mechanical metamaterial actuator, and 3D printed the design for verification with FDM. Tak et al.[125] 3D printed W-band slotted waveguide array antenna and applied NN to optimize the process parameters. Calik et al.[126] built a CNN to predict the capacitive feed antenna performance measures with geometrical design parameters and used the CNN to help antenna design. The design is then justified with 3D printing. Wolfe et al.[127] applied RNN and novelty search to help design gear mechanisms and 3D printed the design for validation. Duchanoy et al.[128] used NN facilitate the design of magnetorheological dampers by predicting hysteretic response from the damper parameters. 3D printing was used to build a damper component. Miao et al.[129] used CNN for segmentation of vertebral bodies and detection of spinal neoplasm lesion and built a GAN for recovering the defective spinal images. Therefore, allowing reconstruction of a complete spinal 3D model that can be 3D printed. Topology optimization is another intelligent approach to a more informed structural design of a 3D object that can withstand specified loads and constraints[130–132]. Deng et al.[133] showed a deep learning approach to topology optimization that can design objects with smooth boundaries which can be used for 3D manufacturing.

1.4.3 Special uses of ML with 3DP

There are other applications of ML and 3D printing concerning domains other than manufacturing and design. One interesting approach is to 3D print devices that can operate

machine learning algorithms physically. Ozcan's team[134,135] proposed an all-optical machine learning system, which is a specifically designed and 3D printed optical device that can implement diffractive deep NN. The optical device can essentially operate as a CNN and can solve computer vision tasks physically. The physical system implies that the system is operating at the speed of light once built, although each device can only work for one specifically designed task.

The security issue and potential negative social impact of 3DP technology have also caused public concerns. With a 3D printer, theoretically any dangerous parts can be made in-house to bypass administration. For example, firearms can be 3D printed without the knowledge of weapon manufacturing. In terms of the security of 3D printing, researchers were developing tools to identify potentially dangerous printable 3D designs. Li et al.[136] developed a classifier with CNN to classify 2D images converted from 3D printable models into 10 object classes. They were specifically concerning the gun object class for the security of 3D printable objects. Pham et al.[137] further explored the detection of weapons, including firearms and knifes, using CNN from D2 vectors extracted from 3D printable object design.

Table 1.1. Summary of machine learning applications in 3D printing.

	Goal	3D Printing Technology	ML and Optimization Algorithms	Reference
Performance prediction and optimization by ML assisted part design	Dimension accuracy	FDM	NN, Nelder-Mead	[55]
		SLA	MLE	[56]
		DLP	CNN, U-Net	[57]
		DLP	CNN, U-Net	[58]
		DLP	CNN, U-Net	[40]
		PBF	NN	[59]
		PBF	NN	[60]
	Mechanical properties	FDM	NN, LSTM	[61]
		SLA	CNN, PointNet	[62]
		DIW	NN	[63]

Table 1.1. Summary of machine learning applications in 3D printing. (Continued)

	Energy consumption	SLA	PCA, NN, stacked AE	[64]
		SLS	NN, PSO	[65]
		SLS	NN	[66]
	Support requirement	Unspecified	CNN	[67]
	4D printing / Part active response	Unspecified	EA	[68]
		DIW	EA	[69]
	Multiple parameters	Unspecified	AE	[70]
		LMD	NN	[71]
Performance prediction and optimization by ML assisted parameters tuning	Dimension accuracy	FDM	NN, grey-Taguchi	[72]
		FDM	Fuzzy inference, grey-Taguchi	[73]
		FDM	NN, CNN, LSTM	[74]
		Extrusion-based 3DP	Random forest	[75]
		Rapid free-form printing	GA	[76]
		biological 3DP	NN, GA	[77]
		SLA	NN	[78]
		CLIP	Various	[79]
	Dimension accuracy (indirect)	FDM	NN, quantum-PSO	[80]
		FDM	NN, quantum-PSO	[81]
		DED	RNN, GRU	[88]
		Laser aided AM	RNN, DNN	[89]
		PBF	NN	[82]
		SLS	NN	[90]
		SLS	NN	[91]
		SLS	NN, GA	[83]
		Binder jetting	NN	[84]
		Wire and arc AM	NN	[85]
		Electron beam melting	SVM	[86]

Table 1.1. Summary of machine learning applications in 3D printing. (Continued)

		Freeform reversible embedding	Hierarchical ML	[87]
	Mechanical properties	FDM	NN, Bayesian optimization	[92]
		FDM	NN, GA	[93]
		SLS	NN	[94]
	Energy consumption	FDM	NN	[95]
	Build time	SLS	NN	[96]
In-situ/In-process performance analysis and control	In-situ part defect/quality	FDM	Naïve Bayes, Decision tree	[97]
		FDM	SVM	[98]
		FDM	CNN	[99]
		FDM	ResNet	[100]
		Arc welding based AM	CNN, SVM	[112]
		SLM	CNN	[101]
		SLM	CNN	[102]
		SLM	CNN	[103]
		PBF	CNN	[104]
		PBF	RL	[105]
		PBF	SVM, CNN	[106]
		L-PBF	Bag of words	[107]
		L-PBF	CNN	[108]
		L-PBF	SVM	[109]
		L-PBF	CNN	[110]
		L-PBF	CNN	[111]
		LMD	CNN	[113]
		LMJP	NN	[114]
	Monitoring quality	L-PBF	Yolo v3	[115]
		L-PBF	CNN	[116]
	Completed part quality	Laser-based AM	NN, CNN	[117]
		Direct laser deposition	CNN	[118]
	Mechanical properties	FDM	LSTM	[119]
		FDM	NN, LSTM	[120]
ML used in 3DP for fast design turnaround	Composite material	FDM	CNN	[121,122]
	Auxetic material	FDM	CNN	[123]
	Mechanical actuator	FDM	RL, NN	[124]
	Antenna	SLA	NN	[125]

Table 1.1. Summary of machine learning applications in 3D printing. (Continued)

	Antenna	FDM	CNN	[126]
	Gear mechanism	FDM	RNN, Novelty Search	[127]
	Damper	FDM	NN	[128]
	Spinal model	Unspecified	CNN, GAN	[129]
	Arbitrary	Unspecified	NN	[133]
Special uses of ML with 3DP	3D print optical NN device	PolyJet	diffractive deep NN	[134,135]
	3D printable object classification	Unspecified	CNN	[136]
	Anti-weapon detection for safe 3DP	Unspecified	CNN	[137]

1.5 Summary and future perspective

Research has shown that ML is a powerful tool to assist 3DP in terms of improving printing quality, modifying print part property, improving in-situ monitoring, and fast designing of 3D printable engineering products. The interplay of these two rapidly growing technologies have great potential in achieving intelligent manufacturing. With more and more smart applications with these two technologies, we will be able to achieve a fully automated 3DP with no need for human expert to adjust the parameters of the 3DP. At the same time, we will have ML applications to replace expert designers which can automatically design any 3D printable parts according to our needs. Together, we can foresee a smart manufacturing system that is capable of ML-assisted designing, and fast and accurate ML-assisted 3DP manufacturing with ML powered monitoring and quality control.

However, there are still unsolved issues and challenges associated with these emerging technologies during their integration. We will discuss the challenges and issues as well as the potential solutions from both the 3DP and ML perspectives.

1.6 3D printing challenges

We have already explored many challenges of 3D printing in Section 1.4.1 and showed that ML can be an excellent solution to many of them. Here we will summarize these challenges and describe whether they are solved by ML or if there is a potential ML-based solution that can be explored.

1.6.1 Geometric data representation

The design for 3D printing with ML is described and demonstrated in Section 1.4.1.1. The examples showed that ML, especially the recent advances of CNN based computer vision techniques, indeed produced promising results on the design of shapes and supporting structures. Unlike traditional designs that only adjust a few parameters of certain geometries, CNN avoids the extra feature extraction step and demonstrated direct analysis and generation of the extremely flexible pixel images of layer design as well as the voxel graphs of volumetric 3D design.

The challenge for CNN here is that the 3D volume in voxel format is very memory costly in computation which means the resolution of generated geometries are limited, for example in [57] the resolution is at most 64*64*64, and fine features disappear after discretization. The trivial solution to this problem is to wait for more powerful computation hardware, and the more applicable alternative solution is to choose 3D data representations that are less memory consuming than voxel format. The main 3D data formats include voxel data, point cloud, surface meshes, RGB-D image, multi-view images, spectral domain, and so on. Ahmed et al.[138] summarized the popular 3D representations and their applications in deep learning as well as their challenges. It is important for the future ML and 3D printing researches to explore more on 3D

representations and select the proper one that can better utilize ML technologies to reach the specific design goal.

1.6.2 Performance control

As described in Section 1.4, the major goals of 3D printing design and process parameter optimization as well as the in-situ control optimization are to reach certain desired product quality, product properties, operation speed, or energy cost. Among these goals, the quality control is most explored. The common quality indicator includes defect, shape deviation, dimension accuracy, surface roughness. There are also 3D printing technology specific quality indicators, like thermal history for DED, welding beads status for Arc welding base AM, nozzle head status for material extrusion type of AM, and melt pool status for PBF. In terms of product properties, the most explored ones are the mechanical properties. The applications in Section 1.4 demonstrated the advantage of using ML for detection, prediction as well as optimization of these performance parameters. The benefit of ML compared to the traditional physical based simulation is the high calculation speed and the ability to learn from real world data which has a better applicability to the physical system. The future trends on performance control are to further explore more product properties other than the mechanical property, and the quality control of multi-material printing and loaded material printing.

1.6.3 Hardware inconsistence issues

Through the advancing of 3D printing technologies, although experts are gradually trying to categorize the various ways of 3D printing in order to create a standard, there is a wide diversity to 3D printing methods. Such diversity is beneficial to exploring the usage of 3D printing, yet

variety often begets inconsistency. It not only causes difficulty to share printing setups between different 3D printers but also creates challenges for ML to have consistent printing quality. An ambitious solution would be to create a universal simulation tool that can convert machine specific control parameters in between each other printers while maintaining the same simulated result. A more gradual approach could be to standardize the parameter settings for printers of the same type, or at least a standard conversion rule among the same type of printers. This could be not only beneficial to 3D printing as a technology but create closer involvement of disparate ML research.

Aside from the issue of hardware differences between 3D printers, there may also be hardware inconsistency issues on any one given 3D printer. There are various ways that can cause error on printing with the same machine, such as physical collision or movement, and ink clogging. This kind of hardware issue can cause severe printing errors on small scale printing. Intuitively, this issue can be solved by ML like any other dimension error problems caused by the 3D printing process. However, the challenge is that the hardware condition could potentially change daily or even hourly, which means that any compensation or calibration mechanism will need to be updated frequently. One potential solution could be to use transfer learning to learn the correct calibration once and frequently update with data from new print jobs.

1.7 ML challenges

The ML's shortcoming on the 3D printing applications mainly comes from its data driven nature. We will discuss these challenges and the possible solutions.

1.7.1 Data availability

The fact that ML is data driven implies that ML is fully dependent on data to learn a system's behavior. Data availability becomes the essential bottleneck of ML application in 3D printing. The hardware compatibility problem described in Section 1.6.3 makes it difficult to get a lot of real prints. Considering that the common 3D printing with ML applications rely on labeled data to do supervised learning, this adds additional difficulty of satisfying labor requirements for labeling. Some labeling tasks, like recognizing defects from layer image, might even require decent knowledge of the 3D printing process, which makes it almost impossible to have rich real world labeled data for any 3D printing task. Therefore, most of the applications rely on synthetic data generated from a physical based simulation software that mimics the 3D printing behavior. This kind of simulators normally have the problem of being slow and cannot fully mimic all the real-world system condition. The benefit though is that it can produce as many data as the ML algorithm needs. However, the ML would only be able to learn to behave like the simulator, faster but not more accurate. In order to exceed simulator and behave more like an actual 3D printer, ML needs to learn from the actual printed and labeled data. To deal with the bias between the need for data and the lack of data, there are two obvious paths, which are increasing data and reducing the need for data.

One way to reduce the need for data is to use transfer learning[139]. Transfer learning is a technique that used a NN that was pretrained on a related-task and then do minimal further finetuning on the target task, therefore reducing the data needed. [100] and [108] demonstrated the use of transfer learning. Reducing needed data can also be achieved by improving the quality of data. The data with good quality means that each different data point contains good amount of new

information about the complete data distribution and of course the data need to be correct with as little error as possible.

The other direction is to increase the data availability. Recall from Section 1.6.3, we can potentially increase the data by building standards and encourage sharing data and even making a public large scale 3D printing dataset, like MNIST[140], ImageNet[141], and large scale datasets for 3D shapes[118]-[121]. Some efforts are already made on making such standard and dataset[142–147].

1.7.2 Generalization and overfitting

Machine learning learns the patterns of the given data and tries to generalize the pattern to other unseen data. Overfitting is a known issue for ML, that the model overfits the given data and as a result loses the generalizability to unseen data. The common fix to this problem is to designate a verification dataset separated from the training dataset, and use the verification data to verify the model's generalizability during the training process. Once the model starts to reduce performance on the verification data, the training process is immediately terminated. As a result, such trained model will normally generalize well on unseen data.

For 3DP with ML, the generalization issue is often caused by the lack of data. When there is little data to use, each data point will be essential to represent the overall patterns. Separating a verification set from the training data in this case will further reduce the already small amount of data used for training, and will result in a big quality drop of the trained ML model. Instead of defining a verification set, we can introduce some human expert knowledge here to manually set a termination condition before the model completely converges, in other word overfits, the train data. The ultimate solution is again to increase the data availability as discussed in the previous.

1.7.3 Parameter tuning

Recall that for the ML learning process, parameters are updated iteratively based on given training data. From this behavior, we can see that it is very difficult for human to make any manual parameter tuning for a trained ML system. This adds difficulty to the situation where minimal changes are made to the 3D printing process, and suddenly the previously working ML system no longer works for the new printing process, and the only solution is to obtain new data and retrain the ML system, which is obviously not ideal. One potential solution to make ML more tunable is to apply hierarchical ML[87,121], and incorporate some of the 3D printing expert knowledge into building the learning system, such that we can somehow manually make changes with respect to the physical printer change.

1.8 Research objectives

Although research has been applying machine learning on 3D printing technologies, there are still many directions underexplored. One important direction that needs more study is the machine learning applications on light-based bioprinting. The following chapters try to address two of the practical problems faced by light-based bioprinters.

One challenge is that the DLP-based 3D printing would have severed reduced printing resolution caused by light scattering effect induced by cells in any bio-fabrication tasks using cell-encapsulated printing material. When the cells in the material scatters light during the photopolymerization process, the dedicated exposure region would have reduced energy deposition while the surrounding regions would be overexposed unexpectedly.

Another challenge is the spatial modulation of the mechanical properties of 3D printed scaffolds. Previous studies have demonstrated the capability of globally adjusting the mechanical properties of material by adjusting the material compositions, which is time consuming and inflexible. Manipulating printing parameters and directly adjust local stiffness on-the-fly would be beneficial and remains less explored for light-based 3D printers.

In Chapter 2, a convolutional neural network-based machine learning algorithm has been developed to calculate an adjusted light distribution mask, which has been applied to the DLP 3D printer to compensate for the light scattering effect, so that the resulting printed structure would meet the initial design and having better resolution compared to using the traditional non-adjusted mask.

In Chapter 3, a custom two-photon polymerization (2PP) 3D printer is introduced to achieve micron resolution fabrication. Detailed fabrication techniques and application showcases are demonstrated.

In Chapter 4, a neural network-based machine learning algorithm is developed to search for proper printing parameters to achieve any arbitrary structure stiffness. The algorithm learns from experimental data and calculates the optimal printing parameter combinations to achieve a given stiffness for DLP 3D printer and 2PP 3D printer. This algorithm allows precise spatial stiffness modulation on both micro and macro structures fabricated with DLP and 2PP 3D printers.

Chapter 5 summarizes the work in this dissertation and discusses the future perspectives of machine learning and intelligent bioprinting.

Acknowledgement

Chapter 1 introduction contains unpublished material coauthored with S. You, J. Alido, H. H. Hwang, S. Chen. The dissertation author was the primary author of this work.

CHAPTER 2 Compensating Cell-induced Scattering Effect Using Deep Learning

Abstract

Digital light processing (DLP)-based 3D printing technology has the advantages of high speed and high precision comparing with other 3D printing technologies like extrusion-based 3D printing. Therefore, it is a promising biomaterial fabrication technique for tissue engineering and regenerative medicine. When printing cell-laden biomaterials, one challenge of DLP-based bioprinting is the light scattering effect of the cells in the bioink, and therefore induce unpredictable effects on the photopolymerization process. In consequence, the DLP-based bioprinting requires extra trial-and-error efforts for parameters optimization for each specific printable structure to compensate the scattering effects induced by cells, which is often difficult and time-consuming for a machine operator. Such trial-and-error style optimization for each different structure is also very wasteful for those expensive biomaterials and cells. Here, we use machine learning to learn from a few trial sample printings and automatically provide printer the optimal parameters to compensate the cell-induced scattering effects. We employ a deep learning method with a learning-based data augmentation which only requires a small amount of training data. After learning from the data, the algorithm can automatically generate the printer parameters to compensate the scattering effects. Our method shows strong improvement in the intra-layer printing resolution for bioprinting, which can be further extended to solve the light scattering problems in multilayer 3D bioprinting processes.

Significance Statement

This work applies a deep learning method with learning-based data augmentation to improve printing fidelity in Digital Light Processing (DLP)-based 3D bioprinting using cell-loaded biomaterials, where cell-induced light scattering tends to decelerate the printing quality. The deep learning algorithm is able to learn the scattering behavior of the bioink and automatically generate a digital mask to compensate this light scattering effect. The learning-based data augmentation method is shown to greatly reduce the required sample prints. Experimental results show that the printing fidelity has been significantly improved through machine learning.

Keywords

3D bioprinting; cell printing; digital light processing; machine learning; deep learning; neural network; genetic algorithm.

2.1 Introduction

Three-dimensional (3D) bioprinting is one of the most important tools for tissue engineering, drug development, and regenerative medicine, due to its excellent ability to build 3D biomimetic tissue constructs and promising potential for printing patient-specific 3D tissues or organs.[148–151] There have been many different bioprinting systems like extrusion-based, inkjet-based, and light-based[152–155]. Because light can be precisely manipulated to induce material polymerization and solidification in micro- and even nano-scale,[156–158] light-based systems have been the most promising method for high-resolution biofabrication. Among the different 3D printing methods, the digital light processing (DLP) 3D printing method, which uses a digital micromirror device (DMD) to control the light pattern and photopolymerize the entire

layer of the exposed region in the bioink, is getting more popular thanks to its fine resolution (a few micro meters) and high printing speed (a few seconds to a few minutes printing time) [154,155,159–162].

For 3D bioprinting, the printing solution (bioink) typically consists of the hydrogel prepolymer biomaterial, the photo-initiator, and the cells. The cells in the bioink will induce a strong scattering effect of the incident light during the photopolymerization process, which may disturb the light pattern and thus result in a undesired print [163,164]. Such scattering arises from refractive index mismatch between the cytoplasm and the external hydrogel environment[165,166], from the Mie scattering caused by the nucleus and organelle, and from the Rayleigh scattering caused by the macro-molecule.[167] The scattering effect will scatter light from the target location, causing reduced light exposure at target location while adding exposure to the surroundings. Therefore, the undesired surrounding location may be polymerized, and some target location may fail to polymerize due to the reduced light exposure (Fig. 2.3(a)).

There have been a few methods on improving the 3D printing fidelity to mitigate the scattering effect of the turbid bioink. Enhancing the material absorption by adding light absorbing species (e.g. food dye) is the most common practice to mitigate the scattering effects. [168,169] In more light-absorbing materials, light, including the scattered photons, will travel a shorter distance. However, the improvement on fabrication resolution is limited, and it also leads to a slower printing speed. A prolonged printing time can significantly reduce the cell viability. You et al. introduced a flashing photopolymerization technique to avoid the scattering effect caused by the hydrogel polymer, however, the scattering caused by cells cannot be resolved by this method[164]. Recently, machine learning algorithms were used to improve 3D printing fidelity by compensating

the scattering effect, which shows a promising approach to address this cell-induced scattering problem [163].

The machine learning algorithms and especially the deep learning algorithms, branching from machine learning based on the use of deep neural network (NN), have been demonstrated for applications in many different fields[170,171]. Machine learning in general is a computer algorithm that learns patterns or rules from the given data or from interacting with a responsive environment without any prior knowledge. The deep learning algorithm uses various NN models to more effectively extract and store information. Researchers have been applying machine learning algorithms to improve the dimensional accuracy in traditional 3D printing [172–175]. Machine learning has also been applied for 3D printing in-situ monitoring and correction [99,176]. In our previous work, NN-based deep learning method was introduced to learn the shape transformation between output structure and input design when using light scattering material for printing. Three hundred trial printings were printed on the actual 3D printer using the light scattering material, and the microscopic images of the printed structures together with their corresponding input digital masks were used to train the NN. The structure images were cropped and resized to match the location and resolution of the input masks. After training, to compensate the scattering effect, the NN was able to generate a digital mask that differs from the original designed pattern. Compare to the conventional method of using a mask that is identical to the designed pattern, using the NN generated mask helps the printer to print the pattern with higher fidelity[163].

While the previous work was applied on a photopolymer material mixed with glass microbeads mimicking a generic class of scattering payload in the printing materials, in this paper, we apply the deep learning method to cell-loaded bioprinting and show the capability of improving

bioprinting quality. We 3D print different structures using various predesigned digital masks, take microscopic images of the structures, and use the mask-structure image pairs as our data set to train the NNs. The trained algorithm can generate a deformed mask for any given target structure to compensate the scattering effect of the cell-loaded bioink. Furthermore, we further improve the previous deep learning method with an additional learning step, which learns parameters from a 3D printer simulator. This simulator serves as a data augmentation tool, which allows us to greatly reduce the required training samples by 10 folds. We show that using only 32 trial printings, which got augmented to 4000 data pairs, is sufficient to train our NN. This reduction of training data requirement is very significant in bioprinting due to the high cost of biomaterials and bioreagent (such as growth factor), limited supply of cells (such as stem cells and primary cells), and the long cell culture time (weeks of culture time).

After we compared our optimized prints guided by machine learning with the conventional printing result, we can see that our deep learning method can indeed improve the printing fidelity for the highly scattering cell-loaded material.

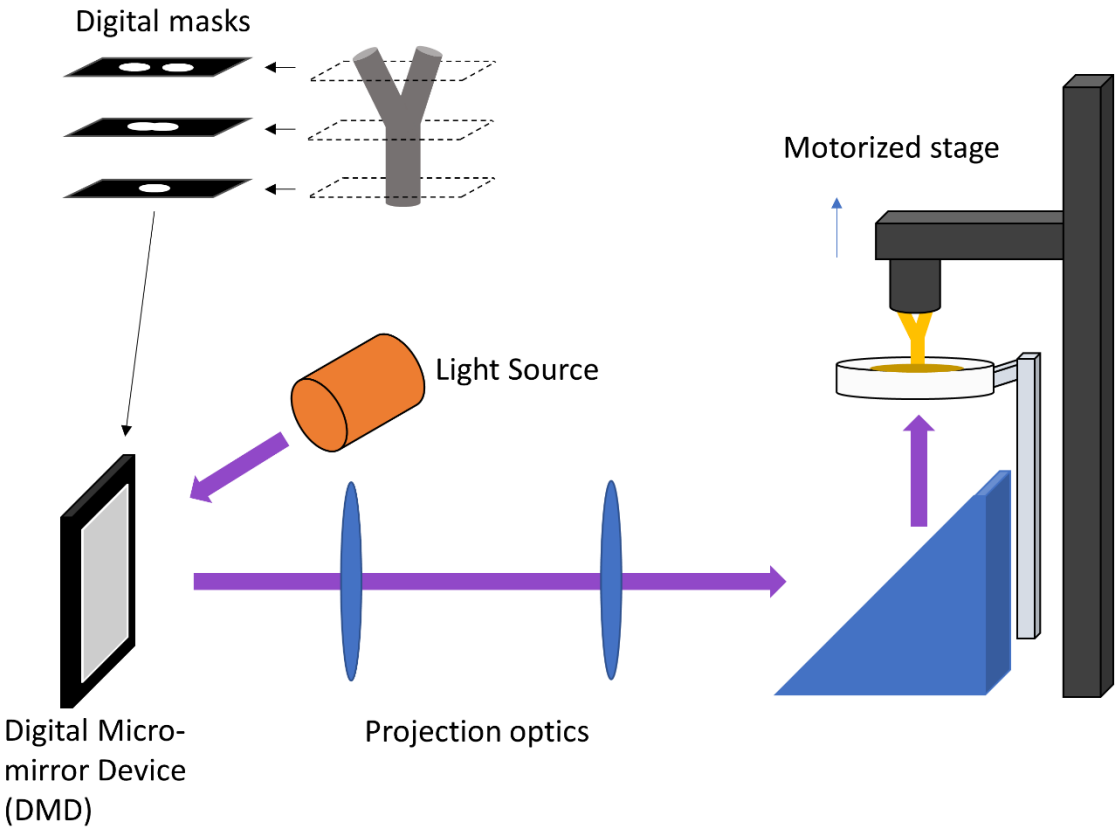

Fig. 2.1. Schematic of the DLP-based 3D bioprinting setup.

2.2 Methods

2.2.1 3D printing method

Our samples are printed with a custom DLP-based 3D printer (Fig. 2.1). A 385 nm wavelength light source first projects the light onto a DMD chip, which contains an array of 2560 by 1600 micro-mirrors. The on-off state of each individual micro-mirror is controlled by flipping the mirror angle, and a pattern will then appear on the micro mirror array. A grayscale pattern can be displayed by controlling the duty ration of the flipping of the mirrors. The patterned light reflected from the DMD is guided by a series of lenses and projects onto the holder with the prepolymer solution. Polymerization occurs at the exposed region, and a solid thin layer of the structure forms. The motorized stage then lifts the solidified structure, normally by tens or

hundreds of microns, and leaves space for the solution to refill and then start the next layer of printing. The process is repeated for all the cross sections of an object model in order to print a 3D object. Our study is focused on the printing process of an individual layer.

A computer software controls the light exposure on the target region. The software controls the light source power, the exposure duration, the DMD mirror array pattern, and local light exposure dose on each micro mirror. A digital mask with grayscale pixel values is used to represent the DMD pattern and the local exposure dose. In this study, the light source power and the exposure duration are set to be constant. We are only controlling a square region in the center of the DMD array, which is represented by a 512-by-512-pixel mask. The rest of the DMD array is set to a fixed state that is designed to localize the center region. In this setup, our 3D printing system can be abstracted as a nonlinear time-invariant system, where the input of the system is a 512x512 grayscale image representing the digital mask, and the output is a 512x512 binary image where 0 and 1 represent void and solid region, respectively (Fig. 2.3(a)). The size is chosen as multiples of 8 (a byte) for efficient CPU and GPU processing, and it is also chosen to not exceed our 8GB GPU memory during the NN training process.

Our prepolymer printing solution is composed of 5% (v/v) gelatin methacryloyl (GelMA) in phosphate-buffered saline (PBS) solution, 1% (w/v) lithium phenyl-2,4,6-trimethylbenzoylphosphinate (LAP) as the photoinitiator, and 10 million/mL C2C12 mouse myoblast cells as the scattering load. The source of our C2C12 cell line was purchased from American Type Culture Collection.

The 3D printed structures are imaged with a fluorescent microscope. Due to the transparent nature of the GelMA polymer, it is hard to detect the printed structures' contour under a bright field microscope. Hence, we apply fluorescent staining to the material in order to obtain high

quality images distinguishing the printed and unprinted part. We obtained the Fluorescein (FAM) NHS ester, 6-isomer from Lumiprobe (MD, USA). The FAM-labeled GelMA was synthesized in accordance to the manufacturer's general NHS ester conjugation protocol. We always wash away the residual solution after printing to avoid the false positive detection of the fluorescent signal in the residual solution. Thanks to the FAM label, the brightness of the fluorescence can directly translate to the density of the structure being polymerized. The fluorescent structure image is cropped, rotated, and resized to match the size and location of the input mask. We use the intensity on the fluorescent image as a measure of the polymerization completeness, and we take a threshold on the fluorescent image to obtain a binary image representing whether each part of the structure is properly polymerized (true, white) or not (false, black) (Fig. 2.3(a)).

The goal of our method is to find an optimal design mask for any printable structure, which represent the light exposure dose on every pixel location with a grayscale value, that help compensate the scattering effect of the cell-loaded material during 3D printing. Our machine learning algorithm is composed of two learning steps, the simulator calibration step for generating augmentation data, and the NN training step to generate desired grayscale masks (Fig. 2.2). The overall workflow of our algorithm is to first acquire image data of real 3D printed structures with a variety of sample masks. Then we use these trial data and apply generic algorithm to learn the parameters of a mathematical simulator to simulate the 3D printer with scattering effects from the cell loading. With the calibrated simulator, we generate thousands of simulated data and train a specially designed deep neural network to learn the optimal mask choice for any desired target structure. For simplicity, all our experiments were done with a single layer of printing instead of multilayer 3D structures. It is worth noting that our method can easily extend to 3D cases by upgrading the simulator and NN design, and the overall learning process remains the same. The

design region is fixed to 512x512 pixels in terms of the mask size with 2.96 micrometers per pixel, which is about 1.5x1.5 mm^2 in physical size of the printing region.

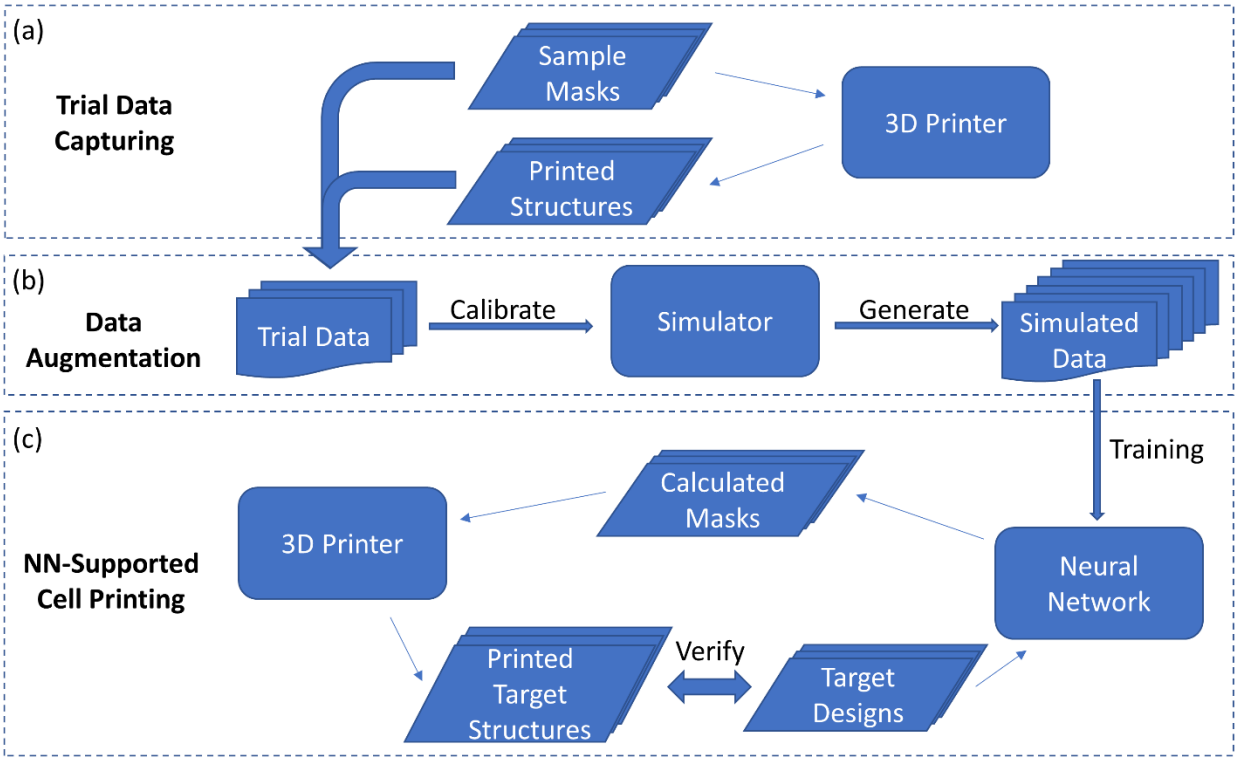

Fig. 2.2. Data Flow and schematic of the learning process. (a) 32 sample masks are used to print 32 single-layer trial prints for training the algorithm. (b) The trial prints calibrate the printer simulator, and the calibrated simulator generates thousands of new training data. (c) The printed samples and the simulator generated samples are used to train the neural network, the trained network calculates the appropriate masks that compensate the cell scattering effect, and the final print quality is tested with some predefined target designs.

2.2.2 Trial data acquisition

The first stage of our algorithm is to acquire real 3D printed structures (Fig. 2.2(a)). The goal of this stage is to collect data for analyzing the inner-layer scattering effects of cell loading. We first generate 32 predesigned masks as demonstrated in Fig. 2.3(a) with MATLAB code. These sample masks have three different types of randomized feature shapes, including random grayscale valued checkerboard shapes, randomly positioned and randomly sized rectangles, and randomly

positioned variety of circular shapes. The design purpose of these masks is to provide various smooth and sharp features as represented by the circles and rectangles.

After we designed the sample masks, we use them as input into our DMD 3D printer. The grayscale value on each pixel of the mask image represents the percentage of light exposure dose of the 3D printer, which is controlled by the duty ration of the flipping of the DMD mirrors. A full valued pixel, which is 255 in 8-bit unsigned integer representation, represents a 100 percent exposure dose. The maximum light exposure dose is also controlled by the exposure time, light source power. For simplicity, we use a constant light source power and manually fix the exposure time to 20 seconds, and the maximum light intensity (at 255 grayscale value on the mask) is measured to be 20.8 mW/cm^2.

The printed structures are imaged using a fluorescence microscope. The intensity of fluorescence can translate to the completeness of polymerization. After a thresholding operation, we obtain the binary image with 0 and 1 representing void and polymerized state respectively. The processed structure images as well as their corresponding masks are then used as input to train our algorithm (Fig. 2.3(a)).

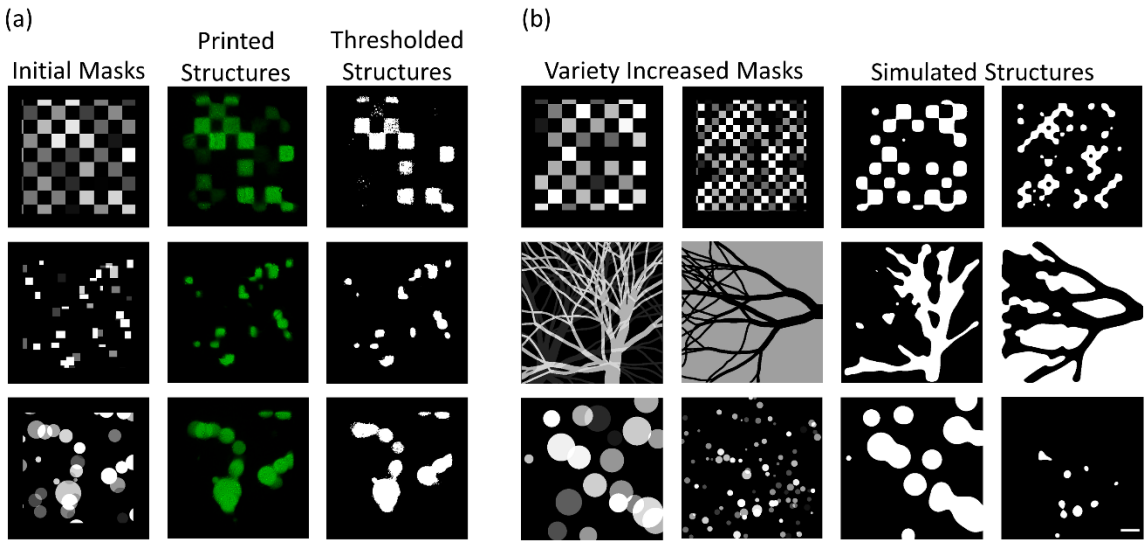

Fig. 2.3. Examples of the calibration and training data. (a) The calibration data for the simulator. (b) The training data generated from the calibrated simulator for NN training. Scale bar is 200 μm.

2.2.3 Simulator calibration

The data augmentation stage is the first learning step that takes the real printing data as input and generates various virtual data as output. The input data, including the sample masks and the postprocessed printed structure images, came from the previous data acquisition stage. The input data is used to calibrate a mathematical simulator that models the local and global deformation caused by the scattering effect of the cell-loaded material during the printing process. We have developed the simulation function according to the interpretation to the physical 3D printing process (Eq. 2.1).

$$\begin{aligned} P &= Sim(M; c_0, c_1, c_2, c_3, c_4, \sigma, T) \\ &= Threshold_T(Gauss_\sigma(ReLU(c_1X^2 + c_2Y^2 + c_3X + c_4Y + c_0) \times M)) \end{aligned} \tag{2.1}$$

The simulator takes a grayscale mask image M of size 512x512 as the input variable, and outputs a binary image P of the same size that shows the polymerization condition of each pixel point on the given region. A true or 1 represents fully polymerized unit, while a false or 0 represents an under-polymerized or unpolymerized unit. The mask is first element-wise multiplied by a basic

light absorption matrix $ReLU(c_1X^2 + c_2Y^2 + c_3X + c_4Y + c_0)$. This matrix is composed of a linear combination of X and Y as well as their quadratics, where X is the first coordinate of each point on the mask, and Y is the second coordinate. Both X and Y are of the same dimension as M. The basic light absorption matrix serves to mimic the light emitting and absorbing process of the DMD 3D printer under a mask with no patterns on it. When it multiplies M pixelwise, the result should represent the light energy absorbed on each patterned pixel without considering the scattering effect. The basic light absorption matrix also provides the simulator the ability to mimic certain locational variant characteristics of the 3D printer, for example the light energy could be slightly stronger at the center of the exposed region compared to the side. The rectifier linear unit (ReLU) function zeros out all the negative values, since we know the light absorption is physically non-negative. After that, we have a 2D Gaussian kernel $Gauss_\sigma(\cdot)$ with standard deviation σ, that simulates the light scattering effect of the cell-loaded material. Finally, the $Threshold_T(\cdot)$ function sets a threshold T that decides under what degree of light exposure should the material be considered as being successfully polymerized. After all the function processes in the simulator, it will calculate a binary map of polymerized versus under- or unpolymerized for each unit area.

The calibration of this simulator is done by optimizing the seven parameters in Eq. 2.1 with genetic algorithm, which is a commonly used non-gradient optimization method in many fields[177]. The optimization objective is set to be the mean squared distance between the real printed structure and the simulator output, averaging among all 32 trial data pairs. Optimization was implemented with MATLAB and the global optimization toolbox[178].

After calibration, we apply a new set of 4,000 masks to the simulator and obtain their corresponding simulated structures. These new masks are designed with the same scheme as the sample masks with a greater variety feature numbers and sizes as well as four additional feature

types, vertical lines with different spacing, horizontal ones, the combination of two, and 2D vasculature shapes. After we get all the simulation results, we proceed to use this data to train the NNs in the final stage.

2.2.4 Neural network training

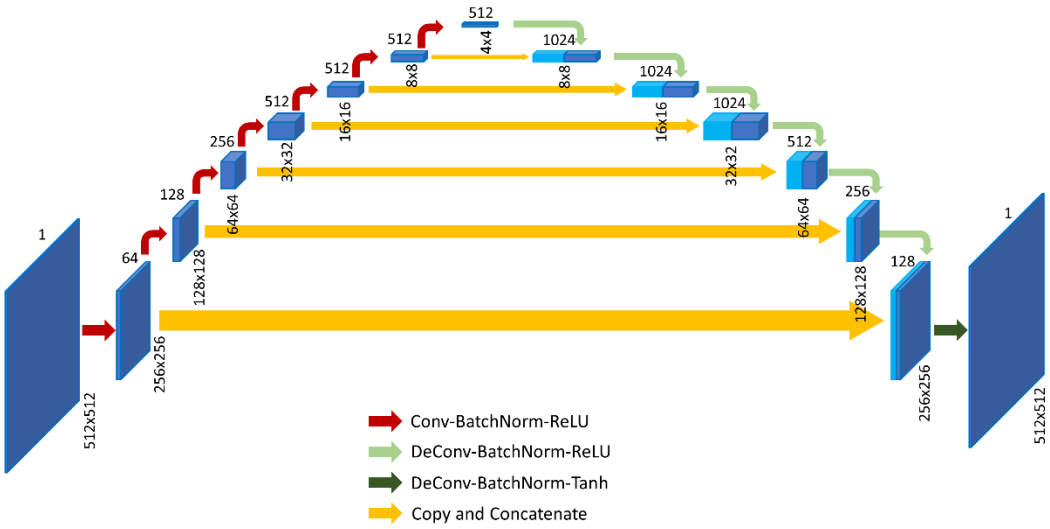

Fig. 2.4. Architecture of the deep neural network. The neural network is composed of fourteen convolution or deconvolution layers with batch normalization, ReLU and Tanh activation function, as well as U-net style skip connections. The cuboids represent the feature maps of the input, intermediate, and output layers of the network. The feature resolution is denoted at bottom of each cuboid, and the corresponding channel size is on the top.

The next step of our machine learning method is the NNs training, which is the key part of our algorithm. We are looking to train a NN that can automatically calculate the appropriate mask for any potential target structure. We are supplying the 4,000 simulated data pairs from the data augmentation stage to train the NN.

Our NN method is composed of two U-Net-like NNs which we call the master NN and the slave NN [163,179]. The slave NN learns the transformation of our physical 3D printer, which is similar to the function of the simulator in the previous stage. The major difference is that the slave

NN is a differentiable function, which provides gradient information to support the training of the master NN. The master NN serves to learn the inverse transformation of the 3D printer. For any given target structure, the master NN will suggest a deformed mask that could allow the printer to print out this target structure under the highly scattering condition.

The network architecture of the master NN is shown in Fig. 2.4. This architecture reproduces the U-net style encoder-decoder architecture with some adaptations [179,180]. The network consists of 14 building blocks. The network takes a 512x512 single-channel image as the input. The first 7 blocks each has a convolution layer with stride 2 to down-sample the images and features, and the convolution layer is followed by a batch normalization layer and a ReLU function[181,182]. The other 7 blocks each has a deconvolution layer with stride 2 to up-sample the features and ensure the output resolution is the same as input. The deconvolution layers are again followed with batch normalization and ReLU, except the last layer uses the hyperbolic tangent function (Tanh) instead of the ReLU. The U-Net style skip connections copy the feature map from the first six block outputs to the last six blocks' input features respectively. These skip connections help the network to learn the local details in the earlier feature maps while retaining the global information extracted from the later features. The slave NN has almost the same architecture as the master NN except the final output layer of the slave NN has 2 channels for the pixel-wise classification output, which outputs the binary structure, instead of the single channel regression output of the master NN.

To train the NNs, we randomly divide the 4,000 data pairs into 3,600 pairs of training data and 400 as testing data. The testing data is used to verify the convergence of the networks. Since we already have the simulator generated data as the augmented data, we are not applying other

data augmentation techniques. The training process is achieved by backpropagation of the following loss function.

$$Loss = E_y\left[L_{Crossentropy}\left(Slave\left(Master(y)\right), y\right)\right] + \lambda_1 * E_{x,y}[L_{L1}(Master(y), x)] + \lambda_2 * E_{x,y}\left[L_{Crossentropy}(Slave(x), y)\right] + \lambda_3 * Sparsity_y(Master(y)) \quad (2.2)$$

In Eq. 2.2, the loss function is the sum of four loss terms, the slave supported master loss, the data supported master loss, the data supported slave loss, and the sparsity loss. The details of the first three loss terms can be found in the Appendix section of [163]. The x here stands for the grayscale mask, which is rescaled to a range between -1 and 1, and y stands for the 3D printer output structure, which is represented in a binary class map with two channels. *E* represents the expectation operator. The $L_{Crossentropy}$ calculates the cross-entropy loss between the two arguments, and L_{L1} is the *L1* loss function or the least absolute deviations. $Master$ is the master NN forward pass, and the $Slave$ is the slave NN forward pass. The $Sparsity$ is a sparsity loss term that sums the pixel grayscale values of a given region. In this case, the sparsity loss sums up the pixel values in the master NN generated mask, where it is outside of the target structure region of y. This term ensures that the NN generated mask does not give unwanted exposure far away from the target structure region. λ_n is the tradeoff coefficient for different loss terms. We are setting the tradeoff coefficients $\lambda_1, \lambda_2, \lambda_3$ to be 1, 1, and 0.05 respectively. We also decay the λ_1 term with factor 0.98 on every training iteration, so that the master NN relies on the training data initially, and it will gradually rely more on the slave NN gradients in the later epochs when the slave NN becomes more trained. This will improve the generalizability of the master NN by promoting it to spend more time on learning the 3D printer transformation instead of repeatedly looking at the training data.

In terms of training implementation, we used the PyTorch framework GPU version 1.2 with Adam solver for the back-propagation process [183,184]. We set the batch size to 10, learning rate to 10^{-5}, gradient decay factor to 0.9, and the squared gradient decay factor to 0.999. A Gaussian noise term is added to the input x to avoid overfitting of slave NN, while the training error of slave NN itself could help avoid the master NN from overfitting[185]. The initialization of model weights is done by sampling from normal distribution with zero mean and 0.02 standard deviation. The training was executed on a desktop computer with Intel i5-7500 CPU and GTX 1070Ti GPU. We trained the networks for 200 epochs for about 26 hours. After the network is trained, it will only require a few seconds on a CPU only machine to execute a forward pass of the master NN, while the GPU enabled machine can process the forward pass in less than a second.

2.3 Results

2.3.1 3D printing with NN-generated masks

To verify our trained NN, we set several testing designs that are unseen from the training data (Fig. 2.5(a)) (Fig. 2.6). The test structure designs mainly demonstrate various concave and convex sharp features as well as the ring shape that could potentially be used to print biological tissue models. We then input these target structures one-by-one to the master NN and get their corresponding NN-calculated masks as the output (Fig. 2.2(c)) (Fig. 2.5(b)).

The NN-calculated masks are indeed different from the target structure. We can interpret that the NN-calculated mask tends to “stretch out” at the protruded sharp regions and “shrink” at the denting regions (Fig. 2.5(e)). The overall behavior of how the NN tries to compensate the scattering effect is similar to our previous research[163]. It is important to note that these kind of mask designs are usually not possible even for an experienced expert in 3D printing.

After we obtain all the NN-calculated masks, we apply each mask to the DMD 3D printer and take microscopic fluorescent images as well as postprocess the images into binary representation, in the same way as we did in preparing the trial data (Fig. 2.5(c-d)). The resulting binary images match nicely to the input target structures.

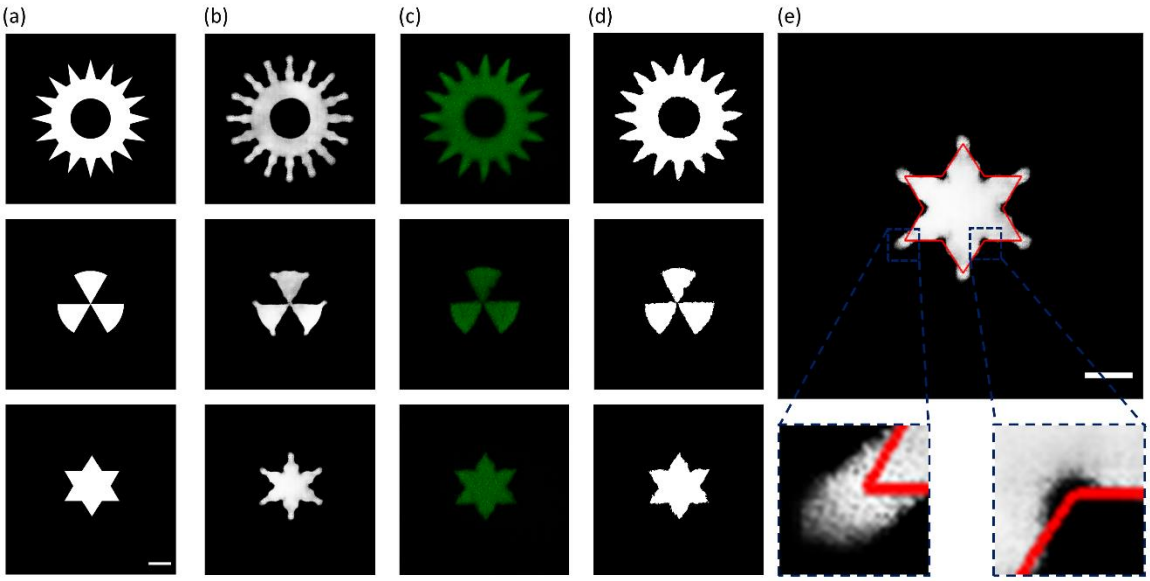

Fig. 2.5. NN-calculated masks and the corresponding images of printing results. (a) The target structures. (b) The grayscale masks calculated by the trained NN. (c) The fluorescent images of the 3D printed structures using the masks from b. (d) The binarized images of c for easier comparison with the target. (e) The NN-calculated mask overlaid with a red contour showing its corresponding target structure. Scale bars are 200 μm.

2.3.2 Printing quality comparison

To better demonstrate the power of our method, we compare the printing results between using the NN-calculated masks and using the traditional identical masks. Traditionally, an operator of the DMD 3D printer usually sets the DMD mask identical to the target design and only changes the overall light exposure dose by tuning the light power and print time. Therefore, we use the 100%, 75%, 70%, and 50% grayscale mask values to mimic the overall light exposure changes of the traditional tuning. Later experiment shows that grayscale value of lower than 50% will hardly print any obvious structures, therefore, we choose 70% as the lower bound of intensity dose (Fig.

2.6). The printing results of these identical masks are then used as benchmark printing samples for comparison with the printing result of NN-calculated masks.

From the results in Fig. 2.6, we can easily see that the NN-calculated masks perform better than the traditional masks across all the testing target structures we had. In the first three rows, we can see that the NN results greatly reserves the sharp features of the target, while the benchmark results always lost the sharpness to the rounded smooth features. For the ring shapes in the bottom two rows, we find that although similar quality has shown on the bigger rings across the different masks, the smaller rings can only be properly printed with the NN-calculated masks. The ring shape with varying diameters shows an example that different patterns would require different manual tuning of the printer settings, since the varying rings under the same printing condition with identical masks would never show the same printing quality. With our machine learning method, we can see that different rings have a more consistent quality. Comparing the smooth ring patterns with the patterns with sharp features, we can see that the smooth features are easier to print even with the traditional identical mask method, while the more complex features can only be properly printed with NN masks to reserve the fine features. The size of the overall patterns also affects the print quality. From the various ring shapes, we can find that the large features are always easier to print, and the small features are very challenging to print under the high scattering effect even with the help of NN (Fig. 2.6).

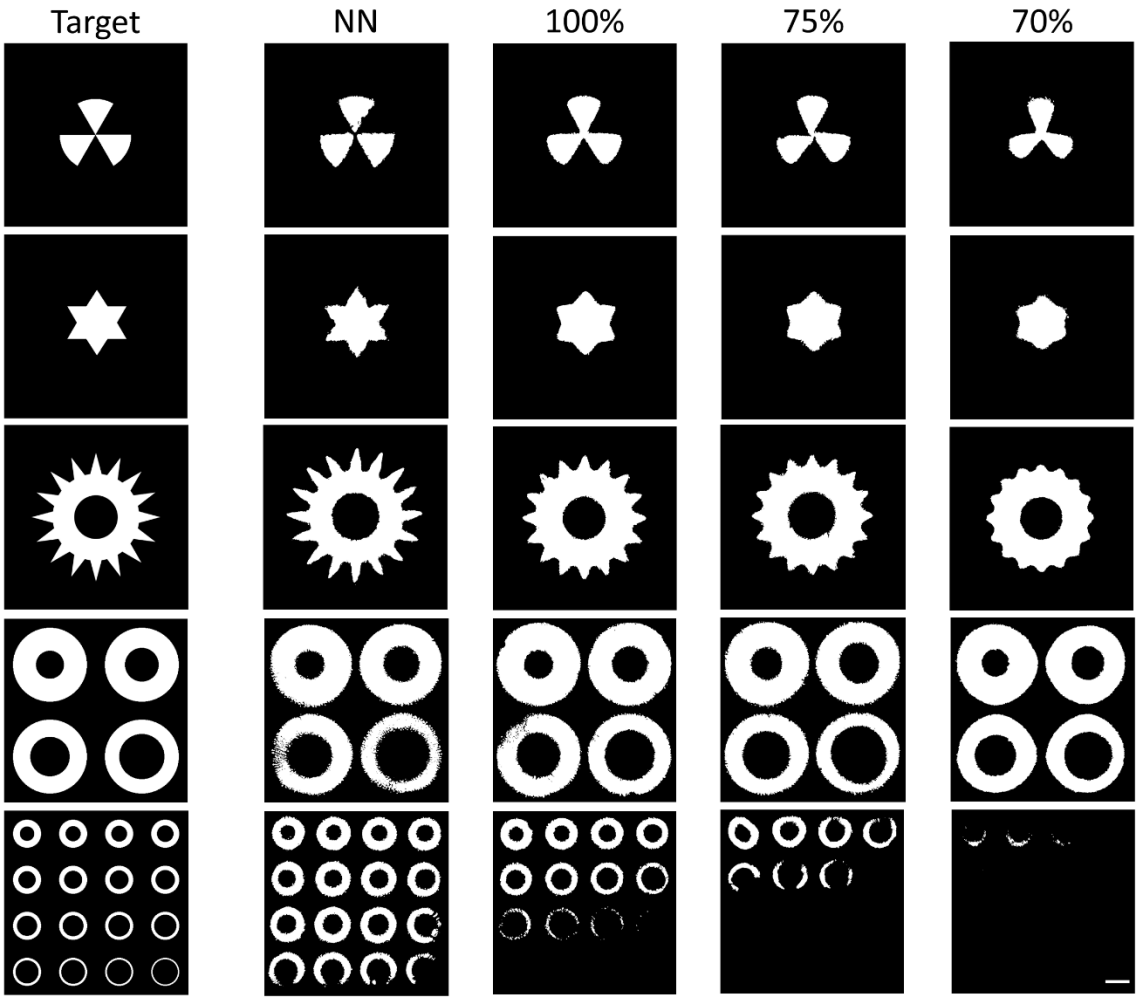

Fig. 2.6. Postprocessed microscopic images of the test printing results. The first column shows the designed target structures. The second column shows the printed structure using NN-calculated masks. The third to fifth column are the printing results using the identical masks with 100%, 75%, and 70% exposure dose respectively. Scale bar is 200 μm.

2.4 Discussion

As 3D bioprinting attracts more and more industrial applications, key challenges emerge: how to improve printing fidelity when cell-induced light scattering effects dominate? How to minimize the traditional trial and error operation in optimizing the printing parameters? As shown in our results, the NN-based deep learning method demonstrate great success on advising the 3D bioprinter by providing the optimal optical masks to improve the printing fidelity when scattering cells present.

One major benefit of our method is the high data efficiency. Common machine learning algorithms would require a large amount of data (i.e. printed samples) in order to get reliable performance. In our algorithm, we are only using 32 actual printing samples as training data, which is an extremely small number compared to the common machine learning data sets that have thousands or even hundreds of thousands of samples. Even with such a small number of trial data, our trained NN showed its power to greatly improve the printing quality. Considering that the 3D bioprinting is normally very expensive to produce many samples due to the cost of the cells, bioinks, and cell cultures, our method is more practically applicable than the normal data heavy deep learning methods. If we are accessible to more printing data, our method can still be applied, and the resulting accuracy could be improved according to the central limit theorem considering the random selection of initial masks and the potential production and imaging noises.

The way we utilize the limited amount of data is to introduce a simple equation, being calibrated with the trial data, to simulate the process of the 3D printer and the scattering effect. Although different from the common data augmentation methods[186], our approach of calibrated simulations can be seen as a heuristic way of data augmentation. By incorporating the understanding of the physical processes of the DMD 3D printing, our simulator only considers seven parameters. Compare to the basic image manipulation type of augmentations like flipping or rotation, our augmentation method shows many more different features by introducing a great variety of new masks than the sample masks in the simulation, which prevents the further overfitting that might be caused with simple augmentations[186].

Beside the calibrated simulation, our slave part of the NN can also be considered a kind of data augmentation, since it predicts the output structure for the input of master NN generated mask which can be potentially unseen from the training data. The slave NN can also be interpreted as a

noise term that will gradually decrease with the training process, since the randomly initialized slave NN can produce very wrong prediction of the output structure at the beginning and improves through training. Adding noise to the NN training process is a known technique to improve the generalization performance of the trained NN[187]. The benefit of the slave NN has been experimentally studied in our previous paper[163].

Although our current experiment is on a single-layer basis, our method can easily be extended to apply on multilayer 3D structures. The only changes in the algorithm will be that the 2D convolution layers in the NNs will be replaced by 3D convolutions, and the simulation function will need to add an extra dimension. The difficulty we foresee is the way to properly image or scan the printed 3D structure. Also, the size of the data we are going to process will be a lot larger if we want to keep the resolution of each dimension. The huge data size could cause trouble in NN training.

Our current experiment is working on a custom DMD based 3D printer, and we are only printing with one specific material and cell composition. However, our method could easily adapt to a different printer or material composition with a new set of sample prints. Our requirement of 32 data samples is relatively easy to obtain comparing to some other deep learning methods that relies on big data[141]. Further online training to improve the performance and the generalizability across different settings would be an interesting future improvement.

2.5 Conclusion

Our deep learning method with learning-based data augmentation greatly improves the fidelity of bioprinting with as few as 32 sample prints to train the learning system. Our experiment shows that using the grayscale masks generated from our trained NN, we can print fine detailed

structures surpassing the traditional manual tuning method with identical masks. Our method allows the use of a very small amount of trial data, which is usually not possible for the common deep learning applications that rely on big dataset. Furthermore, our method could easily be applied on different materials or different printer settings with a new set of sample prints. Considering the high cost of cells, reagent, and bioinks, our deep learning method provides a powerful solution for bioprinting with reduced cost, high fidelity, and shorter time to product, paving the way for future large scale organ printing.

Acknowledgements

Chapter 2, in full, is a reprint of the published article “Compensating the cell-induced light scattering effect in light-based bioprinting using deep learning”, J. Guan, S. You, Y. Xiang, J. Schimelman, J. Alido, X. Ma, M. Tang, S. Chen. *Biofabrication*, 2022. The dissertation author was the primary researcher and first author of this paper.

This work was supported in part by National Institutes of Health (R21AR074763, R33HD090662, R21HD100132) and National Science Foundation (1907434, 1937653). Part of the work is performed at San Diego Nanotechnology Infrastructure (SDNI) of UCSD, a member of the National Nanotechnology Coordinated Infrastructure (NNCI), which is supported by NSF (Grant ECCS-1542148).

Chapter 3 Two-Photon Polymerization 3D Printing and Applications

3.1 Introduction

Two-photon polymerization (2PP) is one of the most precise light-based 3D printing technologies in the field. The 2PP 3D printer could fabricate scaffolds at submicron or nanoscale resolution [188]. The 2PP technology was invented based on the two-photon absorption (2PA) concept, where a molecule was excited into a high energy state from the simultaneous absorption of two consecutive photons. The excitation energy for the molecule was equal to the total energy of two photons being absorbed. The 2PA concept was applied to build the 2PP system where a femtosecond ultrafast infrared laser was used to provide high energy consecutive pulsing photon emissions. The laser beam got focused onto the bioink material and the photoinitiator molecules at the laser focused region started to absorb two consecutive photons and reached the critical energy to reach the high energy state followed up by releasing free radicals. The free radicals then initiated the polymerization chain reaction of the monomers in the bioink and started forming solidified polymer chains near the reaction site. Due to the extremely high power density at the focal point and the Gaussian distribution of the fsec laser beam, only the most focused spot was able to trigger the 2PA photopolymerization reaction, which prevented unwanted polymerization before and after the focal spot. The ultrahigh nanoscale resolution 2PP 3D printing could then be achieved by precisely controlling the printing speed and laser energy [156].

Thanks to the ultrahigh resolution, the 2PP printer could achieve fine feature fabrication tasks that were not achievable with other types of 3D printers, allowing a broad range of applications like micro biomedical devices, micro lenses, microneedles, and so on[189].

3.2 Two-photon polymerization 3D printing system

Our custom 2PP 3D printing system was composed of a laser source, a set of optics and lens, an electrical shutter, a motorized stage system, a camera monitoring system, and a removable printing platform (Fig. 3.1). The femtosecond (fsec) laser source was essential to all 2PP systems, as the short and rapid pulses introduced much higher peak power than other type of lasers enabled the precise energy deployment, resulting in just enough energy on the most focused portion of the laser beam to trigger photopolymerization reaction without affecting the surrounding out-of-focus regions[190]. Our system used a 780 nm fsec laser source (Calmar Laser, USA), which could reach a source power of over 500 mW/cm^2. An electrical shutter (Sutter Instrument, USA) enabled real-time control of the laser switching. The motorized stage system was composed of three linear stages to enable a full three-dimensional precise movement control of the printing platform on top. A digital microscope camera (AmScope, USA) was mounted to monitor the fabrication process. The 3-axis stage system, the electrical shutter, and the camera were all connected to a desktop computer with a custom program to simultaneously control the 3D printing process. The optics was used to guide the laser, and a 50x, NA 0.5 objective lens (Carl Zeiss AG, Germany) was used to focus the laser beam onto the printing platform. The printing platform attached to the stage system was built with a glass slide base with two 250 μm thick polydimethylsiloxane (PDMS) spacers on top of it to hold a methacrylated coverslip. Prepolymer bioink was loaded in between the coverslip and the glass slide, and the laser would start to project on the top surface of the bioink and patterns could form with the motion of the stages. Once the 3D printing process was finished, the printed scaffold would attach to the top coverslip, and we could then remove the coverslip together with the printed scaffolds for further processing. The rest of the printing platform could be reused by placing a new coverslip on top and loading new bioinks (Fig. 3.1).

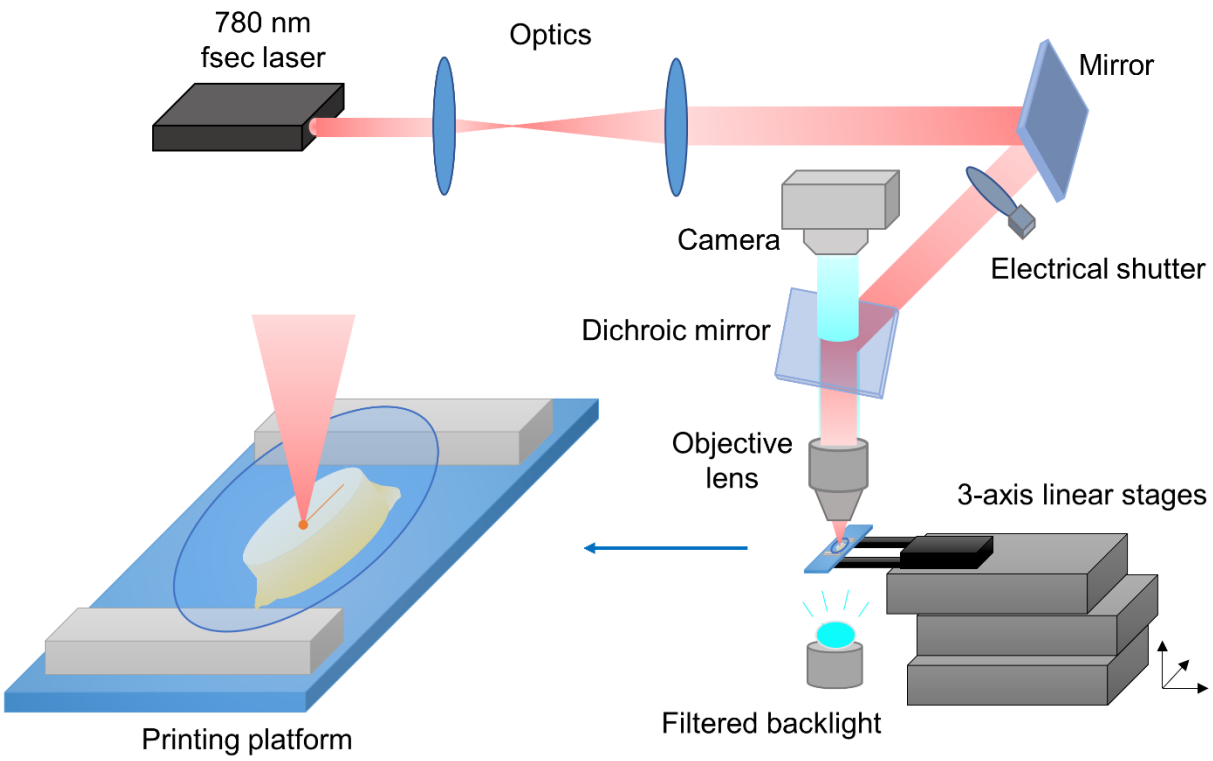

Fig. 3.1. Schematic of the two-photon polymerization 3D printing system.

With the 2PP 3D printing system, the fabrication of micron and even submicron scaffolds were achievable. In order to fabricate a 3D structure, a 3D computer-aided design (CAD) model file was needed. We apply the open-source slicing software Slic3r (Slic3r v1.3.0) to convert the given 3D model into a toolpath in the form of G-code, which could guide the motions of the stages to properly walk through the whole object and guide the electrical shutter to only allow laser pass through when the exposure was needed.

3.3 Fabrication of microscale 2D and 3D scaffolds

A bioink or photoresist used for 2PP fabrication typically consists of a photopolymer and a photoinitiator, where the photoinitiator release free radicals when excited by the laser and initiates the photopolymerization reaction of the photopolymer and forms a solidified structure.

There were a range of different photopolymers and photoinitiator studied for biological and tissue engineering applications[191]. In the following study, we used dipentaerythritol penta-/hexa-acrylate (DPPHA), polyethylene glycol diacrylate (PEGDA), and poly (glycerol-co-sebacate) acrylate (PGSA) as the photopolymer, and Irgacure 819 and diphenyl(2,4,6-trimethylbenzoyl)phosphine oxide (TPO) as the photoinitiator. In addition, we added tartrazine as the photo-inhibitor to add light attenuation to the bioink which could provide better vertical 3D printing resolution. A small amount of sodium fluorescein was also added in the bioink, so that when focused laser excites the fluorescein, we were able to observe the laser projected spot under the preview camera. The following examples showcased the capabilities of our 2PP printer to fabricate different microstructures using the three different polymer materials.

The first bioink we used to showcase our 2PP printer capability was composed of DPPHA mixed with 1% (w/v) of Irgacure 819. The resulting solution was then mixed 100:1 to the sodium fluorescein. The DPPHA is a multifunctional hydrophobic monomer which is biodegradable and biocompatible[192,193]. With its high crosslinking efficiency, we demonstrated the fabrication of stiff DPPHA scaffolds using the 2PP printer (Fig. 3.2). We first demonstrated printing ring structures with varying diameters varying from 2 μm inner diameter (Fig. 3.2 A) up to 35 μm (Fig. 3.2 B). This showed that the micron level small channels were able to be fabricated through 2PP. On top of that, we also fabricated a square block scaffold with vertical channels in the middle (Fig. 3.2 C). The ability to fabricate micron channels in the structure could be useful in many biological applications such as biomimicking arteries and engineered channels to guide tissue growth.

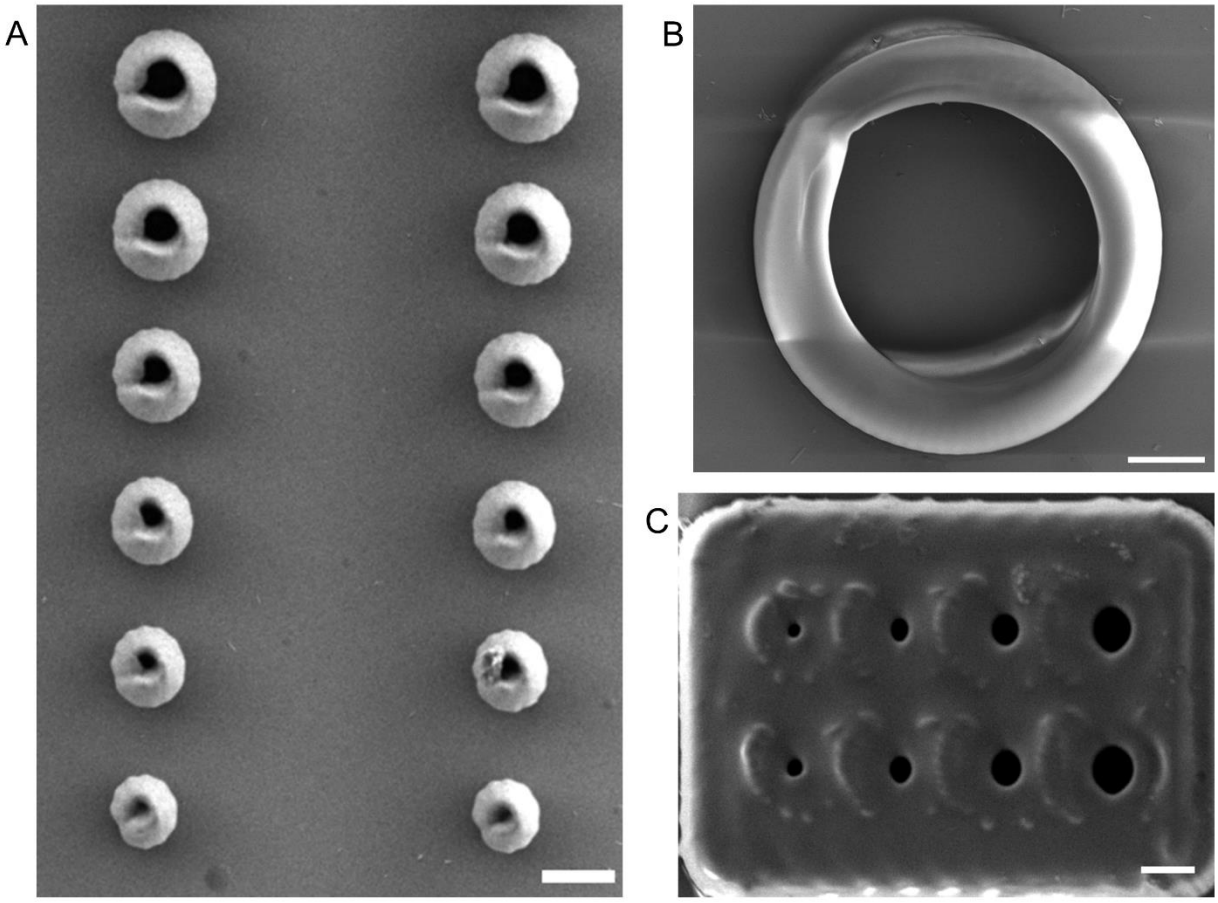

Fig. 3.2. SEM images of 2PP fabricated DPPHA scaffolds. (A) SEM images of ring structures with varying diameters. (B) The zoomed-in view of a larger ring structure. (C) A block scaffold with engineered holes in the middle. Scalebars are 10 μm for A-C.

The second bioink was composed of PEGDA and 1% (w/v) of Irgacure 819 and further mixed 100:1 with sodium fluorescein. The PEGDA hydrogel was broadly used in tissue engineering due to its relatively soft mechanical property and biocompatibility[190]. A mobius strip structure was printed to showcase the PEGDA fabrication of complex 3D structures. We demonstrated that the mobius strip structure could be fabricated both on top of a flat coverslip surface as well as on top of a square block base structure (Fig. 3.3). Our printing plate form design enabled the top to bottom fabrication process, where the printed structure was hanging upside down in the bioink during the printing. The bioink buoyancy together with gravity stabilized the printed structure, allowing the overhanging mobius strip structure to be printed without collapsing

halfway through the printing process. Given this flexible fabrication capability of the PEGDA, we could potentially apply such printing technique to achieve complex overhanging structures for potential tissue engineering applications like 3D cell culture.

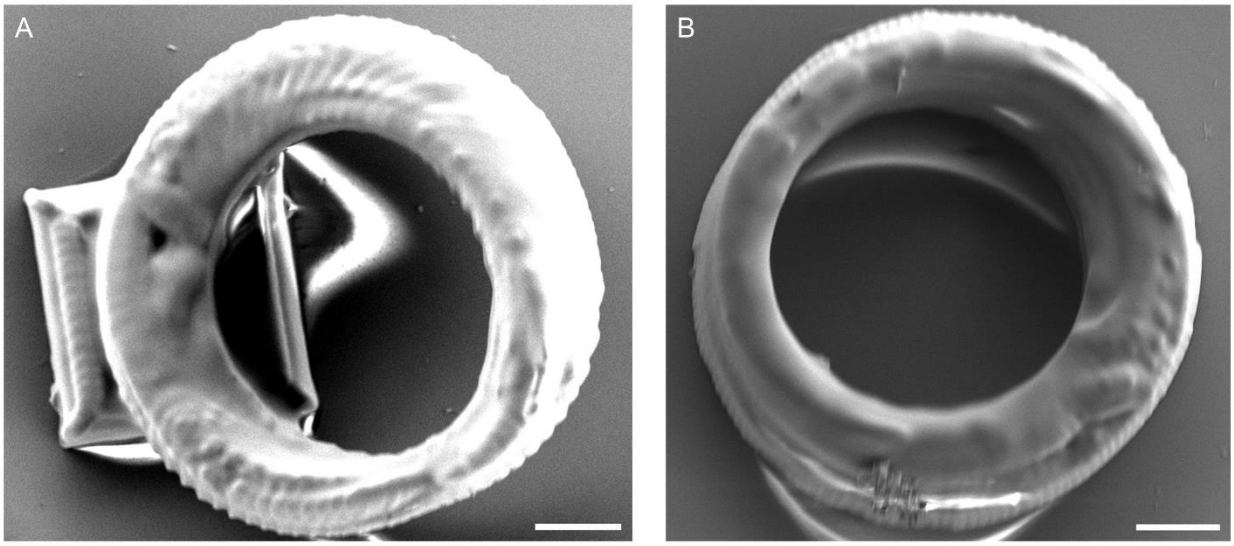

Fig. 3.3. SEM images of 2PP fabricated PEGDA scaffolds. (A) SEM image of a mobius strip structure on a square base. (B) SEM image of a mobius strip structure directly on a coverslip surface. Scalebars are 10 μm for A and B.

The third bioink was composed of the PGSA elastomer with 4% (w/v) TPO and 0.01% (w/v) tartrazine. The resulting solution was also mixed 100:1 with sodium fluorescein. The PGSA material was recognized as a stiff biodegradable elastomer which was previously investigated with other 3D printing methods such as digital-light-processing (DLP) based 3D printing[194,195]. While the PGSA remained understudied with 2PP systems, we demonstrated that we could fabricate various PGSA scaffolds using the 2PP printer (Fig. 3.4). We first fabricated parallel repeating wavy lines to show the feasibility of making complex and smooth 2D patterns on a flat surface. The curvy lines resolve about 3 μm lateral line width. As previously discussed, the vertical height was not perfectly optimized, ending up with a relatively tall wall structure for each line. However, the curvy structure self-stabilized the tall wall so that the lines or walls did not fall down,

but instead self-supported by neighboring part of the curved lines. This structure could potentially enable a design where tall 2D channels are desired while the material is not strong enough to self-support straight channel lines. The capability of fabricating such curvy lines with 2PP for structural self-supporting 2D channels had the potential to achieve this application. After this, we also demonstrated fabricating other complex structures, like the engineered thunder bolt and snowflake structures, where the smallest feature was in less than 5 μm. The UC San Diego logo, composed of the known Geisel library shape on top and the UCSD characters on bottom, was also fabricated with 2PP printer.

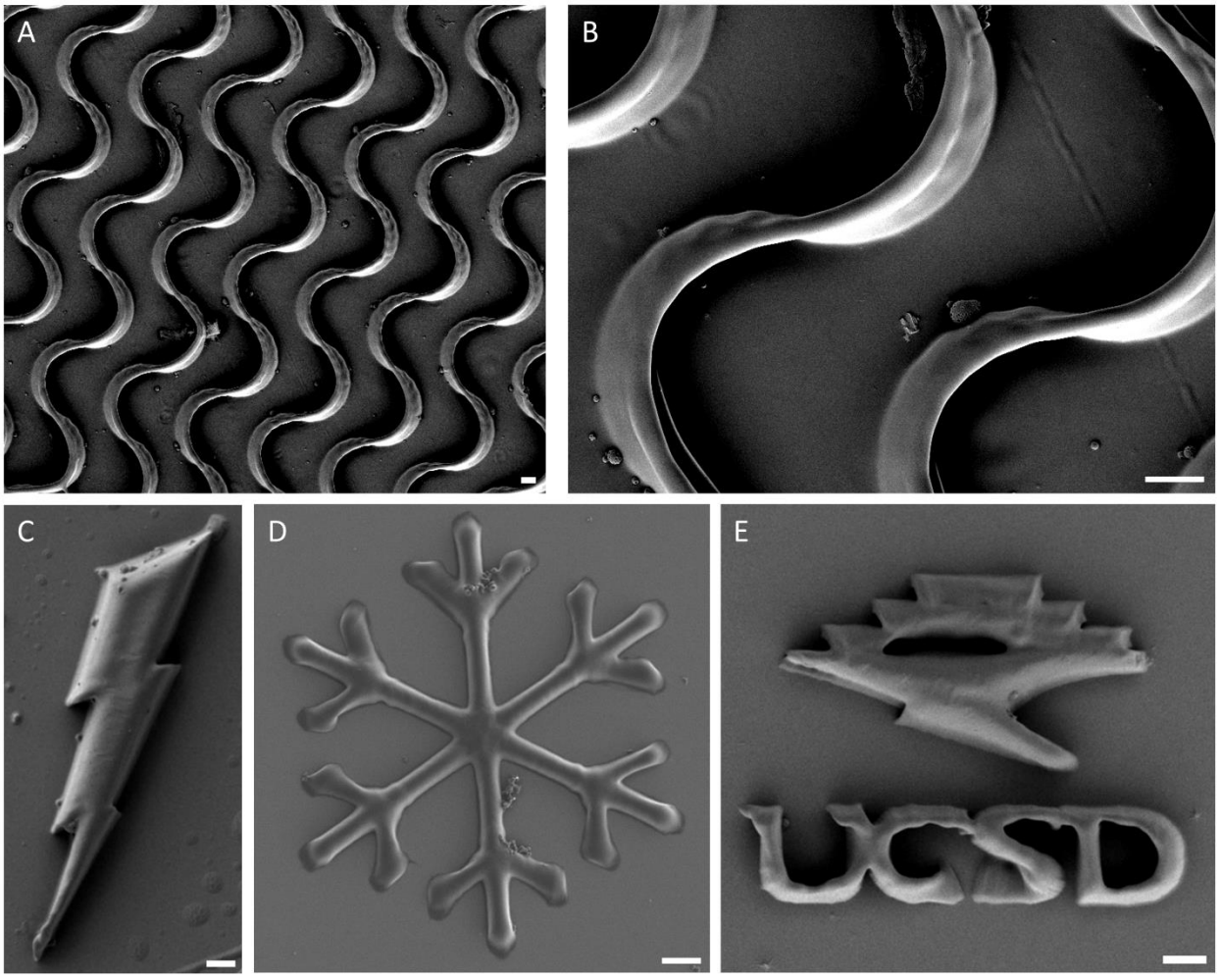

Fig. 3.4. SEM images of 2PP fabricated PGSA scaffolds. (A) SEM images of repeating wavy patterns. (B) Zoomed-in view of A. (C) A thunder bult structure. (D) A snowflake structure. (E) A 2D structure showing UCSD logo. Scalebars are 10 μm for A-E.

Summary

In this chapter, we built a custom 2PP 3D printing system and demonstrated its capabilities of fabricating microscale scaffolds using three different types of bioink polymers, DPPHA, PEGDA, and PGSA. The 2PP printer enabled the flexible fsec laser-based fine microstructure fabrication. The variety of bioinks and the feasibility of fabricating complex 2D and 3D microstructures could enable many different biological and tissue engineering applications. As an example, the fabrication of 2D surface walls or channels could help guide the cell growth, and the 3D cavities and channels could potentially allow biomimicking features and 3D cell culture.

Chapter 4 Machine Learning Assisted Scaffold Stiffness Modulation for Light-based 3D Printing

4.1 Introduction

Recently, machine learning has drawn increased attention in many areas including 3D printing [8]. Previously we have applied machine learning algorithms to assist DLP-based 3D printing to increase resolution of scaffolds due to the light scattering effect in acellular and cellular scaffolds [163,196]. However, the ability to precisely control mechanical properties of printed scaffolds using machine learning has not been previously explored. By applying a machine learning model to predict mechanical properties of a scaffold given trained stiffness data under a range of printing parameters and 3D printers, a new method to fabricate smart tissue engineered scaffolds with precise digital stiffness modulation is demonstrated. Utilizing the advantages of machine learning with both DLP-based and 2PP-based printing systems, a new workflow to analyze sample scaffolds and fabricate precision engineered scaffold is introduced (Fig. 4.1). This workflow applied a neural network (NN)-based machine learning algorithm to learn from previously fabricated scaffolds stiffness data and enabled precise local stiffness control of the DLP and 2PP fabricated scaffolds with the ease of only adjusting printing parameters on-the-fly during the printing process and would not need any adjustments to the bioink composition. Extending the fast fabrication speed of DLP printer and the precise microfabrication of 2PP printer, our system could modulate the complex geometry together with the mechanical property of the scaffolds in micro- and milli-meter scales.

This study chose PGSA as the polymer material for the bioink to demonstrate the capability of modulating scaffold stiffness by only adjusting the 3D printing parameters. As mentioned in the previous chapters, PGSA is a biocompatible and biodegradable elastomer material that is often

used for fabricating tough scaffolds in tissue engineering that has been used for muscle regeneration and other tissue engineering tasks thanks to its achievable range of mechanical properties. PGSA prepolymer could be 3D printed with both DLP and 2PP light-based 3D printing systems after mixing with 4% (w/v) TPO as photoinitiator [194,195,197]. For 2PP printer, the PGSA bioink was further mixed with sodium fluorescein at 100 to 1 dilution to trigger fluorescent marking upon exposing to the laser. In our system, the stiffness of PGSA could be precisely modulated locally in both DLP and 2PP 3D printing systems, enabling a broad range of tissue engineering applications that requires a specific range of scaffold stiffness and customizable geometry.

Our study applied a machine learning method to analyze and learn from sample stiffness data to achieve precise stiffness modulation of PGSA scaffolds on DLP and 2PP printers. For DLP printer, the sample data was collected by first 3D printing a set of block scaffolds using a range of different DLP printing parameters, namely exposure time and light intensity. Then, the stiffness of the printed scaffolds was accessed with nanoindentation. From the nanoindentation experiments, we could calculate the Young's modulus from the amount of stress exerted and the strain of the indented region. Using the input 3D printing parameters and the measured stiffness values, we could then train a NN model to predict the scaffold stiffness with arbitrary combination of printing parameters. With this trained NN model, we could then simply use brute-force searching algorithm to find a set of printing parameters given any target stiffness. We also proceeded additional 3D printing and nanoindentation experiments to verify that the algorithm found parameters could indeed help us 3D print scaffolds with the desired stiffness. In addition, we also applied the same workflow on 2PP 3D printer instead of the DLP 3D printer, where the 3D printing parameters were changed to printing speed, laser current, and infill density (Fig. 4.1).

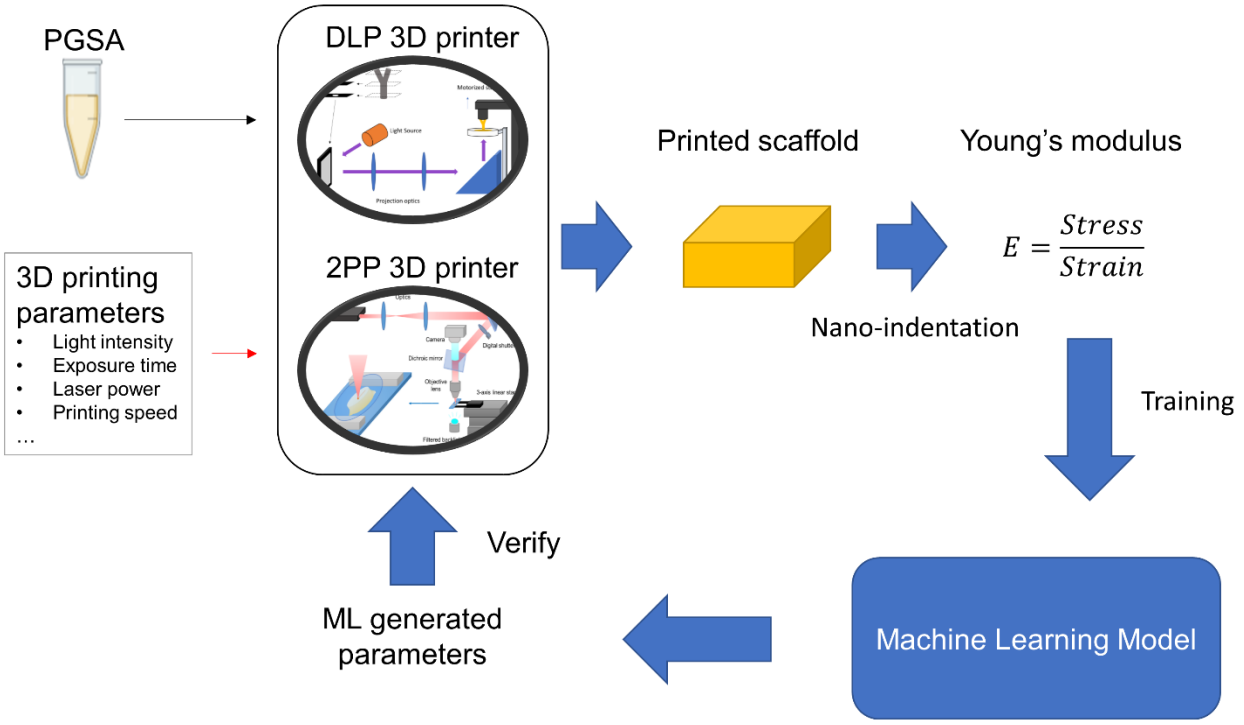

Fig. 4.1. Machine learning workflow for finding optimal 3D printing parameters to achieve arbitrary scaffold stiffness. The workflow shows the scaffold fabrication of PGSA material using DLP and 2PP 3D printers, obtaining Young's modulus through nano-indentation, machine learning model training using the stiffness data, and verifying the ML model generated 3D printing parameters for any desired stiffness by repeating the 3D printing and nano-indentation process with the generated parameters.

4.2 Material and method

4.2.1 Materials

The PGSA bioink for both DLP and 2PP 3D printing was composed of PGSA prepolymer, 4% (w/v) TPO photoinitiator, and 0.01% (w/v) tartrazine. The PGSA bioink for 2PP was further mixed with sodium fluorescein salt at 100:1 dilution as fluorescent tracer to trace the laser projection spot. The PGSA prepolymer that was used was from the same batch as synthesized and used in a previous published literature with the degree of acrylation of 57% [195].

4.2.2 Light-based 3D printing methods

This study utilized two light-based 3D printing systems, the DLP-based 3D printing system and the 2PP 3D printing system. The DLP-based 3D printing system was built in-lab with a 385 nm wavelength ultraviolet light source that projected onto a digital-micromirror-device (DMD) chip to form specific 2D patterns, then projected through a series of lenses and mirrors onto a vat of photopolymer material to trigger photopolymerization reaction and the exposed regions will form a layer of pattern (Fig. 2.1). While the motorized stage lifted the printing probe together with the printed structure, the remaining prepolymer solution would flow into the cavity and the next layer of fabrication would proceed and gradually form a full 3D structure. The DMD chip contains an array of 2560 by 1600 micro-mirrors, which would individually be flipped on or off, that would form patterns on the reflected light beam. While the DLP 3D printing method would typically fabricate complex multilayer 3D scaffolds, we only used it for fabricating a thin square slab for mechanical testing purpose, and therefore, the motorized stage was not used, and only a single layer of material was printed for every scaffold. The height of the scaffold was secured by using two PDMS spacers on the material vat which holds a coverslip on top. The bioink prepolymer material was sandwiched in between the coverslip and the material vat, which was a transparent petri dish. The petri dish was coated with a thin PDMS layer on the surface to prevent sticking with the polymerized material while the coverslip was treated with methacrylation to ensure a strong connection with polymer scaffold. Therefore, the 3D printed scaffold could be easily transferred and washed together with the methacrylated coverslip. For DLP printer, the light exposure time and light intensity were both essential printing parameters that would control the amount of energy exerted onto the bioink, thus directly correlated to the printed scaffold stiffness.

One of the goals of this study was to precisely modulate stiffness by changing these two printing parameters, namely exposure time and light intensity.

The custom built 2PP 3D printing system was composed of a 780 nm wavelength infrared femtosecond pulsing laser source to project laser through a set of optics and focused by an objective lens onto a removable printing platform. A custom computer software controls an electrical shutter on the laser path to turn on and off the laser, a 3-axis motorized stage system to precisely maneuver the printing platform, and a microscope camera to monitor the fabrication process and to trace the laser triggered fluorescent spot. Similar to the DLP printing platform, the 2PP removable printing platform was made of a glass slide base with two PDMS spacers on top to hold a methacrylated coverslip, while the bioink was loaded and sandwiched in between the coverslip and the glass slide (Fig. 3.1). Note the 2PP printing always started at the bottom surface of the coverslip, and gradually printed downwards into the material, so that the resulting printed scaffold would always connect to the coverslip on top. A 3D structure was printed with 2PP by turning on the laser to trigger polymerization at the focused spot and moving this focused spot through a certain toolpath that traversed through the whole 3D model. This motion was controlled by the stages to move the printing platform, which in turn also controls the motion of the focused laser spot. The motion speed while the laser was on was called printing speed, which was one of the essential parameters that controls the exposure time on the printed path. Faster printing speed would result in a shorter exposure time on the material, which means less energy has been exerted onto the material, thus affecting the resulting scaffold stiffness. Intuitively, the laser seed current which controls the laser power would also affect the printed scaffold stiffness. In addition, the way laser maneuvers the 3D model would also have a big effect on scaffold stiffness. One could imagine that a 3D model that was only loosely traversed with laser would be less stiff than a

thoroughly and densely traversed one. This density of traversal was described as infill density percentage and was one of the toolpath parameters for the open-source Slic3r software, which was used to generate laser traversal toolpath from any 3D CAD model. For the 2PP printer, our goal was to precisely modulate the printed scaffold stiffness by only adjusting the three parameters, printing speed, laser current, and infill density.

4.2.3 Mechanical testing

The Piuma nanoindenter (Optics11 Life, Netherlands) was used to measure the compressive stiffness or Young's modulus of the 3D printed samples. For DLP printer, 2 mm by 2mm by 300 μm rectangular slab specimens were fabricated at varying exposure time and light intensities as nanoindentation samples. For 2PP printer, 400 μm by 400 μm by 10 μm specimens were made under different printing speed, laser current, and infill density for nanoindentation testing. At least three indentations were tested on different surface regions of each sample, and the average measurement was used to represent the stiffness of this sample. For each condition, we repeatedly fabricated and tested scaffold stiffness using the same printing parameters, where the extreme outliers that were magnitude different were considered as fault samples caused by human error during fabrication or handling and were discarded. At least 5 non-fault samples were tested and collected for each condition. The average value for a condition could then be used as one data point for further statistical analysis and machine learning training process. Considering the difficulty to fabricate and test samples, there were only 8 different conditions collected for DLP printer and 9 different conditions collected for 2PP printer. The machine learning generated printing parameters were verified through the same process of 3D printing and testing.

4.2.4 Machine learning algorithm

Once the Young's Moduli of the samples printed under different printer parameters was obtained, a machine learning algorithm was applied to analyze the correlation between the printing parameters and the resulting scaffold stiffness. A NN regression algorithm was applied to predict the scaffold stiffness with arbitrary parameters for both the DLP printer and 2PP printer [17]. On top of that, a brute-force searching method was used to search for the most probable printing parameter combinations for any desired scaffold stiffness.

The NN regressor, also named as multi-layer perceptron, deep NN, artificial NN, or NN, was composed of multiple hidden layers and an output layer (Fig. 4.2). Each layer applied an affine transformation and rectifying linear unit (ReLU) activation function to the feature from the previous layer, and the resulting new features were sent to the next layer. The NN architecture took the printer parameters as input features, where there were three input parameters for the 2PP printer and two input parameters for the DLP printer, and the input features were sent through three hidden NN layers with 20, 10, and 5 hidden features respectively. After that, the last layer of hidden features went to the output layer and ended up with the output feature which was a scalar value representing the predicted Young's modulus [17].

The NN regressor was written in Python with the PyTorch package [183]. The NN model was trained using the nanoindentation data obtained from the corresponding printing parameters with mean square error loss function and the Adam stochastic optimization algorithm [184] for backpropagation. After training, the NN regressor could accurately predict the scaffold stiffness for arbitrary printing parameters. After obtaining a fully trained NN to predict the stiffness, a simple brute-force searching method was applied to find the printing parameter combinations that could reach any desired stiffness value (Fig. 4.2).

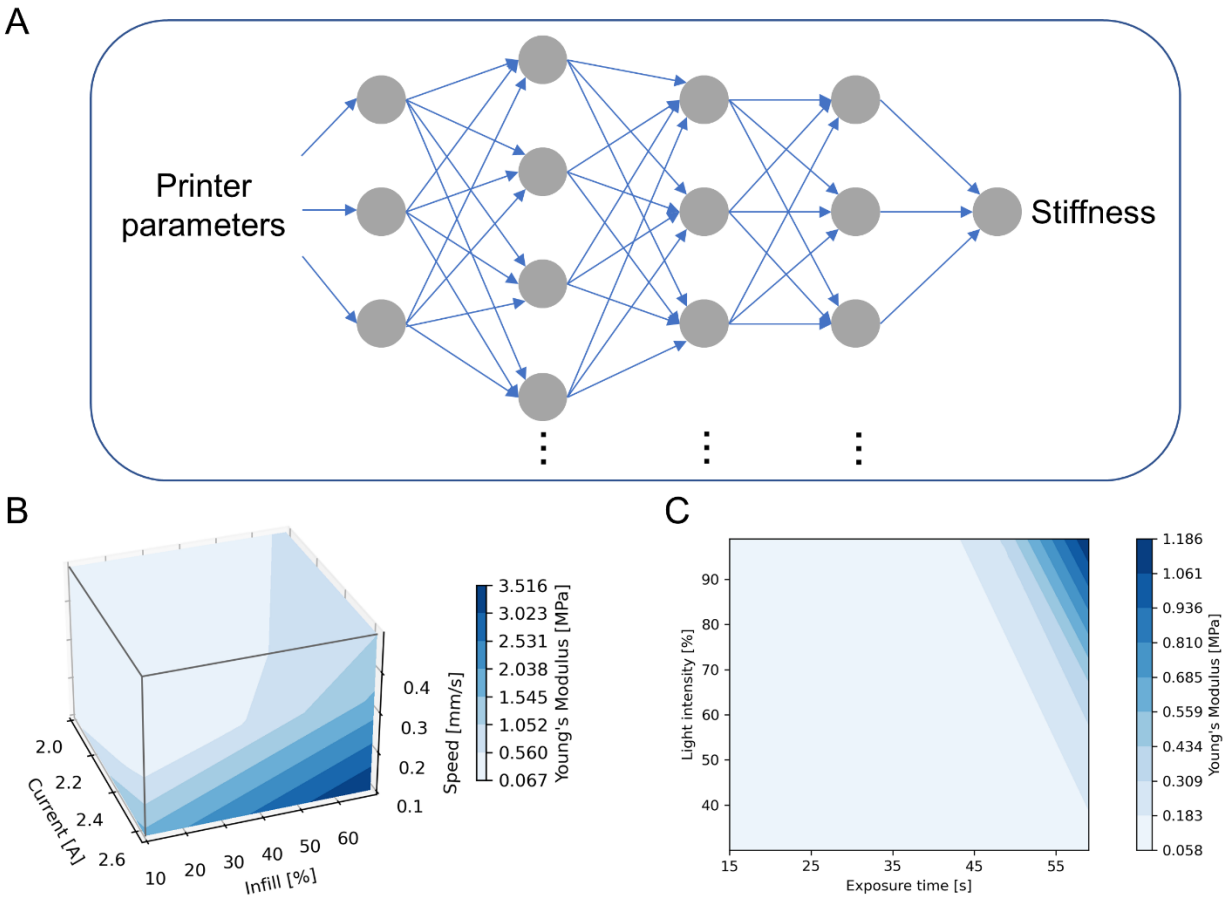

Fig. 4.2. Neural network architecture for the machine learning algorithm and the stiffness prediction results. (A) A four-layer NN architecture diagram with printer parameters as input and the printed scaffold stiffness as the output. (B) The 3D heat map representing the stiffness distribution predicted by the fully trained NN with respect to the changes of three 2PP printer parameters, namely printing speed, laser current, and infill density. (C) The 2D heat map representing the stiffness distribution predicted by the fully trained NN with respect to the changes of two DLP printer parameters, namely exposure time and light intensity.

Results and discussion

4.3 Result and discussion

4.3.1 Compressive stiffness measurements

For DLP-based 3D printer, we ran 8 conditions of experiments, each with a different set of printing parameters. The parameters we modified for DLP printer were exposure time and light intensity. We set the range of exposure time to be less than 60 seconds, and selected four evenly spaced exposure times 15, 30, 45, and 60 s to be examined. The light intensity was limited by our

light source, which had a peak light intensity of 18.5 mW/cm^2 on the printing platform. The peak intensity was set to be 100% intensity, and we chose 30%, 40%, 60%, 80%, and 100% for our sample scaffolds. Note 20% intensity was too low to observe any reasonable amount of polymerization, thus we chose the minimum light intensity to be at 30%. As we could intuitively imagine the exposure time and light intensity both would positively affect the scaffold stiffness, we chose the maximum exposure time 60 s and the maximum light intensity 100% to be the default value so to collect the maximum achievable stiffness value from the given parameter ranges. Following that, the 3 non-default different exposure times were paired with the default light intensity as 3 different conditions, while the 4 non-default light intensities were paired with the default exposure time as 4 different conditions. Together with the one default condition, a total of 8 different conditions were designed and experimented. The data collection in terms of 3D printing and nanoindentation were described in the previous method sections.

After all the experiments, we collected 8 unique data points for the DLP scaffold stiffness. The average stiffness values for the scaffolds printed with a constant 100% light intensity and 15, 30, and 45 s exposure time were tested to be 49.3 kPa, 67.1 kPa, and 236.0 kPa respectively. The stiffness values for the scaffolds printed with a constant 60 s exposure time while varying light intensity of 30%, 40%, 60%, and 80% were measured to be 148.3 kPa, 225.8 kPa, 337.5 kPa, 864.7 kPa. The default condition, 60 s exposure and 100% intensity, was given an average scaffold stiffness of 1.3 MPa. We could easily find that the scaffold stiffness values changed with the exposure time and light intensity in a highly non-linear fashion.

For 2PP printer, we executed 9 different conditions of experiments. The printing parameters we adjusted for 2PP printer were printing speed, laser current, and infill density. The printing speed was chosen to be from 100, 300, and 500 μm/s. The laser current was selected from

2, 2.25, 2.5, and 2.65 A (equivalent laser power of 40, 58.5, 80.5, and 95.4 mW/cm^2 respectively). The reason we capped the upper limit of the laser current at 2.65 was due to that higher laser current had a high chance of burning the PGSA bioink during the 3D printing process and causing abnormal air bubbles or damages at the fabricated scaffolds. For the infill density, we selected 10%, 30%, 50% and 70%. The 300 μm/s printing speed, 2.5 A laser current, and 50% infill density were selected as the default set of printing parameters. For each parameter, we also tested with the non-default values pairing with other two default parameters, resulting in a total of 8 different combinations. Together with the case with all three default parameters, we have total of 9 different parameter combinations to test.

After the 2PP printing and nanoindentation experiments, we collected 9 unique data points. The average stiffness values printed with a constant 2.5 A laser current and 50% infill density, while using 100 and 500 μm/s speeds were 2.7 MPa and 618.2kPa respectively. The average stiffness values printed with a constant 300 μm/s printing speed and 2.5A laser current, together with 2, 2.25, or 2.65 A laser current values were tested to be 396.7 kPa, 762.4 kPa, and 1.3 MPa respectively. The average stiffness values printed using a constant 300 μm/s printing speed and 2.5 A laser current, while having 10%, 30%, or 70% infill density would be 67.1 kPa, 396.5 kPa, and 1.6 MPa respectively. The default condition with 300 μm/s printing speed and 2.5 A laser current, and 50% infill density resulted in a scaffold stiffness of 942.8 kPa.

Note that for the default printing parameters, we were choosing middle values from the range of parameters in 2PP printer experiments, which was different from the strategy of the DLP printer experiments where we chose the highest values of all parameters to be the default. The reason was that we wanted to test out the generalizability of the machine learning model for both data collection strategies, where our DLP data collection strategy was trying to collect from the

higher stiffness side, while the 2PP data collection was starting from the middle parameter values. Although we could not accurately predict the final printed stiffness values just by looking at the printing parameters, having the heuristic assumptions could help us better understand the generalizability of the analysis of the resulting data considering the small amount of data points we could get.

4.3.2 Stiffness modulation assisted with machine learning

The previous experiments explored the feasibility of fabricating stiffness modulated 3D scaffolds given a variety of printing parameters. However, to fabricate scaffolds with user defined mechanical properties that were not attained given the standardized printing parameters, a NN-based algorithm was developed. After training the NN as described in section 4.2.4, the NN could then generate a mapping from arbitrary printing parameters to the expected scaffold stiffness for both the DLP printer and the 2PP printer (Fig. 4.2). Once the parameter-stiffness mapping was ready, a brute-force search on the mapping data could be applied to retrieve the printing parameters that could print a scaffold with user defined stiffness.

To verify that the NN informed printing parameters yielded accurate predictions for stiffness, the printing parameters for scaffolds with intended stiffness values of 500 kPa and 1.0 MPa were generated from the NN module on the DLP-based 3D printer. A similar approach was applied to the 2PP printer to print structures with intended stiffness values of 125 kPa, 1.5 MPa, and 3 MPa based on printing parameters generated from the NN module. Then, the accuracy of the developed NN module was analyzed by comparing the actual stiffness values of the scaffolds printed with the AI-generated printing parameters to the aforementioned intended stiffness values.

For the intended stiffness of 500 kPa for DLP-based printed scaffolds, the output AI-generated printing parameters were light intensity of 70% (12.95 mW/cm^2) and exposure time of

59 s. PGSA scaffolds that were DLP-printed with those AI-generated printing parameters were mechanically tested with nanoindentation and were shown to have Young's modulus value of 533.4 ± 24.6 kPa (Fig. 4.3B). For the intended stiffness of 1.0 MPa DLP-based printed scaffolds, the output AI-generated printing parameters were light intensity of 91% (16.84 mW/cm^2) and exposure time of 59 s. PGSA scaffolds that were DLP-printed with those AI-generated printing parameters were mechanically tested with nanoindentation and were shown to have Young's modulus value of 1.1 ± 0.1 MPa (Fig. 4.3B).

For the intended stiffness of 125 kPa for 2PP printed structures, the output AI-generated printing parameters were 36% infill, 2A printing current (40 mW/cm^2), and 0.36 mm/s printing speed. PGSA scaffolds that were 2PP-printed with those AI-generated printing parameters were mechanically tested with nanoindentation and were shown to have Young's modulus value of 133.2 ± 13.8 kPa (Fig. 4.3A). For the intended stiffness of 1.5 MPa for 2PP printed structures, the output AI-generated printing parameters were 60% infill, 2.29A printing current (61.8 mW/cm^2), and 0.22 mm/s printing speed. PGSA scaffolds that were 2PP-printed with those AI-generated printing parameters were mechanically tested with nanoindentation and were shown to have Young's modulus value of 1.5 ± 0.1 MPa (Fig. 4.3A). For the intended stiffness of 3.0 MPa for 2PP printed structures, the output AI-generated printing parameters were 63% infill, 2.64A printing current (94.3 mW/cm^2), and 0.14 mm/s printing speed. PGSA scaffolds that were 2PP-printed with those AI-generated printing parameters were mechanically tested with nanoindentation and were shown to have Young's modulus value of 2.8 ± 0.3 MPa (Fig. 4.3A).

To understand the amount of variance in the NN to predict material properties given a set of printing parameters, R^2 was calculated. The R^2 between NN predicted and measured stiffness was 0.95 for these experiments, meaning that high predictive capacity for mechanical properties

was accounted for by the machine learning model (Fig. 4.3C). To minimize the error between target stiffness *vs.* measured stiffness, one could potentially train the machine learning model with a larger number of printing parameters. One key aspect of this workflow is the ability to precisely control the stiffness of a 3D printed scaffold by printing it at specified parameters in a single step rather than requiring a more complex fabrication approach (i.e. multi material, multi-acrylation ratio). In addition, this workflow can be applied to other material systems that are compatible with light-based or femtosecond laser 3D printing systems.

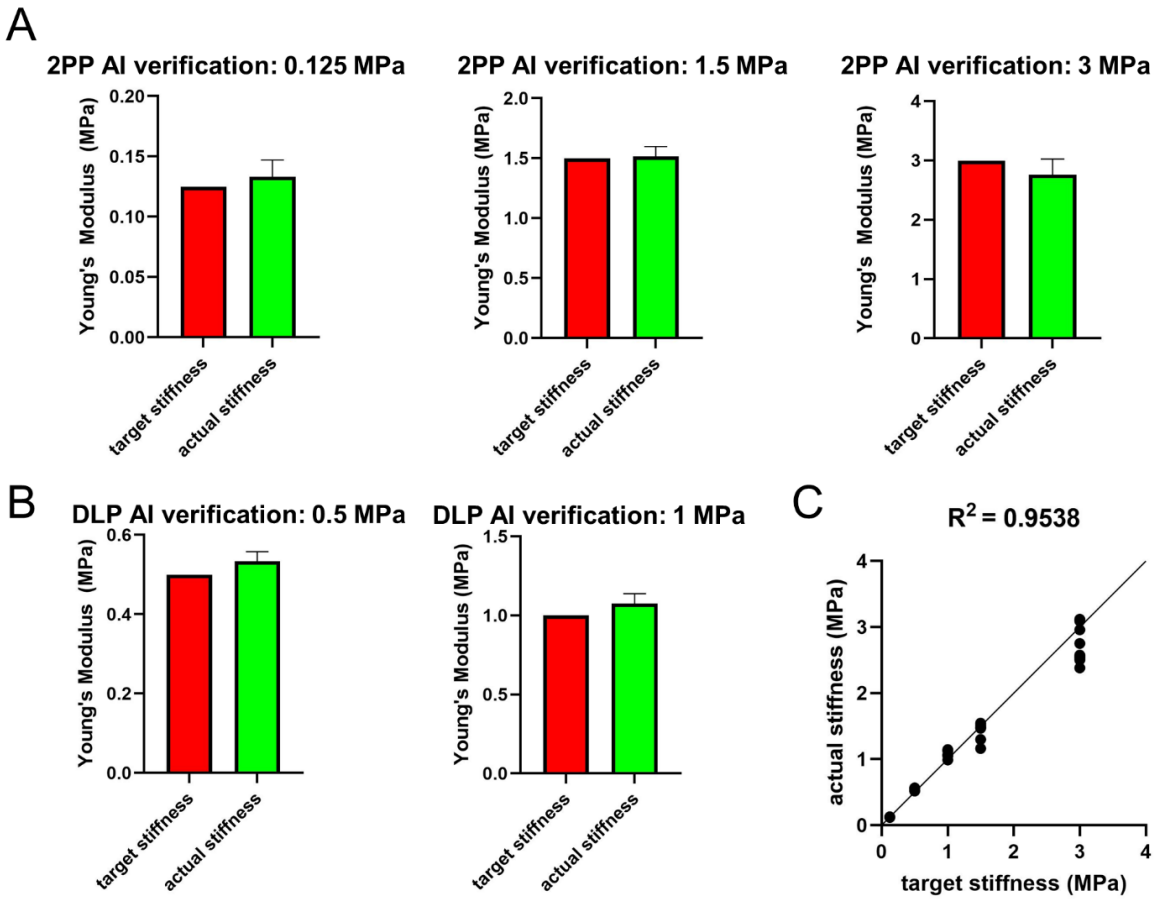

Fig. 4.3. Machine learning result verifications. (A) The comparison between the desired stiffness and the 2PP printed scaffold stiffness using machine learning generated printing parameters for 0.125MPa, 1.5MPa, and 3 MPa respectively. (B) The comparison between the desired stiffness and the DLP printed sample stiffness using machine learning generated printing parameters for 0.5MPa and 1 MPa respectively. (C) The uniformity plot where the points represent the actual measured stiffness of the printed samples versus the target stiffness, and the coefficient of determination for all the data points on the plot.

We have proved the ability of the trained ML model to help us fabricate precise stiffness modulated scaffolds. One extension of the application was to fabricate a gradient stiffness scaffold with each point of the material having modulated stiffness using our ML model. This could help us fabricate some functional materials that have a full customized stiffness distribution along a dedicated scaffold of complex geometry. One example would be 3D printing a muscle-tendon junction tissue mimicry that could assist disease modeling or wound recovery.

5 Conclusion

This study achieved precise PGSA scaffold stiffness control using DLP and 2PP 3D printing methods assisted by a NN-based machine learning algorithm. The NNs were trained from limited amount of data points collected by measuring DLP and 2PP printed scaffolds stiffness with nanoindentation, and were able to precisely predict unseen stiffness values for an arbitrary set of printing parameters. Together with a brute-force searching method, the machine learning algorithm was able to suggest a reasonable combination of printing parameters that could achieve any target stiffness within the feasible range. Assisted by this machine learning algorithm, our DLP and 2PP printers could fabricate stiffness modulated PGSA scaffolds from microstructures up to millimeter ranges by only modifying printing parameters on-the-fly. Furthermore, this machine learning workflow could be easily transferred and applied to other materials and 3D printing systems following the same data collection and NN training methods. This machine learning approach would extend the future study of fine mechanical property-controlled fabrication techniques, potentially generalize simultaneous geometry and mechanical property modulation, which would open great opportunities for organoid fabrication and many tissue engineering applications.

Acknowledgements

Chapter 4, in part, has been submitted for publication entitled, “Multi-modal Vat Photopolymerization for Microscale Modulation of Scaffold Stiffness Assisted via Machine Learning”, W. Kiratitanaporn, J. Guan, D. Berry, A. Lao, S. Chen, as it may appear in Additive Manufacturing 2023. The dissertation author was one of the primary researchers and a co-first author of this paper.

This work was supported in part by grants to S.C. from the NIH (R21ES034455) and National Science Foundation (NSF) (1907434, 2135720, 2026236). This work was performed in part at the San Diego Nanotechnology Infrastructure (SDNI) of UCSD, a member of the National Nanotechnology Coordinated Infrastructure, which is supported by the National Science Foundation (Grant ECCS-2025752).

Chapter 5 Conclusions and Future Perspectives

Machine learning has brought much recent attention by achieving difficult tasks through analyzation of big data. The 3D printing and bioprinting fields however, were struggling with many difficult tasks such as improvement of fabrication precision, defect prevention, structure mechanical property control, and so on. While recent research has already been exploring the use of ML on assisting 3D printing technologies and solving these tasks, many problems still remain understudied.

My dissertation focuses on exploring the future of intelligent 3D bioprinting, for both precise geometry control as well as mechanical property modulation on light-based bioprinting technologies, using ML algorithms. My study aimed to explore two general directions of applying machine learning to achieve intelligent bioprinting.

One major direction of my study was to apply a specifically designed complex ML algorithm to fully utilize the limited amount of data from a particular bioprinting application and use this specific ML algorithm to solve a dedicated bioprinting task when the answer was in a high dimensional vector space that was difficult to search with traditional algorithms. As an example, we explored one challenge in the DLP-based bioprinting that cell-encapsulated bioinks would induce strong light scattering effect and thus severely reduce the printing fidelity. When cells in the bioink scatters light during the light triggered photopolymerization process, the expected exposure site would get reduced energy while the surrounding unwanted positions would absorb the extra energy and start solidifying, making the final printed scaffolds looking different from the initial design. This challenge could be potentially solved by finding a modified input mask for the DLP printer so that the mask would compensate for the cell-induced scattering effect and result in a printed structure that matches the target design. The difficulty was that the DLP mask was of

extremely high dimensions which would be not practical to solve by typical searching algorithms, especially considering the redundant search time needed for each and every different target structure design. In my study, I collected 32 DLP printed samples using bioink mixed with 10 M cells per ml, applied specially designed data augmentation algorithm, and developed and trained a U-Net style CNN-based ML model to generated modified DLP input masks so that the resulting printed scaffold would better match the initial target design. This study solved this challenge in bioprinting, by compensating the cell-induced light scattering problem in DLP-based bioprinting with a dedicated ML algorithm. This direction of ML application also proved that sophisticatedly engineered ML algorithms could achieve dedicated bioprinting tasks, with high dimensional search space, even when there was limited amount of available data, which was very common in the bioprinting field due to the long fabrication time and expensive biological materials.

The other major direction of my study was to apply a highly generalizable ML algorithm to solve a general and transferable bioprinting task. As an example of this direction for applying ML on bioprinting, we demonstrated a task to modulate scaffold mechanical property by adjusting 3D printing parameters using a simple ML algorithm. More specifically, we use a 3-layer NN-based ML algorithm with brute-force searching to help adjust 3D printing parameters for both DLP and 2PP bioprinters and achieved precise PGSA scaffold stiffness modulation. Note that this task was very general, and our ML algorithm could be easily transferred to study the same type of problems with a different bioprinter, bioink material, and target scaffold properties. Using such a general ML algorithm, we successfully solved one particular task in this type of challenges, which proves that with the same workflow and the same ML algorithm, we have the potential to easily beat down a broad range of bioprinting challenges of the same nature.

Both ML algorithms demonstrated not only a task-specific solution, but also a task-free generalizable ML workflow, emphasizing two ways to solve future bioprinting challenges with ML. The challenges with a specific high dimensional search space would be suggested to follow the first route to engineer a dedicated ML which involves prior knowledge to fully utilize the limited amount of bioprinting data. The challenges that share common nature and has a relatively smaller dimensions of parameter space could then rely on simple generalizable ML workflows, which could greatly speed up the problem-solving process, due to the removal of algorithm developing and researching which was previously required for all bioprinting tasks. The two high-level directions for applying ML in bioprinting could help enable a more intelligent future of bioprinting.

Aside from the ML assisted bioprinting, we also built a custom 2PP printer which was the state-of-the-art highest precision 3D printing technology. By developing the 2PP bioprinter, we demonstrated a range of microstructure fabrication with different biocompatible photopolymers, which enhanced further study of high precision bioprinting. Together with the ML algorithms we developed, we were aiming to step into an intelligent bioprinting technology for finer geometry as well as precise mechanical property controls of the biocompatible material fabrication.

REFERENCES

[1] R.Y. Zhong, X. Xu, E. Klotz, S.T. Newman, Intelligent Manufacturing in the Context of Industry 4.0: A Review, Engineering. 3 (2017) 616–630. https://doi.org/10.1016/J.ENG.2017.05.015.

[2] J. Lee, B. Bagheri, H.-A. Kao, A Cyber-Physical Systems architecture for Industry 4.0-based manufacturing systems, Manufacturing Letters. 3 (2015) 18–23. https://doi.org/10.1016/j.mfglet.2014.12.001.

[3] A.G. Frank, L.S. Dalenogare, N.F. Ayala, Industry 4.0 technologies: Implementation patterns in manufacturing companies, International Journal of Production Economics. 210 (2019) 15–26. https://doi.org/10.1016/j.ijpe.2019.01.004.

[4] J. Zhou, P. Li, Y. Zhou, B. Wang, J. Zang, L. Meng, Toward New-Generation Intelligent Manufacturing, Engineering. 4 (2018) 11–20. https://doi.org/10.1016/j.eng.2018.01.002.

[5] F.W. Baumann, A. Sekulla, M. Hassler, B. Himpel, M. Pfeil, Trends of machine learning in additive manufacturing, IJRAPIDM. 7 (2018) 310. https://doi.org/10.1504/IJRAPIDM.2018.095788.

[6] C. Yu, J. Jiang, A perspective on Using Machine Learning in 3D Bioprinting, Int J Bioprint. 6 (2020). https://doi.org/10.18063/ijb.v6i1.253.

[7] X. Qi, G. Chen, Y. Li, X. Cheng, C. Li, Applying Neural-Network-Based Machine Learning to Additive Manufacturing: Current Applications, Challenges, and Future Perspectives, Engineering. 5 (2019) 721–729. https://doi.org/10.1016/j.eng.2019.04.012.

[8] G.D. Goh, S.L. Sing, W.Y. Yeong, A review on machine learning in 3D printing: applications, potential, and challenges, Artif Intell Rev. (2020). https://doi.org/10.1007/s10462-020-09876-9.

[9] W. Zhu, X. Ma, M. Gou, D. Mei, K. Zhang, S. Chen, 3D printing of functional biomaterials for tissue engineering, Current Opinion in Biotechnology. 40 (2016) 103–112. https://doi.org/10.1016/j.copbio.2016.03.014.

[10] H.H. Hwang, W. Zhu, G. Victorine, N. Lawrence, S. Chen, 3D-Printing of Functional Biomedical Microdevices via Light- and Extrusion-Based Approaches, Small Methods. 2 (2018) 1700277. https://doi.org/10.1002/smtd.201700277.

[11] M. Vaezi, H. Seitz, S. Yang, A review on 3D micro-additive manufacturing technologies, Int J Adv Manuf Technol. 67 (2013) 1957–1957. https://doi.org/10.1007/s00170-013-4962-5.

[12] T.D. Ngo, A. Kashani, G. Imbalzano, K.T.Q. Nguyen, D. Hui, Additive manufacturing (3D printing): A review of materials, methods, applications and challenges, Composites Part B: Engineering. 143 (2018) 172–196. https://doi.org/10.1016/j.compositesb.2018.02.012.

[13] P.K. Gokuldoss, S. Kolla, J. Eckert, Additive Manufacturing Processes: Selective Laser Melting, Electron Beam Melting and Binder Jetting—Selection Guidelines, Materials. 10 (2017) 672. https://doi.org/10.3390/ma10060672.

[14] N. Guo, M.C. Leu, Additive manufacturing: technology, applications and research needs, Front. Mech. Eng. 8 (2013) 215–243. https://doi.org/10.1007/s11465-013-0248-8.

[15] S. You, K. Miller, S. Chen, Chapter 1. Microstereolithography, in: D.-W. Cho (Ed.), Biomaterials Science Series, Royal Society of Chemistry, Cambridge, 2019: pp. 1–21. https://doi.org/10.1039/9781788012683-00001.

[16] W.E. Frazier, Metal Additive Manufacturing: A Review, J. of Materi Eng and Perform. 23 (2014) 1917–1928. https://doi.org/10.1007/s11665-014-0958-z.

[17] I. Goodfellow, Y. Bengio, A. Courville, Deep Learning, United Kingdom:MIT Press, 2016.

[18] M.I. Jordan, T.M. Mitchell, Machine learning: Trends, perspectives, and prospects, Science. 349 (2015) 255–260. https://doi.org/10.1126/science.aaa8415.

[19] A. Dey, Machine Learning Algorithms: A Review, 7 (2016) 6.

[20] C.M. Bishop, Pattern recognition and machine learning, springer, 2006.

[21] K.P. Murphy, Machine learning: a probabilistic perspective, MIT press, 2012.

[22] E. Chong, C. Han, F.C. Park, Deep learning networks for stock market analysis and prediction: Methodology, data representations, and case studies, Expert Systems with Applications. 83 (2017) 187–205. https://doi.org/10.1016/j.eswa.2017.04.030.

[23] Y. Guo, Y. Liu, A. Oerlemans, S. Lao, S. Wu, M.S. Lew, Deep learning for visual understanding: A review, Neurocomputing. 187 (2016) 27–48. https://doi.org/10.1016/j.neucom.2015.09.116.

[24] A. Voulodimos, N. Doulamis, A. Doulamis, E. Protopapadakis, Deep Learning for Computer Vision: A Brief Review, Computational Intelligence and Neuroscience. 2018 (2018) e7068349. https://doi.org/10.1155/2018/7068349.

[25] A.E. Sallab, M. Abdou, E. Perot, S. Yogamani, Deep Reinforcement Learning framework for Autonomous Driving, Electronic Imaging. 2017 (2017) 70–76. https://doi.org/10.2352/ISSN.2470-1173.2017.19.AVM-023.

[26] K.H. Huebner, D.L. Dewhirst, D.E. Smith, T.G. Byrom, The Finite Element Method for Engineers, John Wiley & Sons, 2001.

[27] I. Zein, D.W. Hutmacher, K.C. Tan, S.H. Teoh, Fused deposition modeling of novel scaffold architectures for tissue engineering applications, Biomaterials. 23 (2002) 1169–1185. https://doi.org/10.1016/S0142-9612(01)00232-0.

[28] D.L. Cohen, E. Malone, H. Lipson, L.J. Bonassar, Direct Freeform Fabrication of Seeded Hydrogels in Arbitrary Geometries, Tissue Engineering. 12 (2006) 1325–1335. https://doi.org/10.1089/ten.2006.12.1325.

[29] S. Maruo, T. Saeki, Femtosecond laser direct writing of metallic microstructures by photoreduction of silver nitrate in a polymer matrix, Opt. Express. 16 (2008) 1174. https://doi.org/10.1364/OE.16.001174.

[30] S. Kumar, Selective laser sintering: A qualitative and objective approach, JOM. 55 (2003) 43–47. https://doi.org/10.1007/s11837-003-0175-y.

[31] S. You, J. Li, W. Zhu, C. Yu, D. Mei, S. Chen, Nanoscale 3D printing of hydrogels for cellular tissue engineering, J. Mater. Chem. B. 6 (2018) 2187–2197. https://doi.org/10.1039/C8TB00301G.

[32] P. Soman, B.T.D. Tobe, J.W. Lee, A.A.M. Winquist, I. Singec, K.S. Vecchio, E.Y. Snyder, S. Chen, Three-dimensional scaffolding to investigate neuronal derivatives of human embryonic stem cells, Biomed Microdevices. 14 (2012) 829–838. https://doi.org/10.1007/s10544-012-9662-7.

[33] W. Zhu, K.R. Tringale, S.A. Woller, S. You, S. Johnson, H. Shen, J. Schimelman, M. Whitney, J. Steinauer, W. Xu, T.L. Yaksh, Q.T. Nguyen, S. Chen, Rapid continuous 3D printing of customizable peripheral nerve guidance conduits, Materials Today. 21 (2018) 951–959. https://doi.org/10.1016/j.mattod.2018.04.001.

[34] J. Shapiro, Genetic Algorithms in Machine Learning, in: G. Paliouras, V. Karkaletsis, C.D. Spyropoulos (Eds.), Machine Learning and Its Applications: Advanced Lectures, Springer, Berlin, Heidelberg, 2001: pp. 146–168. https://doi.org/10.1007/3-540-44673-7_7.

[35] Y. Zhang, S. Wang, G. Ji, A Comprehensive Survey on Particle Swarm Optimization Algorithm and Its Applications, Mathematical Problems in Engineering. 2015 (2015) 1–38. https://doi.org/10.1155/2015/931256.

[36] S.P. Jena, S. Mahapatra, Application of Taguchi Method for Process Optimization on Different Fields of Engineering- A review, (2019) 6.

[37] B. Shahriari, K. Swersky, Z. Wang, R.P. Adams, N. de Freitas, Taking the Human Out of the Loop: A Review of Bayesian Optimization, Proceedings of the IEEE. 104 (2016) 148–175. https://doi.org/10.1109/JPROC.2015.2494218.

[38] S. Boyd, L. Vandenberghe, Convex Optimization, Cambridge University Press, 2004.

[39] V.V. Estrela, H.A. Magalhães, O. Saotome, Total Variation Applications in Computer Vision, (n.d.) 24.

[40] S. You, J. Guan, J. Alido, H.H. Hwang, R. Yu, L. Kwe, H. Su, S. Chen, Mitigating Scattering Effects in Light-based 3D Printing Using Machine Learning, Journal of Manufacturing Science and Engineering. (2020) 1–23. https://doi.org/10.1115/1.4046986.

[41] A. Singh, N. Thakur, A. Sharma, A review of supervised machine learning algorithms, in: 2016 3rd International Conference on Computing for Sustainable Global Development (INDIACom), 2016: pp. 1310–1315.

[42] P.C. Sen, M. Hajra, M. Ghosh, Supervised Classification Algorithms in Machine Learning: A Survey and Review, in: J.K. Mandal, D. Bhattacharya (Eds.), Emerging Technology in Modelling and Graphics, Springer, Singapore, 2020: pp. 99–111. https://doi.org/10.1007/978-981-13-7403-6_11.

[43] M.E. Celebi, K. Aydin, eds., Unsupervised Learning Algorithms, Springer International Publishing, Cham, 2016. https://doi.org/10.1007/978-3-319-24211-8.

[44] K. Arulkumaran, M.P. Deisenroth, M. Brundage, A.A. Bharath, Deep Reinforcement Learning: A Brief Survey, IEEE Signal Processing Magazine. 34 (2017) 26–38. https://doi.org/10.1109/MSP.2017.2743240.

[45] M. Botvinick, S. Ritter, J.X. Wang, Z. Kurth-Nelson, C. Blundell, D. Hassabis, Reinforcement Learning, Fast and Slow, Trends in Cognitive Sciences. 23 (2019) 408–422. https://doi.org/10.1016/j.tics.2019.02.006.

[46] V. Cheplygina, M. de Bruijne, J.P.W. Pluim, Not-so-supervised: A survey of semi-supervised, multi-instance, and transfer learning in medical image analysis, Medical Image Analysis. 54 (2019) 280–296. https://doi.org/10.1016/j.media.2019.03.009.

[47] Z.-H. Zhou, A brief introduction to weakly supervised learning, National Science Review. 5 (2018) 44–53. https://doi.org/10.1093/nsr/nwx106.

[48] M.A. Nielsen, Neural networks and deep learning, Determination press San Francisco, CA, 2015.

[49] C.C. Aggarwal, Neural networks and deep learning, Springer, 2018.

[50] K. Hornik, Approximation capabilities of multilayer feedforward networks, Neural Networks. 4 (1991) 251–257. https://doi.org/10.1016/0893-6080(91)90009-T.

[51] A. Choromanska, M. Henaff, M. Mathieu, G.B. Arous, Y. LeCun, The loss surfaces of multilayer networks, in: Artificial Intelligence and Statistics, 2015: pp. 192–204.

[52] M.K. Thompson, G. Moroni, T. Vaneker, G. Fadel, R.I. Campbell, I. Gibson, A. Bernard, J. Schulz, P. Graf, B. Ahuja, F. Martina, Design for Additive Manufacturing: Trends, opportunities, considerations, and constraints, CIRP Annals. 65 (2016) 737–760. https://doi.org/10.1016/j.cirp.2016.05.004.

[53] N. Boddeti, D.W. Rosen, K. Maute, M.L. Dunn, Multiscale optimal design and fabrication of laminated composites, Composite Structures. 228 (2019) 111366. https://doi.org/10.1016/j.compstruct.2019.111366.

[54] I.F. Ituarte, N. Boddeti, V. Hassani, M.L. Dunn, D.W. Rosen, Design and additive manufacture of functionally graded structures based on digital materials, Additive Manufacturing. 30 (2019) 100839. https://doi.org/10.1016/j.addma.2019.100839.

[55] A. Noriega, D. Blanco, B.J. Alvarez, A. Garcia, Dimensional accuracy improvement of FDM square cross-section parts using artificial neural networks and an optimization algorithm, Int J Adv Manuf Technol. 69 (2013) 2301–2313. https://doi.org/10.1007/s00170-013-5196-2.

[56] Q. Huang, Y. Wang, M. Lyu, W. Lin, Shape Deviation Generator–A Convolution Framework for Learning and Predicting 3-D Printing Shape Accuracy, IEEE Transactions on Automation Science and Engineering. (2020) 1–15. https://doi.org/10.1109/TASE.2019.2959211.

[57] M. Zhao, G. Xiong, X. Shang, C. Liu, Z. Shen, H. Wu, Nonlinear Deformation Prediction and Compensation for 3D Printing Based on CAE Neural Networks, in: 2019 IEEE 15th International Conference on Automation Science and Engineering (CASE), 2019: pp. 667–672. https://doi.org/10.1109/COASE.2019.8843210.

[58] Z. Shen, X. Shang, M. Zhao, X. Dong, G. Xiong, F.-Y. Wang, A Learning-Based Framework for Error Compensation in 3D Printing, IEEE Transactions on Cybernetics. 49 (2019) 4042–4050. https://doi.org/10.1109/TCYB.2019.2898553.

[59] S. Chowdhury, S. Anand, Artificial Neural Network Based Geometric Compensation for Thermal Deformation in Additive Manufacturing Processes, in: American Society of Mechanical Engineers Digital Collection, 2016. https://doi.org/10.1115/MSEC2016-8784.

[60] S. Chowdhury, K. Mhapsekar, S. Anand, Part Build Orientation Optimization and Neural Network-Based Geometry Compensation for Additive Manufacturing Process, J. Manuf. Sci. Eng. 140 (2018). https://doi.org/10.1115/1.4038293.

[61] A. Koeppe, C.A. Hernandez Padilla, M. Voshage, J.H. Schleifenbaum, B. Markert, Efficient numerical modeling of 3D-printed lattice-cell structures using neural networks, Manufacturing Letters. 15 (2018) 147–150. https://doi.org/10.1016/j.mfglet.2018.01.002.

[62] A. Khadilkar, J. Wang, R. Rai, Deep learning–based stress prediction for bottom-up SLA 3D printing process, Int J Adv Manuf Technol. 102 (2019) 2555–2569. https://doi.org/10.1007/s00170-019-03363-4.

[63] Y. Fan, B. Feng, L. Yang, Y. Zhang, Application of artificial neural network optimization for resilient ceramic parts fabricated by direct ink writing, International Journal of Applied Ceramic Technology. 17 (2020) 217–226. https://doi.org/10.1111/ijac.13394.

[64] Y. Yang, M. He, L. Li, Power consumption estimation for mask image projection stereolithography additive manufacturing using machine learning based approach, Journal of Cleaner Production. 251 (2020) 119710. https://doi.org/10.1016/j.jclepro.2019.119710.

[65] J. Qin, Y. Liu, R. Grosvenor, F. Lacan, Z. Jiang, Deep learning-driven particle swarm optimisation for additive manufacturing energy optimisation, Journal of Cleaner Production. 245 (2020) 118702. https://doi.org/10.1016/j.jclepro.2019.118702.

[66] J. Qin, Y. Liu, R. Grosvenor, Multi-source data analytics for AM energy consumption prediction, Advanced Engineering Informatics. 38 (2018) 840–850. https://doi.org/10.1016/j.aei.2018.10.008.

[67] J. Huang, T.-H. Kwok, C. Zhou, W. Xu, Surfel convolutional neural network for support detection in additive manufacturing, Int J Adv Manuf Technol. 105 (2019) 3593–3604. https://doi.org/10.1007/s00170-019-03792-1.

[68] C.M. Hamel, D.J. Roach, K.N. Long, F. Demoly, M.L. Dunn, H.J. Qi, Machine-learning based design of active composite structures for 4D printing, Smart Mater. Struct. 28 (2019) 065005. https://doi.org/10.1088/1361-665X/ab1439.

[69] S. Wu, C.M. Hamel, Q. Ze, F. Yang, H.J. Qi, R. Zhao, Evolutionary Algorithm-Guided Voxel-Encoding Printing of Functional Hard-Magnetic Soft Active Materials, Advanced Intelligent Systems. 2 (2020) 2000060. https://doi.org/10.1002/aisy.202000060.

[70] C. McComb, C. Murphey, N. Meisel, T.W. Simpson, Predicting Part Mass, Required Support Material, and Build Time Via Autoencoded Voxel Patterns, in: Austin, TX, Aug, 2018: pp. 1–15.

[71] F. Caiazzo, A. Caggiano, Laser Direct Metal Deposition of 2024 Al Alloy: Trace Geometry Prediction via Machine Learning, Materials. 11 (2018) 444. https://doi.org/10.3390/ma11030444.

[72] Parametric appraisal of fused deposition modelling process using the grey Taguchi method - A K Sood, R K Ohdar, S S Mahapatra, 2010, (n.d.). https://journals.sagepub.com/doi/10.1243/09544054JEM1565 (accessed April 5, 2020).

[73] A. Equbal, A.K. Sood, S. s. Mahapatra, Prediction of dimensional accuracy in fused deposition modelling: a fuzzy logic approach, International Journal of Productivity and Quality Management. 7 (2010) 22–43. https://doi.org/10.1504/IJPQM.2011.03773.

[74] D. Chen, Re-perceive 3D printing with Artificial Intelligence, in: Sousa, JP, Xavier, JP and Castro Henriques, G (Eds.), Architecture in the Age of the 4th Industrial Revolution - Proceedings of the 37th ECAADe and 23rd SIGraDi Conference - Volume 1, University of Porto, Porto, Portugal, 11-13 September 2019, Pp. 443-450, CUMINCAD, 2019. http://papers.cumincad.org/cgi-bin/works/BrowseTree=series=AZ/Show?ecaadesigradi2019_034 (accessed April 5, 2020).

[75] M.A. Conev, M.E. Litsa, M.M. Perez, D.M. Diba, D.A.G. Mikos, P.L. Kavraki, Machine Learning Guided 3D Printing of Tissue Engineering Scaffolds, Https://Home.Liebertpub.Com/Tea. (2020). https://doi.org/10.1089/ten.TEA.2020.0191.

[76] T.I. Zohdi, Dynamic thermomechanical modeling and simulation of the design of rapid free-form 3D printing processes with evolutionary machine learning, Computer Methods in Applied Mechanics and Engineering. 331 (2018) 343–362. https://doi.org/10.1016/j.cma.2017.11.030.

[77] Z. Jiang, Y. Liu, H. Chen, Q. Hu, Optimization of Process Parameters for Biological 3D Printing Forming Based on BP Neural Network and Genetic Algorithm., in: ISPE CE, 2014: pp. 351–358.

[78] S.H. Lee, W.S. Park, H.S. Cho, W. Zhang, M.C. Leu, A neural network approach to the modelling and analysis of stereolithography processes, Proceedings of the Institution of Mechanical Engineers, Part B: Journal of Engineering Manufacture. 215 (2001) 1719–1733. https://doi.org/10.1177/095440540121501206.

[79] H. He, Y. Yang, Y. Pan, Machine learning for continuous liquid interface production: Printing speed modelling, Journal of Manufacturing Systems. 50 (2019) 236–246. https://doi.org/10.1016/j.jmsy.2019.01.004.

[80] A.K. Sood, R.K. Ohdar, S.S. Mahapatra, Experimental investigation and empirical modelling of FDM process for compressive strength improvement, Journal of Advanced Research. 3 (2012) 81–90. https://doi.org/10.1016/j.jare.2011.05.001.

[81] A.K. Sood, A. Equbal, V. Toppo, R.K. Ohdar, S.S. Mahapatra, An investigation on sliding wear of FDM built parts, CIRP Journal of Manufacturing Science and Technology. 5 (2012) 48–54. https://doi.org/10.1016/j.cirpj.2011.08.003.

[82] W. Zhang, A. Mehta, P.S. Desai, C.F. Higgs, Machine learning enabled powder spreading process map for metal additive manufacturing (AM), in: Int. Solid Free Form Fabr. Symp. Austin, TX, 2017: pp. 1235–1249.

[83] W. Rong-Ji, L. Xin-hua, W. Qing-ding, W. Lingling, Optimizing process parameters for selective laser sintering based on neural network and genetic algorithm, Int J Adv Manuf Technol. 42 (2009) 1035–1042. https://doi.org/10.1007/s00170-008-1669-0.

[84] H. Chen, Y.F. Zhao, Learning Algorithm Based Modeling and Process Parameters Recommendation System for Binder Jetting Additive Manufacturing Process, in: American Society of Mechanical Engineers Digital Collection, 2016. https://doi.org/10.1115/DETC2015-47627.

[85] Y. Li, Y. Sun, Q. Han, G. Zhang, I. Horváth, Enhanced beads overlapping model for wire and arc additive manufacturing of multi-layer multi-bead metallic parts, Journal of Materials Processing Technology. 252 (2018) 838–848. https://doi.org/10.1016/j.jmatprotec.2017.10.017.

[86] K. Aoyagi, H. Wang, H. Sudo, A. Chiba, Simple method to construct process maps for additive manufacturing using a support vector machine, Additive Manufacturing. 27 (2019) 353–362. https://doi.org/10.1016/j.addma.2019.03.013.

[87] A. Menon, B. Póczos, A.W. Feinberg, N.R. Washburn, Optimization of Silicone 3D Printing with Hierarchical Machine Learning, 3D Printing and Additive Manufacturing. 6 (2019) 181–189. https://doi.org/10.1089/3dp.2018.0088.

[88] M. Mozaffar, A. Paul, R. Al-Bahrani, S. Wolff, A. Choudhary, A. Agrawal, K. Ehmann, J. Cao, Data-driven prediction of the high-dimensional thermal history in directed energy deposition processes via recurrent neural networks, Manufacturing Letters. 18 (2018) 35–39. https://doi.org/10.1016/j.mfglet.2018.10.002.

[89] K. Ren, Y. Chew, Y.F. Zhang, J.Y.H. Fuh, G.J. Bi, Thermal field prediction for laser scanning paths in laser aided additive manufacturing by physics-based machine learning, Computer Methods in Applied Mechanics and Engineering. 362 (2020) 112734. https://doi.org/10.1016/j.cma.2019.112734.

[90] X. Shen, J. Yao, Y. Wang, J. Yang, Density Prediction of Selective Laser Sintering Parts Based on Artificial Neural Network, in: F.-L. Yin, J. Wang, C. Guo (Eds.), Advances in Neural Networks - ISNN 2004, Springer, Berlin, Heidelberg, 2004: pp. 832–840. https://doi.org/10.1007/978-3-540-28648-6_133.

[91] R.-J. Wang, J. Li, F. Wang, X. Li, Qingding Wu, ANN model for the prediction of density in Selective Laser Sintering, International Journal of Manufacturing Research. 4 (2009) 362–373. https://doi.org/10.1504/IJMR.2009.026579.

[92] M. Malviya, K. Desai, Build Orientation Optimization for Strength Enhancement of FDM Parts Using Machine Learning based Algorithm, CADandA. 17 (2019) 783–796. https://doi.org/10.14733/cadaps.2020.783-796.

[93] D. Yadav, D. Chhabra, R. Kumar Garg, A. Ahlawat, A. Phogat, Optimization of FDM 3D printing process parameters for multi-material using artificial neural network, Materials Today: Proceedings. 21 (2020) 1583–1591. https://doi.org/10.1016/j.matpr.2019.11.225.

[94] Prediction of Sintering Strength for Selective Laser Sintering of Polystyrene Using Artificial Neural Network--《Journal of Donghua University(English Edition)》2015年05期, (n.d.). http://www.cnki.com.cn/Article/CJFDTotal-DHDY201505022.htm (accessed April 5, 2020).

[95] C. Junwen, Z. Gang, Z. Hua, Energy Consumption Prediction of Fused Deposition 3D Printer Based on Improved Regularized BP Neural Network, IOP Conf. Ser.: Earth Environ. Sci. 295 (2019) 032001. https://doi.org/10.1088/1755-1315/295/3/032001.

[96] J. Munguía, J. Ciurana, C. Riba, Neural-network-based model for build-time estimation in selective laser sintering, Proceedings of the Institution of Mechanical Engineers, Part B: Journal of Engineering Manufacture. 223 (2009) 995–1003. https://doi.org/10.1243/09544054JEM1324.

[97] M. Wu, V.V. Phoha, Y.B. Moon, A.K. Belman, Detecting Malicious Defects in 3D Printing Process Using Machine Learning and Image Classification, in: American Society of

Mechanical Engineers Digital Collection, 2017. https://doi.org/10.1115/IMECE2016-67641.

[98] U. Delli, S. Chang, Automated Process Monitoring in 3D Printing Using Supervised Machine Learning, Procedia Manufacturing. 26 (2018) 865–870. https://doi.org/10.1016/j.promfg.2018.07.111.

[99] Z. Jin, Z. Zhang, G.X. Gu, Autonomous in-situ correction of fused deposition modeling printers using computer vision and deep learning, Manufacturing Letters. 22 (2019) 11–15. https://doi.org/10.1016/j.mfglet.2019.09.005.

[100] Z. Jin, Z. Zhang, G.X. Gu, Automated Real-Time Detection and Prediction of Interlayer Imperfections in Additive Manufacturing Processes Using Artificial Intelligence, Advanced Intelligent Systems. 2 (2020) 1900130. https://doi.org/10.1002/aisy.201900130.

[101] A. Caggiano, J. Zhang, V. Alfieri, F. Caiazzo, R. Gao, R. Teti, Machine learning-based image processing for on-line defect recognition in additive manufacturing, CIRP Annals. 68 (2019) 451–454. https://doi.org/10.1016/j.cirp.2019.03.021.

[102] S.A. Shevchik, C. Kenel, C. Leinenbach, K. Wasmer, Acoustic emission for in situ quality monitoring in additive manufacturing using spectral convolutional neural networks, Additive Manufacturing. 21 (2018) 598–604. https://doi.org/10.1016/j.addma.2017.11.012.

[103] K. Wasmer, C. Kenel, C. Leinenbach, S.A. Shevchik, In situ quality monitoring in am using acoustic emission: a machine learning approach, Proc. Materials Science and Technology. (2017) 8–12.

[104] S.A. Shevchik, G. Masinelli, C. Kenel, C. Leinenbach, K. Wasmer, Deep Learning for In Situ and Real-Time Quality Monitoring in Additive Manufacturing Using Acoustic Emission, IEEE Transactions on Industrial Informatics. 15 (2019) 5194–5203. https://doi.org/10.1109/TII.2019.2910524.

[105] K. Wasmer, T. Le-Quang, B. Meylan, S.A. Shevchik, In Situ Quality Monitoring in AM Using Acoustic Emission: A Reinforcement Learning Approach, J. of Materi Eng and Perform. 28 (2019) 666–672. https://doi.org/10.1007/s11665-018-3690-2.

[106] Y. Zhang, G.S. Hong, D. Ye, K. Zhu, J.Y.H. Fuh, Extraction and evaluation of melt pool, plume and spatter information for powder-bed fusion AM process monitoring, Materials & Design. 156 (2018) 458–469. https://doi.org/10.1016/j.matdes.2018.07.002.

[107] L. Scime, J. Beuth, Anomaly detection and classification in a laser powder bed additive manufacturing process using a trained computer vision algorithm, Additive Manufacturing. 19 (2018) 114–126. https://doi.org/10.1016/j.addma.2017.11.009.

[108] L. Scime, J. Beuth, A multi-scale convolutional neural network for autonomous anomaly detection and classification in a laser powder bed fusion additive manufacturing process, Additive Manufacturing. 24 (2018) 273–286. https://doi.org/10.1016/j.addma.2018.09.034.

[109] L. Scime, J. Beuth, Using machine learning to identify in-situ melt pool signatures indicative of flaw formation in a laser powder bed fusion additive manufacturing process, Additive Manufacturing. 25 (2019) 151–165. https://doi.org/10.1016/j.addma.2018.11.010.

[110] Z. Yang, Y. Lu, H. Yeung, S. Krishnamurty, Investigation of Deep Learning for Real-Time Melt Pool Classification in Additive Manufacturing, in: 2019 IEEE 15th International Conference on Automation Science and Engineering (CASE), 2019: pp. 640–647. https://doi.org/10.1109/COASE.2019.8843291.

[111] F. Imani, R. Chen, E. Diewald, E. Reutzel, H. Yang, Deep Learning of Variant Geometry in Layerwise Imaging Profiles for Additive Manufacturing Quality Control, Journal of Manufacturing Science and Engineering. 141 (2019) 111001. https://doi.org/10.1115/1.4044420.

[112] S. Tang, G. Wang, H. Zhang, R. Wang, An online surface defects detection system for AWAM based on deep learning, in: Solid Freeform Fabrication 2017: Proc. of the 28th Annual International Solid Freeform Fabrication Symposium–An Additive Manufacturing Conference, 1965.

[113] C. Gonzalez-Val, A. Pallas, V. Panadeiro, A. Rodriguez, A convolutional approach to quality monitoring for laser manufacturing, J Intell Manuf. 31 (2020) 789–795. https://doi.org/10.1007/s10845-019-01495-8.

[114] T. Wang, T.-H. Kwok, C. Zhou, S. Vader, In-situ droplet inspection and closed-loop control system using machine learning for liquid metal jet printing, Journal of Manufacturing Systems. 47 (2018) 83–92. https://doi.org/10.1016/j.jmsy.2018.04.003.

[115] S. Patel, J. Mekavibul, J. Park, A. Kolla, R. French, Z. Kersey, G.C. Lewin, Using Machine Learning to Analyze Image Data from Advanced Manufacturing Processes, in: 2019 Systems and Information Engineering Design Symposium (SIEDS), 2019: pp. 1–5. https://doi.org/10.1109/SIEDS.2019.8735603.

[116] J. Williams, P. Dryburgh, A. Clare, P. Rao, A. Samal, Defect Detection and Monitoring in Metal Additive Manufactured Parts through Deep Learning of Spatially Resolved Acoustic Spectroscopy Signals, Smart and Sustainable Manufacturing Systems. 2 (2018) 20180035. https://doi.org/10.1520/SSMS20180035.

[117] J. Francis, L. Bian, Deep Learning for Distortion Prediction in Laser-Based Additive Manufacturing using Big Data, Manufacturing Letters. 20 (2019) 10–14. https://doi.org/10.1016/j.mfglet.2019.02.001.

[118] B. Zhang, S. Liu, Y.C. Shin, In-Process monitoring of porosity during laser additive manufacturing process, Additive Manufacturing. 28 (2019) 497–505. https://doi.org/10.1016/j.addma.2019.05.030.

[119] J. Zhang, P. Wang, R.X. Gao, Modeling of Layer-wise Additive Manufacturing for Part Quality Prediction, Procedia Manufacturing. 16 (2018) 155–162. https://doi.org/10.1016/j.promfg.2018.10.165.

[120] J. Zhang, P. Wang, R.X. Gao, Deep learning-based tensile strength prediction in fused deposition modeling, Computers in Industry. 107 (2019) 11–21. https://doi.org/10.1016/j.compind.2019.01.011.

[121] G. X. Gu, C.-T. Chen, D. J. Richmond, M. J. Buehler, Bioinspired hierarchical composite design using machine learning: simulation, additive manufacturing, and experiment, Materials Horizons. 5 (2018) 939–945. https://doi.org/10.1039/C8MH00653A.

[122] G.X. Gu, C.-T. Chen, M.J. Buehler, De novo composite design based on machine learning algorithm, Extreme Mechanics Letters. 18 (2018) 19–28. https://doi.org/10.1016/j.eml.2017.10.001.

[123] J.K. Wilt, C. Yang, G.X. Gu, Accelerating Auxetic Metamaterial Design with Deep Learning, Advanced Engineering Materials. n/a (n.d.) 1901266. https://doi.org/10.1002/adem.201901266.

[124] S. Bonfanti, R. Guerra, F.F. Clos, D. Rayneau-Kirkhope, S. Zapperi, Automatic Design of Mechanical Metamaterial Actuators, ArXiv:2002.03032 [Cond-Mat]. (2020). http://arxiv.org/abs/2002.03032 (accessed April 6, 2020).

[125] J. Tak, A. Kantemur, Y. Sharma, H. Xin, A 3-D-Printed W-Band Slotted Waveguide Array Antenna Optimized Using Machine Learning, IEEE Antennas and Wireless Propagation Letters. 17 (2018) 2008–2012. https://doi.org/10.1109/LAWP.2018.2857807.

[126] N. Calik, M.A. Belen, P. Mahouti, Deep learning base modified MLP model for precise scattering parameter prediction of capacitive feed antenna, International Journal of Numerical Modelling: Electronic Networks, Devices and Fields. 33 (2020) e2682. https://doi.org/10.1002/jnm.2682.

[127] C.R. Wolfe, C.C. Tutum, R. Miikkulainen, Functional generative design of mechanisms with recurrent neural networks and novelty search, in: Proceedings of the Genetic and Evolutionary Computation Conference, Association for Computing Machinery, Prague, Czech Republic, 2019: pp. 1373–1380. https://doi.org/10.1145/3321707.3321785.

[128] C.A. Duchanoy, M.A. Moreno-Armendáriz, J.C. Moreno-Torres, C.A. Cruz-Villar, A Deep Neural Network Based Model for a Kind of Magnetorheological Dampers, Sensors. 19 (2019) 1333. https://doi.org/10.3390/s19061333.

[129] Y. Miao, Y. Sun, S. Li, P. Zhang, Y. Yang, Y. Hu, Spinal Neoplasm Image Inpainting with Deep Convolutional Neutral Networks, in: 2019 IEEE International Conference on Robotics and Biomimetics (ROBIO), 2019: pp. 2619–2624. https://doi.org/10.1109/ROBIO49542.2019.8961840.

[130] Y. Sui, X. Peng, Chapter 3 - Stress-constrained topology optimization for continuum structures, in: Y. Sui, X. Peng (Eds.), Modelling, Solving and Application for Topology Optimization of Continuum Structures, Butterworth-Heinemann, 2018: pp. 79–137. https://doi.org/10.1016/B978-0-12-812655-4.00003-1.

[131] S. Bobby, S.M.J. Spence, A. Kareem, Data-driven performance-based topology optimization of uncertain wind-excited tall buildings, Struct Multidisc Optim. 54 (2016) 1379–1402. https://doi.org/10.1007/s00158-016-1474-6.

[132] E. Ulu, R. Zhang, M.E. Yumer, L.B. Kara, A Data-Driven Investigation and Estimation of Optimal Topologies under Variable Loading Configurations, in: Y.J. Zhang, J.M.R.S. Tavares (Eds.), Computational Modeling of Objects Presented in Images. Fundamentals, Methods, and Applications, Springer International Publishing, Cham, 2014: pp. 387–399. https://doi.org/10.1007/978-3-319-09994-1_38.

[133] H. Deng, A.C. To, Topology optimization based on deep representation learning (DRL) for compliance and stress-constrained design, Comput Mech. 66 (2020) 449–469. https://doi.org/10.1007/s00466-020-01859-5.

[134] X. Lin, Y. Rivenson, N.T. Yardimci, M. Veli, Y. Luo, M. Jarrahi, A. Ozcan, All-optical machine learning using diffractive deep neural networks, Science. 361 (2018) 1004–1008. https://doi.org/10.1126/science.aat8084.

[135] Y. Luo, D. Mengu, N.T. Yardimci, Y. Rivenson, M. Veli, M. Jarrahi, A. Ozcan, Design of task-specific optical systems using broadband diffractive neural networks, Light: Science & Applications. 8 (2019) 1–14. https://doi.org/10.1038/s41377-019-0223-1.

[136] H. Li, X. Ma, A.S. Rathore, Z. Li, Q. An, C. Song, W. Xu, Y. Wang, Image Dataset for Visual Objects Classification in 3D Printing, (2018). https://openreview.net/forum?id=SyyBVIJwG (accessed April 6, 2020).

[137] G.N. Pham, S.-H. Lee, K.-R. Kwon, Convolutional neural networks-based anti-weapon detection for safe 3D printing, in: International Forum on Medical Imaging in Asia 2019, International Society for Optics and Photonics, 2019: p. 110501B. https://doi.org/10.1117/12.2519447.

[138] E. Ahmed, A. Saint, A.E.R. Shabayek, K. Cherenkova, R. Das, G. Gusev, D. Aouada, B. Ottersten, A survey on Deep Learning Advances on Different 3D Data Representations, ArXiv:1808.01462 [Cs]. (2019). http://arxiv.org/abs/1808.01462 (accessed April 8, 2020).

[139] K. Weiss, T.M. Khoshgoftaar, D. Wang, A survey of transfer learning, Journal of Big Data. 3 (2016) 9. https://doi.org/10.1186/s40537-016-0043-6.

[140] Y. Lecun, L. Bottou, Y. Bengio, P. Haffner, Gradient-based learning applied to document recognition, Proceedings of the IEEE. 86 (1998) 2278–2324. https://doi.org/10.1109/5.726791.

[141] J. Deng, W. Dong, R. Socher, L.-J. Li, Kai Li, Li Fei-Fei, ImageNet: A large-scale hierarchical image database, in: 2009 IEEE Conference on Computer Vision and Pattern Recognition, 2009: pp. 248–255. https://doi.org/10.1109/CVPR.2009.5206848.

[142] Q. Zhou, A. Jacobson, Thingi10K: A Dataset of 10,000 3D-Printing Models, ArXiv:1605.04797 [Cs]. (2016). http://arxiv.org/abs/1605.04797 (accessed April 29, 2020).

[143] B. Lane, H. Yeung, Process Monitoring Dataset from the Additive Manufacturing Metrology Testbed (AMMT): "Three-Dimensional Scan Strategies," J. RES. NATL. INST. STAN. 124 (2019) 124033. https://doi.org/10.6028/jres.124.033.

[144] A.X. Chang, T. Funkhouser, L. Guibas, P. Hanrahan, Q. Huang, Z. Li, S. Savarese, M. Savva, S. Song, H. Su, J. Xiao, L. Yi, F. Yu, ShapeNet: An Information-Rich 3D Model Repository, ArXiv:1512.03012 [Cs]. (2015). http://arxiv.org/abs/1512.03012 (accessed April 28, 2020).

[145] Z. Wu, S. Song, A. Khosla, F. Yu, L. Zhang, X. Tang, J. Xiao, 3D ShapeNets: A Deep Representation for Volumetric Shapes, ArXiv:1406.5670 [Cs]. (2015). http://arxiv.org/abs/1406.5670 (accessed April 28, 2020).

[146] S. Choi, Q.-Y. Zhou, S. Miller, V. Koltun, A Large Dataset of Object Scans, ArXiv:1602.02481 [Cs]. (2016). http://arxiv.org/abs/1602.02481 (accessed April 28, 2020).

[147] K. Mo, S. Zhu, A.X. Chang, L. Yi, S. Tripathi, L.J. Guibas, H. Su, PartNet: A Large-Scale Benchmark for Fine-Grained and Hierarchical Part-Level 3D Object Understanding, in: 2019 IEEE/CVF Conference on Computer Vision and Pattern Recognition (CVPR), IEEE, Long Beach, CA, USA, 2019: pp. 909–918. https://doi.org/10.1109/CVPR.2019.00100.

[148] D.B. Berry, S. You, J. Warner, L.R. Frank, S. Chen, S.R. Ward, A 3D Tissue-Printing Approach for Validation of Diffusion Tensor Imaging in Skeletal Muscle, Tissue Engineering Part A. 23 (2017) 980–988. https://doi.org/10.1089/ten.tea.2016.0438.

[149] X. Ma, X. Qu, W. Zhu, Y.-S. Li, S. Yuan, H. Zhang, J. Liu, P. Wang, C.S.E. Lai, F. Zanella, G.-S. Feng, F. Sheikh, S. Chien, S. Chen, Deterministically patterned biomimetic human iPSC-derived hepatic model via rapid 3D bioprinting, Proc Natl Acad Sci USA. 113 (2016) 2206–2211. https://doi.org/10.1073/pnas.1524510113.

[150] H.H. Hwang, S. You, X. Ma, L. Kwe, G. Victorine, N. Lawrence, X. Wan, H. Shen, W. Zhu, S. Chen, High throughput direct 3D bioprinting in multiwell plates, Biofabrication. (2020). https://doi.org/10.1088/1758-5090/ab89ca.

[151] W. Zhu, K.R. Tringale, S.A. Woller, S. You, S. Johnson, H. Shen, J. Schimelman, M. Whitney, J. Steinauer, W. Xu, T.L. Yaksh, Q.T. Nguyen, S. Chen, Rapid continuous 3D printing of customizable peripheral nerve guidance conduits, Materials Today. 21 (2018) 951–959. https://doi.org/10.1016/j.mattod.2018.04.001.

[152] Y.-J. Seol, H.-W. Kang, S.J. Lee, A. Atala, J.J. Yoo, Bioprinting technology and its applications, European Journal of Cardio-Thoracic Surgery. 46 (2014) 342–348. https://doi.org/10.1093/ejcts/ezu148.

[153] I.T. Ozbolat, M. Hospodiuk, Current advances and future perspectives in extrusion-based bioprinting, Biomaterials. 76 (2016) 321–343. https://doi.org/10.1016/j.biomaterials.2015.10.076.

[154] A.B. Dababneh, I.T. Ozbolat, Bioprinting Technology: A Current State-of-the-Art Review, Journal of Manufacturing Science and Engineering. 136 (2014). https://doi.org/10.1115/1.4028512.

[155] S. Derakhshanfar, R. Mbeleck, K. Xu, X. Zhang, W. Zhong, M. Xing, 3D bioprinting for biomedical devices and tissue engineering: A review of recent trends and advances, Bioactive Materials. 3 (2018) 144–156. https://doi.org/10.1016/j.bioactmat.2017.11.008.

[156] S. You, J. Li, W. Zhu, C. Yu, D. Mei, S. Chen, Nanoscale 3D printing of hydrogels for cellular tissue engineering, J. Mater. Chem. B. 6 (2018) 2187–2197. https://doi.org/10.1039/C8TB00301G.

[157] S. You, W. Zhu, P. Wang, S. Chen, Projection Printing of Ultrathin Structures with Nanoscale Thickness Control, ACS Applied Materials & Interfaces. 11 (2019) 16059–16064. https://doi.org/10.1021/acsami.9b02728.

[158] S. You, K. Miller, S. Chen, Chapter 1. Microstereolithography, in: D.-W. Cho (Ed.), Biomaterials Science Series, Royal Society of Chemistry, Cambridge, 2019: pp. 1–21. https://doi.org/10.1039/9781788012683-00001.

[159] C. Yu, J. Schimelman, P. Wang, K.L. Miller, X. Ma, S. You, J. Guan, B. Sun, W. Zhu, S. Chen, Photopolymerizable Biomaterials and Light-Based 3D Printing Strategies for Biomedical Applications, Chem. Rev. 120 (2020) 10695–10743. https://doi.org/10.1021/acs.chemrev.9b00810.

[160] W. Zhu, X. Ma, M. Gou, D. Mei, K. Zhang, S. Chen, 3D printing of functional biomaterials for tissue engineering, Current Opinion in Biotechnology. 40 (2016) 103–112. https://doi.org/10.1016/j.copbio.2016.03.014.

[161] M. Lin, N. Firoozi, C.-T. Tsai, M.B. Wallace, Y. Kang, 3D-printed flexible polymer stents for potential applications in inoperable esophageal malignancies, Acta Biomaterialia. 83 (2019) 119–129. https://doi.org/10.1016/j.actbio.2018.10.035.

[162] M. Lin, M. Vatani, J.-W. Choi, S. Dilibal, E.D. Engeberg, Compliant underwater manipulator with integrated tactile sensor for nonlinear force feedback control of an SMA actuation system, Sensors and Actuators A: Physical. 315 (2020) 112221. https://doi.org/10.1016/j.sna.2020.112221.

[163] S. You, J. Guan, J. Alido, H.H. Hwang, R. Yu, L. Kwe, H. Su, S. Chen, Mitigating Scattering Effects in Light-Based Three-Dimensional Printing Using Machine Learning, Journal of Manufacturing Science and Engineering. 142 (2020) 081002. https://doi.org/10.1115/1.4046986.

[164] S. You, P. Wang, J. Schimelman, H.H. Hwang, S. Chen, High-fidelity 3D printing using flashing photopolymerization, Additive Manufacturing. 30 (2019) 100834. https://doi.org/10.1016/j.addma.2019.100834.

[165] W. Choi, C. Fang-Yen, K. Badizadegan, S. Oh, N. Lue, R.R. Dasari, M.S. Feld, Tomographic phase microscopy, Nat Methods. 4 (2007) 717–719. https://doi.org/10.1038/nmeth1078.

[166] M. Schürmann, J. Scholze, P. Müller, J. Guck, C.J. Chan, Cell nuclei have lower refractive index and mass density than cytoplasm, J. Biophoton. 9 (2016) 1068–1076. https://doi.org/10.1002/jbio.201500273.

[167] V.V. Tuchin, Tissue Optics: Light Scattering Methods and Instruments for Medical Diagnosis, Society of Photo-Optical Instrumentation Engineers (SPIE), 2015. https://doi.org/10.1117/3.1003040.

[168] L.-H. Han, G. Mapili, S. Chen, K. Roy, Projection Microfabrication of Three-Dimensional Scaffolds for Tissue Engineering, Journal of Manufacturing Science and Engineering. 130 (2008). https://doi.org/10.1115/1.2823079.

[169] B. Grigoryan, S.J. Paulsen, D.C. Corbett, D.W. Sazer, C.L. Fortin, A.J. Zaita, P.T. Greenfield, N.J. Calafat, J.P. Gounley, A.H. Ta, F. Johansson, A. Randles, J.E. Rosenkrantz, J.D. Louis-Rosenberg, P.A. Galie, K.R. Stevens, J.S. Miller, Multivascular networks and functional intravascular topologies within biocompatible hydrogels, Science. 364 (2019) 458–464. https://doi.org/10.1126/science.aav9750.

[170] S. Angra, S. Ahuja, Machine learning and its applications: A review, in: 2017 International Conference on Big Data Analytics and Computational Intelligence (ICBDAC), 2017: pp. 57–60. https://doi.org/10.1109/ICBDACI.2017.8070809.

[171] P.P. Shinde, S. Shah, A Review of Machine Learning and Deep Learning Applications, in: 2018 Fourth International Conference on Computing Communication Control and Automation (ICCUBEA), 2018: pp. 1–6. https://doi.org/10.1109/ICCUBEA.2018.8697857.

[172] F.W. Baumann, A. Sekulla, M. Hassler, B. Himpel, M. Pfeil, Trends of machine learning in additive manufacturing, International Journal of Rapid Manufacturing. 7 (2018) 310. https://doi.org/10.1504/IJRAPIDM.2018.095788.

[173] L. Meng, B. McWilliams, W. Jarosinski, H.-Y. Park, Y.-G. Jung, J. Lee, J. Zhang, Machine Learning in Additive Manufacturing: A Review, JOM. 72 (2020) 2363–2377. https://doi.org/10.1007/s11837-020-04155-y.

[174] S.S. Razvi, S. Feng, A. Narayanan, Y.-T.T. Lee, P. Witherell, A Review of Machine Learning Applications in Additive Manufacturing, in: American Society of Mechanical Engineers Digital Collection, 2019. https://doi.org/10.1115/DETC2019-98415.

[175] X. Qi, G. Chen, Y. Li, X. Cheng, C. Li, Applying Neural-Network-Based Machine Learning to Additive Manufacturing: Current Applications, Challenges, and Future Perspectives, Engineering. 5 (2019) 721–729. https://doi.org/10.1016/j.eng.2019.04.012.

[176] Z. Jin, Z. Zhang, X. Shao, G.X. Gu, Monitoring Anomalies in 3D Bioprinting with Deep Neural Networks, ACS Biomater. Sci. Eng. (2021). https://doi.org/10.1021/acsbiomaterials.0c01761.

[177] D.E. Goldberg, Genetic algorithms in search, optimization, and machine learning, Addison-Wesley Pub. Co, Reading, Mass, 1989.

[178] MATLAB R2021a and Global Optimization Toolbox 4.5, (2021).

[179] O. Ronneberger, P. Fischer, T. Brox, U-Net: Convolutional Networks for Biomedical Image Segmentation, in: N. Navab, J. Hornegger, W.M. Wells, A.F. Frangi (Eds.), Medical Image Computing and Computer-Assisted Intervention – MICCAI 2015, Springer International Publishing, Cham, 2015: pp. 234–241. https://doi.org/10.1007/978-3-319-24574-4_28.

[180] P. Isola, J.-Y. Zhu, T. Zhou, A.A. Efros, Image-to-Image Translation with Conditional Adversarial Networks, in: 2017 IEEE Conference on Computer Vision and Pattern Recognition (CVPR), IEEE, Honolulu, HI, 2017: pp. 5967–5976. https://doi.org/10.1109/CVPR.2017.632.

[181] S. Ioffe, C. Szegedy, Batch normalization: accelerating deep network training by reducing internal covariate shift, in: Proceedings of the 32nd International Conference on International Conference on Machine Learning - Volume 37, JMLR.org, Lille, France, 2015: pp. 448–456.

[182] V. Nair, G.E. Hinton, Rectified linear units improve restricted boltzmann machines, in: Proceedings of the 27th International Conference on Machine Learning (ICML-10), Haifa, Israel, 2010: pp. 807–814.

[183] A. Paszke, S. Gross, S. Chintala, G. Chanan, E. Yang, Z. DeVito, Z. Lin, A. Desmaison, L. Antiga, A. Lerer, Automatic differentiation in PyTorch, (2017).

[184] D.P. Kingma, J. Ba, Adam: A Method for Stochastic Optimization, in: Y. Bengio, Y. LeCun (Eds.), 3rd International Conference on Learning Representations, ICLR 2015, San Diego, CA, USA, May 7-9, 2015, Conference Track Proceedings, 2015. http://arxiv.org/abs/1412.6980 (accessed April 26, 2020).

[185] C.M. Bishop, Neural networks for pattern recognition, Oxford university press, 1995.

[186] C. Shorten, T.M. Khoshgoftaar, A survey on Image Data Augmentation for Deep Learning, Journal of Big Data. 6 (2019) 60. https://doi.org/10.1186/s40537-019-0197-0.

[187] G. An, The Effects of Adding Noise During Backpropagation Training on a Generalization Performance, Neural Computation. 8 (1996) 643–674. https://doi.org/10.1162/neco.1996.8.3.643.

[188] X. Zhou, Y. Hou, J. Lin, A review on the processing accuracy of two-photon polymerization, AIP Advances. 5 (2015) 030701. https://doi.org/10.1063/1.4916886.

[189] A. Marino, C. Filippeschi, V. Mattoli, B. Mazzolai, G. Ciofani, Biomimicry at the nanoscale: current research and perspectives of two-photon polymerization, Nanoscale. 7 (2015) 2841–2850. https://doi.org/10.1039/C4NR06500J.

[190] W. Zhang, S. Chen, Femtosecond laser nanofabrication of hydrogel biomaterial, MRS Bulletin. 36 (2011) 1028–1033. https://doi.org/10.1557/mrs.2011.275.

[191] A.K. Nguyen, R.J. Narayan, Two-photon polymerization for biological applications, Materials Today. 20 (2017) 314–322. https://doi.org/10.1016/j.mattod.2017.06.004.

[192] R. Ajay, J.S. Sivakumar, S. Ahamed, N. Nilofernisha, B. Saravanakarthikeyan, S. Krishnaraj, In Vitro Cytocompatibility of Dental Restorative Composite Resin Photopolymerized with a Novel Multifunctional Crosslinking Comonomer, World Journal of Dentistry. 12 (2021) 403–408. https://doi.org/10.5005/jp-journals-10015-1858.

[193] D.W. Johnson, C.R. Langford, M.P. Didsbury, B. Lipp, S.A. Przyborski, N.R. Cameron, Fully biodegradable and biocompatible emulsion templated polymer scaffolds by thiol-acrylate polymerization of polycaprolactone macromonomers, Polym. Chem. 6 (2015) 7256–7263. https://doi.org/10.1039/C5PY00721F.

[194] P. Wang, D.B. Berry, Z. Song, W. Kiratitanaporn, J. Schimelman, A. Moran, F. He, B. Xi, S. Cai, S. Chen, 3D Printing of a Biocompatible Double Network Elastomer with Digital Control of Mechanical Properties, Adv. Funct. Mater. 30 (2020) 1910391. https://doi.org/10.1002/adfm.201910391.

[195] W. Kiratitanaporn, D.B. Berry, A. Mudla, T. Fried, A. Lao, C. Yu, N. Hao, S.R. Ward, S. Chen, 3D printing a biocompatible elastomer for modeling muscle regeneration after volumetric muscle loss, Biomaterials Advances. 142 (2022) 213171. https://doi.org/10.1016/j.bioadv.2022.213171.

[196] J. Guan, S. You, Y. Xiang, J. Schimelman, J. Alido, X. Ma, M. Tang, S. Chen, Compensating the cell-induced light scattering effect in light-based bioprinting using deep learning, Biofabrication. 14 (2022) 015011. https://doi.org/10.1088/1758-5090/ac3b92.

[197] S. Pashneh-Tala, R. Owen, H. Bahmaee, S. Rekštytė, M. Malinauskas, F. Claeyssens, Synthesis, Characterization and 3D Micro-Structuring via 2-Photon Polymerization of Poly(glycerol sebacate)-Methacrylate–An Elastomeric Degradable Polymer, Front. Phys. 6 (2018) 41. https://doi.org/10.3389/fphy.2018.00041.